



5-2008

Flavonoids and Related Compounds as Nucleoside Transporter Inhibitors

Surekha Ravaji Pimple

University of Tennessee Health Science Center

Follow this and additional works at: <https://dc.uthsc.edu/dissertations>

 Part of the [Medicinal and Pharmaceutical Chemistry Commons](#), and the [Pharmaceutics and Drug Design Commons](#)

Recommended Citation

Pimple, Surekha Ravaji, "Flavonoids and Related Compounds as Nucleoside Transporter Inhibitors" (2008). *Theses and Dissertations (ETD)*. Paper 200. <http://dx.doi.org/10.21007/etd.cghs.2008.0245>.

This Thesis is brought to you for free and open access by the College of Graduate Health Sciences at UTHSC Digital Commons. It has been accepted for inclusion in Theses and Dissertations (ETD) by an authorized administrator of UTHSC Digital Commons. For more information, please contact jwelch30@uthsc.edu.

Flavonoids and Related Compounds as Nucleoside Transporter Inhibitors

Document Type

Thesis

Degree Name

Master of Science (MS)

Program

Pharmaceutical Sciences

Research Advisor

John K. Buolamwini, Ph.D.

Committee

Peter K. Bridson, Ph.D. Issac O. Donkor, Ph.D. Duane D. Miller, Ph.D.

DOI

10.21007/etd.cghs.2008.0245

**FLAVONOIDS AND RELATED COMPOUNDS AS NUCLEOSIDE
TRANSPORTER INHIBITORS**

A Dissertation
Presented for
The Graduate Studies Council
The University of Tennessee
Health Science Center

In Partial Fulfillment
Of the Requirements for the Degree
Master of Science
From The University of Tennessee

By
Surekha Ravaji Pimple
May 2008

Copyright © 2008 by Surekha Ravaji Pimple
All rights reserved

Dedication

This dissertation is dedicated to my husband,
Dr. Yogeshwar Gulabrao Bachhav

Acknowledgements

I would like to thank my major advisor, Dr. John K. Buolamwini for his constant help, guidance and support during the course of this work. In the past two and a half years the encouragement and training that I have received from Dr. Buolamwini has helped develop my independent thinking and skills as a researcher. I am also very grateful to my other committee members, Dr. Peter K. Bridson, Dr. Isaac O. Donkor, and Dr. Duane D. Miller for their valuable suggestions.

I extend my sincere thanks to the following past and present members of our laboratory: Dr. Shantaram Kamath, Dr. Shivaputra Patil, Dr. Chunmei Wang, Dr. Amol Gupte, Dr. Zhengxiang Zhu, Dr. Wenwei Lin, JaWanda Grant, Horrick Sharma, and Peihong Guan for all the help and support that they have given me during the tenure of this work. I would like to thank my colleagues at work and my friends, Himabindu, Sucharita, Bharati, Renuka and Varun, at the University of Tennessee for their support and cooperation.

I would also like to thank my husband Dr. Yogeshwar Bachhav for the encouragement and support that he has always given. Finally, I would like to express my sincere gratitude to my parents, parent in-laws, and siblings who have always been a constant source of inspiration and support.

Abstract

Mammalian nucleoside transporters can be classified into two main categories, namely, equilibrative nucleoside transporters (ENTs) and concentrative nucleoside transporters (CNTs). ENTs are ubiquitous, and mediate sodium-independent bi-directional facilitated diffusion nucleoside transport processes. CNTs on the other hand, are secondary active unidirectional transporters that are sodium-dependent. Both the equilibrative and the concentrative nucleoside transporters have several family members which are ENT1 to ENT4 and CNT1 to CNT6. Over the past two decades, important advances in the understanding of nucleoside transporter functions have been made. Identification and molecular cloning of the ENT and CNT families from mammals and protozoan parasites have provided much information about the structure, function, regulation, and tissue and cellular localization. Structure–function analyses of various nucleoside transporter chimeras and mutants have revealed important elements involved in substrate and inhibitor recognition and binding. However, the mechanisms that regulate nucleoside transporters in various tissues and cell types are just beginning to be understood. Because of the ability of these transporters to handle nucleoside analogues used in the treatment of patients with cancer and viral diseases, ongoing research should allow the design of more specifically targeted new compounds or improvements to existing drugs. New drugs are welcome not only in the treatment of cancer and viral diseases, but also in cardiovascular disorders and parasitic infections.

Due to the absence of crystal structures and limited information regarding the active sites of nucleoside transporters, the designing of novel inhibitors is confined to ligand-based methods. In an effort to search for novel classes of inhibitors other than the existing ones, a series of 95 different flavone and flavone-like compounds was screened against concentrative nucleoside transporters (CNT 1, 2 and 3) and equilibrative nucleoside transporters (ENT 1 and 2). The results obtained in the form of IC_{50} values were further utilized to perform quantitative structure–activity relationship studies which indeed helped to understand the effects of different functionalities in the inhibition of nucleoside transporters. The validated 3D-QSAR models were used for design and activity prediction of new compounds. Pharmacophore hypotheses were also generated for hCNT3 using the PHASE pharmacophore mapping program to establish structural criteria for inhibitor design, and for database searching to find new hit molecules. Additionally, fifteen compounds were selected based on SAR and screened for equilibrative nucleoside transporter inhibition for validation of QSAR models. One novel compound, **XI** was designed with reduced complexity in further attempts to identify the ENT pharmacophore. But the synthetic route followed to prepare compound **XI**, resulted in the synthesis of compounds **XII** and **XIII**, which were evaluated as a mixture and exhibited substantial inhibitory activity against hENT1, but had no significant effect on hENT2 or hCNT3.

This work has identified a novel class of CNT and ENT nucleoside transporter inhibitors and delineated structural determinants of potency and transporter subtype selectivity.

Table of Contents

Chapter 1: Human Nucleoside Transporters	1
1.1 Nucleoside Transporters	1
1.2 Concentrative Nucleoside Transporters	5
1.2.1 Molecular Characteristics	5
1.2.2 Tissue Distribution	7
1.2.3 Transport of Physiologic Nucleosides and Nucleoside Analogs	7
1.2.4 Molecular Determinants of Concentrative Nucleoside Transporter Substrates	8
1.2.5 Concentrative Nucleoside Transporter Inhibitors	9
1.2.5.1 Phloridzin	9
1.2.5.2 5'-Position Modified Nucleoside Derivatives of Adenosine	9
1.2.5.3 Ribofuranoside Compounds with Benzimidazole Moiety	10
1.2.5.4 8-Position Modified Purine Nucleoside Derivatives	10
1.3 Equilibrative Nucleoside Transporters	11
1.3.1 Molecular Characteristics	11
1.3.2 Tissue Distribution	14
1.3.3 Transport of Physiologic Nucleosides and Nucleoside Analogs	14
1.3.4 Equilibrative Nucleoside Transporter Inhibitors	16
1.4 Applications of Nucleoside Transporter Inhibitors	16
1.4.1 Antimetabolite Potentiation	16
1.4.1.1 Cancer Chemotherapy	16
1.4.1.2 Viral Infections	17
1.4.2 Adenosine Potentiation	17
1.4.2.1 Cardioprotection	17
1.4.2.2 Ischemic Preconditioning and Heart Transplantation	17
1.4.2.3 Neuroprotection and Stroke	18
1.4.2.4 Anti-inflammatory Effects	18
1.4.3 Host Tissue Protection	18
1.4.3.1 Protection Against Nucleoside Anticancer Drugs Toxicity	18
1.4.3.2 Antiprotozoal Chemotherapy	19
Chapter 2: Research Objectives	20
Chapter 3: Biological Evaluation and 3D-QSAR Studies on Flavone Analogs for Human Concentrative Nucleoside Transporter Inhibition	22
3.1 Introduction	22
3.2 Uridine Uptake Assay	22
3.3 IC ₅₀ Curves of Active Flavones	22
3.4 Materials and Methods	30
3.5 Molecular Modeling	30
3.6 CoMFA and CoMSIA Models	31
3.7 Results of 3D-QSAR Analyses	34

3.8	PLS Contour Maps	38
3.8.1	PLS Contour Interpretation for CNT1 CoMFA	38
3.8.2	PLS Contour Interpretation for CNT1 CoMSIA	38
3.8.3	PLS Contour Interpretation for CNT2 CoMFA	42
3.8.4	PLS Contour Interpretation for CNT2 CoMSIA	42
3.8.5	PLS Contour Interpretation for CNT3 CoMFA	42
3.8.6	PLS Contour Interpretation for CNT3 CoMSIA	42
3.9	Activity Prediction of <i>In silico</i> Designed Compounds Using 3D-QSAR Models for hCNT3.	43
3.10	Discussion	48
3.11	Conclusion	49
3.12	Experimental Section: [³ H]-Uridine Uptake Assay	49

**Chapter 4: Biological Evaluation and 3D-QSAR Studies on Flavones
Analogues for Human Equilibrative Nucleoside Transporter
Inhibition**

		50
4.1	Introduction	50
4.2	Biological Evaluation: Uridine Uptake Assay	50
4.3	3D-QSAR Analyses	59
4.3.1	Materials and Methods	59
4.3.2	Molecular Modeling	59
4.3.3	CoMFA and CoMSIA Models	59
4.3.4	Results of 3D-QSAR Analyses	61
4.3.5	PLS Contour Maps	64
4.3.5.1	PLS Contour Interpretation for ENT1 CoMFA	72
4.3.5.2	PLS Contour Interpretation for ENT1 CoMSIA	72
4.3.5.3	PLS Contour Interpretation for ENT2 CoMFA	72
4.3.5.4	PLS Contour Interpretation for ENT2 CoMSIA	73
4.4	Activity Prediction of <i>In silico</i> Designed Compounds Using 3D-QSAR Models for hENT.	73
4.5	Evaluation of Related Analogues	77
4.6	Synthesis and Testing of a New Lead as an Equilibrative Nucleoside Transporter Specific Inhibitor	77
4.7	Discussion	77
4.8	Conclusion	85
4.9	Experimental Section: Chemistry	85
4.9.1	Reaction Procedure	86
4.9.2	Mixture of Compounds XII and XIII	86

**Chapter 5: Pharmacophore Mapping of Flavone Derivatives for hCNT3
Inhibition**

		87
5.1	Introduction	87
5.2	Materials and Methods	87
5.2.1	Preparation of Ligands	90
5.2.2	Creation of Pharmacophoric Sites	90
5.2.3	Finding a Common Pharmacophore	90

5.2.4	Scoring Hypotheses	90
5.2.5	Building a QSAR Model	93
5.3	Results and Discussion	97
5.4	Pharmacophore Based Database Searching	101
5.5	Summary	101
List of References			103
Appendix: Proton and Mass Spectrum of Compounds XII and XIII			118
Vita			121

List of Tables

Table 3.1:	Compounds evaluated for CNT inhibition with IC ₅₀ values	24
Table 3.2:	PLS statistics of CoMFA and CoMSIA 3D-QSAR models for CNT	32
Table 3.3:	Field contribution by CoMFA and CoMSIA descriptors for CNT	33
Table 3.4:	Results of group cross validation, randomization and bootstrapping for CNT	33
Table 3.5:	Residuals of predictions of test set by CoMFA and CoMSIA models for hCNT3 inhibition	37
Table 3.6:	Predictive R ² values of test set by CoMFA and CoMSIA models for hCNT3 inhibition.	37
Table 3.7:	Predicted activities for <i>in silico</i> designed compounds for hCNT3-inhibition	44
Table 4.1:	Compounds evaluated for ENT inhibition with IC ₅₀ values	54
Table 4.2:	PLS statistics of CoMFA and CoMSIA 3D-QSAR models for ENT	62
Table 4.3:	Field contribution by CoMFA and CoMSIA descriptors for ENT	63
Table 4.4:	Results of group cross validation, randomization and bootstrapping for ENT	63
Table 4.5:	Residuals of predictions of internal test set by CoMFA and CoMSIA models for hENT1 and hENT2 inhibition	67
Table 4.6:	Residuals of predictions of external test set by CoMFA and CoMSIA models for hENT1 and hENT2 inhibition	68
Table 4.7:	R ² predictivity of internal and external test sets by CoMFA and CoMSIA models for hENT1 and hENT2 inhibition	69
Table 4.8:	Predicted activities for <i>in silico</i> designed compounds	74
Table 4.9:	Biological activity data of compounds 101 to 115 ^{ab}	79
Table 5.1:	Compounds used in pharmacophore mapping	88
Table 5.2:	Pharmacophore generation	92

Table 5.3: Scoring results	94
Table 5.4: QSAR results	98

List of Figures

Figure 1.1: Structures of physiological nucleosides	2
Figure 1.2: Structures of representative antiviral and anticancer nucleoside analogs	3
Figure 1.3: Classification of human nucleoside transporters	4
Figure 1.4: Nucleoside transport mediated by Na ⁺ -dependent (CNT) and Na ⁺ -independent (ENT) nucleoside transporters	4
Figure 1.5: Topographical model of concentrative nucleoside transporter	6
Figure 1.6: CNT inhibitors	10
Figure 1.7: Topographical model of equilibrative nucleoside transporter	12
Figure 1.8: Potent ENT inhibitors	13
Figure 2.1: Structural resemblance of phloridzin to flavone	20
Figure 3.1: Comparison graph of % of inhibition at 10 μM concentration by compounds against hCNT1, hCNT2 and hCNT3	23
Figure 3.2: IC ₅₀ curves of active compounds for CNT3 inhibition	29
Figure 3.3: Atoms used in MATCH alignment shown in bold face	30
Figure 3.4: Atom-by-atom superposition used for 3D-QSAR analysis	31
Figure 3.5: Prediction curves for CoMFA and CoMSIA model for hCNT1 inhibition	35
Figure 3.6: Prediction curves for CoMFA and CoMSIA models for hCNT2 inhibition	35
Figure 3.7: Prediction curves for CoMFA training set and test set for hCNT3 inhibition	36
Figure 3.8: Prediction curves for CoMSIA training set and test set for hCNT3 inhibition	36

Figure 3.9: PLS contours from CoMFA steric and electrostatic (A) and CoMSIA steric, electrostatic and hydrophobic (B) descriptors for hCNT1 inhibition	39
Figure 3.10: PLS contours from CoMFA steric and electrostatic (A), CoMSIA steric and electrostatic (B) and CoMSIA hydrophobic and hydrogen bond donor and acceptor (C) descriptors for hCNT2 inhibition	40
Figure 3.11: PLS contours from CoMFA steric and electrostatic (A), CoMSIA steric and electrostatic (B) and CoMSIA hydrophobic and hydrogen bond donor and acceptor (C) descriptors for hCNT3 inhibition	41
Figure 3.12: <i>In silico</i> compounds with high predicted hCNT3 inhibition activity	47
Figure 4.1: Comparison graph of % of inhibition at 10 μ M.	51
Figure 4.2: IC ₅₀ curves of compounds in study for ENT1 inhibition	52
Figure 4.3: IC ₅₀ curves of compounds in study for ENT2 inhibition	53
Figure 4.4: Atoms used in MATCH alignment shown in bold face.	60
Figure 4.5: Atom-by-atom superposition used for 3D-QSAR analysis	60
Figure 4.6: Predicted vs actual pK_i graphs for CoMFA training set and test set for hENT1 inhibition	65
Figure 4.7: Predicted vs actual pK_i graphs for CoMSIA training set and test set for hENT1 inhibition	65
Figure 4.8: Predicted vs actual pK_i graphs for CoMFA training set and test set for hENT2 inhibition	66
Figure 4.9: Predicted vs actual pK_i graphs for CoMSIA training set and test set for hENT2 inhibition	66
Figure 4.10: Predicted vs actual pK_i graphs for external test set for hENT1 inhibition (A) CoMFA & (B) CoMSIA.	69
Figure 4.11: Predicted vs actual pK_i graphs for external test set for hENT2 Inhibition (A) CoMFA & (B) CoMSIA.	69
Figure 4.12: PLS contours from CoMFA steric and electrostatic (A), CoMSIA steric and electrostatic (B) and CoMSIA hydrophobic and hydrogen bond donor & acceptor (C) descriptors for hENT1 transporter inhibitors	70

Figure 4.13: PLS contours from CoMFA steric and electrostatic (A), CoMSIA steric and electrostatic (B) and CoMSIA hydrophobic and hydrogen bond donor & acceptor (C) descriptors for hENT2 transporter inhibitors	71
Figure 4.14: <i>In silico</i> compounds with high inhibitory activity against ENT1 and ENT2	78
Figure 4.15: Structures of compounds 101 to 115	80
Figure 4.16: (A) Screening at 10 μ M on ENT1 and ENT2, (B) IC ₅₀ curves for ENT1 and (C) IC ₅₀ curves for ENT2	81
Figure 4.17: Structural similarity between active flavones and compound XI	82
Figure 4.18: Synthetic scheme	82
Figure 4.19: Comparison graph of mixture of compounds XII and XIII screening	83
Figure 5.1: General structure of compounds used in the study	87
Figure 5.2: (A) All ligands with pharmacophoric sites, (B) active ligand set and (C) inactive ligand set.	91
Figure 5.3: Hypotheses belonging to pharmacophore AAADRRR	95
Figure 5.4: Hypotheses belonging to pharmacophore AAAADDR	96
Figure 5.5: Training and test set used for building QSAR models for hypotheses AAADRRR (A, B) and AAAADDR (C, D)	99
Figure 5.6: Contribution of sites to pharmacophores AAADRRR (A, B, C) & AAAADDR (D, E, F)	100
Figure 5.7: PHASE hypotheses (A and B) and UNITY query (C and D) to be used for database searching	102
Figure A.1: Proton spectrum	119
Figure A.2: ES mass spectrum	120

List of Abbreviations

Ara-C	Cytarabine
AZT	Azidothymidine
cAMP	cyclic Adenosine Monophosphate
CNT1	Concentrative Nucleoside Transporter 1
CNT2	Concentrative Nucleoside Transporter 2
CNT3	Concentrative Nucleoside Transporter 3
CNTs	Concentrative Nucleoside Transporters
CoMFA	Comparative Molecular Field Analysis
CoMSIA	Comparative Molecular Similarity Indices Analysis
DNA	Deoxyribonucleic Acid
ENT1	Equilibrative Nucleoside Transporter 1
ENT2	Equilibrative Nucleoside Transporter 2
ENT3	Equilibrative Nucleoside Transporter 3
ENT4	Equilibrative Nucleoside Transporter 4
ENTs	Equilibrative Nucleoside Transporters
hCNT1.	human Concentrative Nucleoside Transporter 1
hCNT2.	human Concentrative Nucleoside Transporter 2
hCNT3.	human Concentrative Nucleoside Transporter 3
hENT1.	human Equilibrative Nucleoside Transporter 1
hENT2.	human Equilibrative Nucleoside Transporter 2
hENT3.	human Equilibrative Nucleoside Transporter 3
hENT4.	human Equilibrative Nucleoside Transporter 4
LOO	Leave One Out
NBMPR	S^6 -(4-Nitrobenzyl)mercaptapurine Riboside
PK15NTD	Porcine Kidney 15 Nucleoside Transporter Deficient
PLS	Partial Least Squares
TM	Transmembrane
3D-QSAR	Three-Dimensional Quantitative Structure-Activity Relationship

Chapter 1: Human Nucleoside Transporters

1.1 Nucleoside Transporters

Naturally occurring human nucleosides are glycosylamines containing a purine or a pyrimidine nitrogenous base attached to a ribose or a deoxyribose ring. The major physiological nucleosides commonly found in living organisms include cytidine, deoxycytidine, thymidine, and uridine obtained from a pyrimidine nitrogenous base and adenosine, deoxyadenosine, guanosine, deoxyguanosine and inosine obtained from a purine nucleobase (Figure 1.1).

Nucleosides and nucleoside analogs can modulate a variety of biochemical and physiological processes. For example, adenosine is known to exert protective cardiovascular effects that make it clinically useful in the treatment of supraventricular tachycardia.¹ Extracellularly, adenosine acts as a signaling molecule affecting a variety of physiological processes such as neurotransmission,² platelet aggregation,³ vasodilation,⁴ and lipolysis.⁵ The 5'-triphosphate nucleotide of adenosine, ATP, is largely responsible for meeting the energy demand in human tissues and acts as the energy currency of the cell, providing energy for a number of different cellular functions.⁶ Nucleotides such as cAMP also play an important role in a myriad of signal transduction processes.⁷ Nucleotides containing ribose or deoxyribose serve as precursors for the biosynthesis of ribonucleic acid (RNA) or deoxyribonucleic acid (DNA), respectively.^{8,9} However, physiological nucleosides are hydrophilic in nature and hence require assistance to cross hydrophobic cell membranes; and this is provided by nucleoside transporters.

Nucleoside analogs commonly used as anticancer¹⁰ and antiviral agents,¹¹ also need to be transported into cells to exert their effects, and nucleoside transporters are responsible for their uptake. Representative examples of nucleoside analogs include the anti-viral agents AZT (1-[4-azido-5-(hydroxymethyl)oxolan-2-yl]-5-methyl-pyrimidine-2,4-dione) and Idoxuridine (1-[(2R,4S,5R)-4-hydroxy-5-(hydroxymethyl)oxolan-2-yl]-5-iodo-pyrimidin e-2,4-dione) and the anticancer agents Ara-C (4-amino-1-[(2R,3S,4R,5R)-3,4-dihydroxy-5-(hydroxymethyl)oxolan-2-yl]pyrimidin-2-one) and Cladribine ((2R,3S,5R)-5-(6-amino-2-chloro-purin-9-yl)-2-(hydroxymethyl)oxolan-3-ol) (Figure 1.2). Nucleoside transporters are thus integral membrane glycoproteins that modulate the cellular uptake of physiological nucleosides and their synthetic analogs.¹² Nucleoside transporter-mediated cellular uptake of nucleosides by mammalian cells was first recognized in Ehrlich cells in 1962.¹³ The different isoforms of nucleoside transporters were not recognized until the early 1980's.^{14,15} In humans, four equilibrative nucleoside transporters and six concentrative nucleoside transporters have been identified as shown in Figure 1.3. This classification has been discussed in detail later in this chapter. Figure 1.4 shows a model of nucleoside transport mediated by concentrative or equilibrative nucleoside transporter.

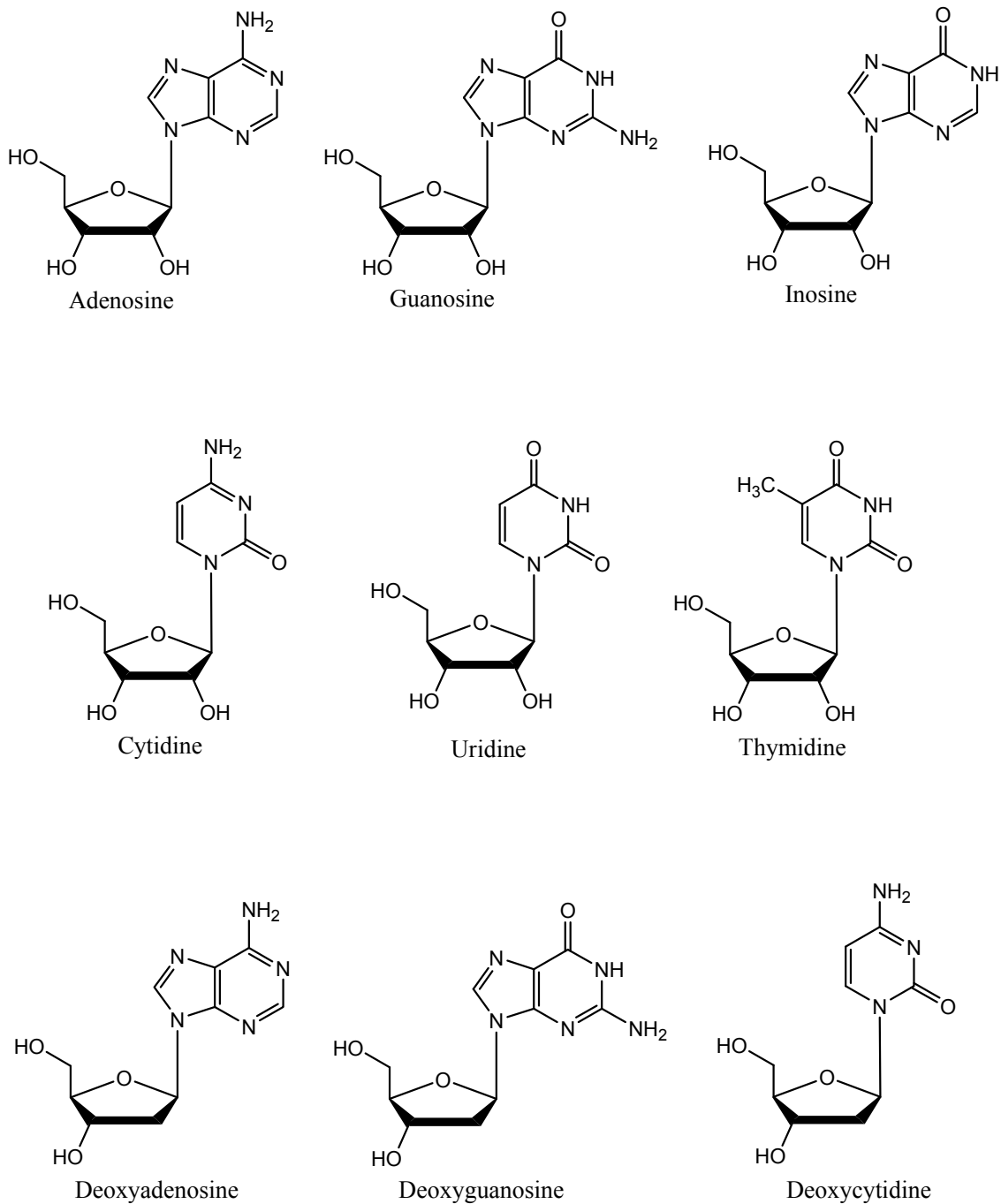
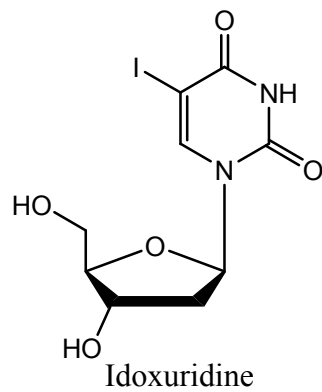
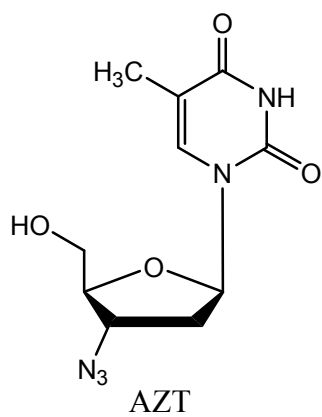
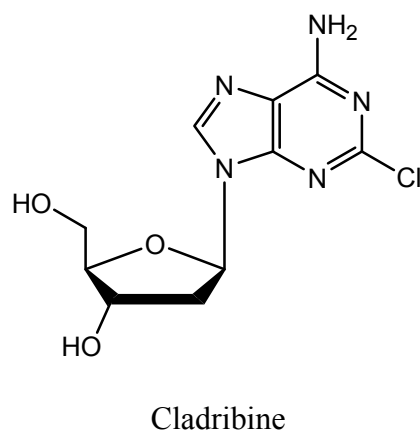
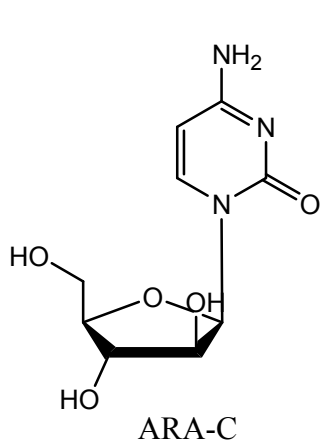


Figure 1.1: Structures of physiological nucleosides



Anti-viral nucleosides



Anticancer nucleosides

Figure 1.2: Structures of representative antiviral and anticancer nucleoside analogs

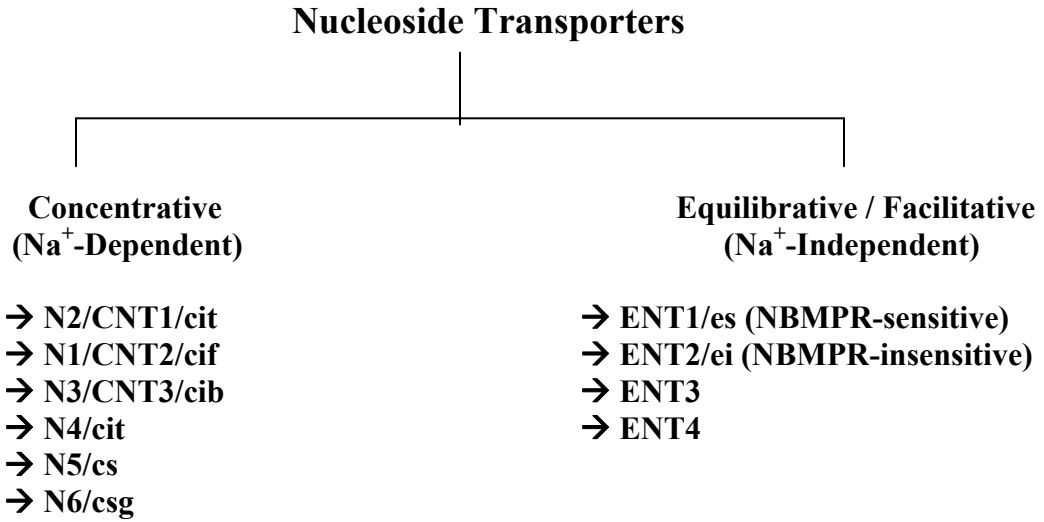


Figure 1.3: Classification of human nucleoside transporters

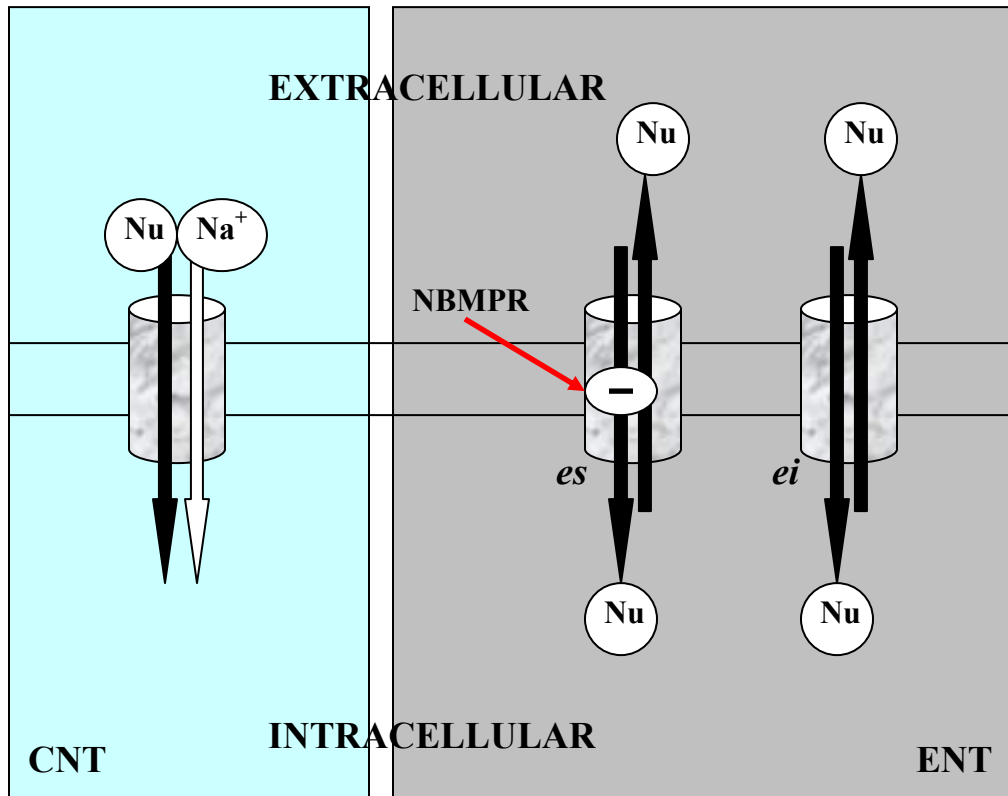


Figure 1.4: Nucleoside transport mediated by Na⁺-dependent (CNT) and Na⁺-independent (ENT) nucleoside transporters

Nu is designated for nucleoside and Na⁺ for sodium ion.

1.2 Concentrative Nucleoside Transporters

Concentrative nucleoside transporters (CNT) belong to the SLC28 family of proteins.¹⁶ Concentrative nucleoside transport processes are high-affinity, sodium-dependent systems that mediate active uphill transport of nucleosides.¹⁷⁻¹⁹ Six concentrative nucleoside transporters have been identified but only three isoforms, CNT1 (SLC28A1), CNT2 (SLC28A2, also termed SPNT) and CNT3 (SLC28A3) have been cloned. The three cloned CNTs have been predicted to be 13 TM domain proteins with the substrate translocation pore formed by TM domains 7 to 9 (Topographical model for CNT is shown in Figure 1.5).²⁰

The six concentrative nucleoside transporters are classified on the basis of their substrate specificities and inhibitor sensitivity as follows:

N1/CNT2/*cif* (insensitive to NBMPR and accepts formycin as a substrate)^{21, 22}
N2/CNT1/*cit* (insensitive to NBMPR and accepts thymidine as a substrate)²⁰
N3/CNT3/*cib* (insensitive to NBMPR and exhibits broad substrate specificity)²³
N4/*cit* (like CNT2 but also accepts guanosine as a permeant)
N5/*cs* (sensitive to NBMPR)
N6/*csg* (sensitive to NBMPR and accepts guanosine as a substrate)

1.2.1 Molecular Characteristics

CNT1 was the first member of the concentrative nucleoside transporter family to be cloned. The rat CNT1 subtype, rCNT1, was the first to be functionally expressed in *Xenopus laevis* oocytes following isolation from rat jejunum.²⁴ The human CNT1 transporter (hCNT1) was cloned from kidney tissue using hybridization and reverse transcriptase polymerase chain reaction (RT-PCR) techniques.²⁵ The hCNT1 nucleoside transporter encodes a protein containing 650 amino acid residues. The substrate and cation recognition sites are both located in the carboxy terminal half of the protein.²⁵ The rat CNT2 isoform, rCNT2, was first isolated from rat liver and functionally expressed in *Xenopus laevis* oocytes.²¹ The cloning of the human ortholog of CNT2, termed SPNT1 or hCNT2, was done using kidney cells.²² The hCNT2 protein has 658 amino acid residues and is predicted to consist of 13 TM domains. The hCNT2 protein is 72 % identical to the hCNT1 protein. Human CNT3, hCNT3, was first cloned from the human mammary gland and differentiated human myeloid HL-60 cells.²³ The mouse ortholog, mCNT3 has also been cloned and characterized from mouse liver cells. The human and the mouse CNT3 are 78 % identical at the protein level. The hCNT3 gene encodes a 691 amino acid protein. The amino acid sequence of CNT3 is 48 % identical to CNT1 and 47 % identical to CNT2. As in the case of the other members of the CNT family, hCNT3 and mCNT3 are predicted to have 13 TM domains.

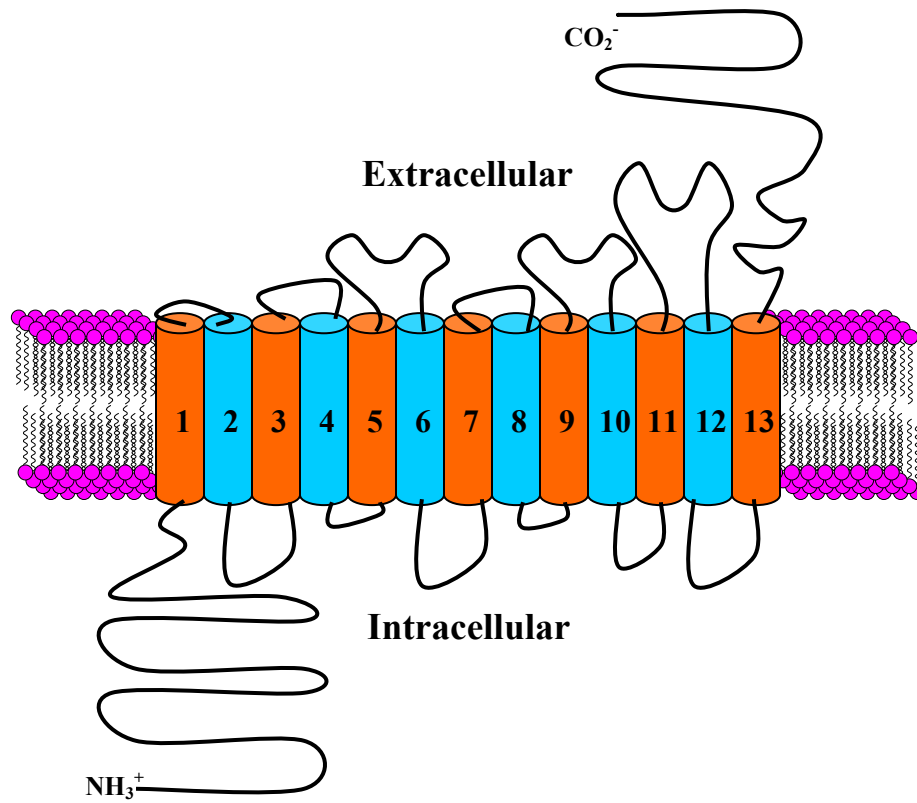


Figure 1.5: Topographical model of concentrative nucleoside transporter

1.2.2 Tissue Distribution

In humans, hCNT1 is predominantly expressed in kidney and liver epithelial tissues²⁶⁻²⁸, with much lower expression in other tissues.²⁹ Even within the kidney, there appears to be large inter-individual differences in hCNT1 mRNA expression. In the epithelia, CNT1 is localized to the apical membrane and works along with equilibrative nucleoside transporters, which are localized predominantly in the baso-lateral membranes of these tissues, to mediate trans-epithelial nucleoside flux.²⁷ Human CNT2 has a wider tissue distribution than hCNT1. It is widely distributed in the kidney, liver, heart, brain, placenta, pancreas, skeletal muscle, colon, rectum, duodenum, jejunum and ileum. hCNT2 is also expressed in normal human leukocytes and a number of neoplastic tissues and cancer cell lines. The distribution pattern of hCNT3 has been studied using an RNA array of 76 human tissues and cell lines.²³ High levels of human CNT3 mRNA transcripts are found in the pancreas, trachea, bone marrow and mammary glands, whereas lower levels are found in the intestine, lung, placenta, prostate, testis, kidney and liver.

1.2.3 Transport of Physiological Nucleosides and Nucleoside Analogs

The hCNT1 nucleoside transporter preferentially transports pyrimidine nucleosides such as thymidine, cytidine, and uridine with high affinity,^{30,31} with K_m values in the low micromolar range. Interestingly, hCNT1 does transport adenosine in a high affinity low capacity manner,^{32,33} but, it does not transport purine nucleosides such as, guanosine and inosine, or their analogs. The hCNT1 protein also does not interact with either nucleobases or nucleotides. Transport across hCNT1 has a sodium to nucleoside ratio of 1:1 (Na^+ /nucleoside).³² The hCNT1 nucleoside transporter also accepts a number of pyrimidine and adenosine analogs as substrates.³⁴ Gemcitabine, an anticancer drug, is a high affinity substrate of hCNT1 which exhibits an efficiency similar to that of hENT1.³⁵ 5'-Deoxy-5-fluorouridine, an intermediate metabolite of the anticancer drug capecitabine is also an hCNT1 substrate.³⁶

The transport of nucleosides across the hCNT2 transporter appears to be mechanistically similar to hCNT1 mediated transport. However, unlike hCNT1, hCNT2 is involved in the transport of purine nucleosides such as adenosine, guanosine and inosine.^{21,22} The only exception is that of the pyrimidine nucleoside, uridine, which is transported by this transporter.³⁷ The ratio of Na^+ to nucleoside transport via hCNT2 is 1:1.³⁸ A number of nucleoside analogs used in therapeutics are known to interact with the hCNT2 transporter. A number of fluorouridine analogs interact with hCNT2 and 5-FU is transported by hCNT2 with kinetics similar to that of uridine.³⁷ However, other drugs such as AZT, ddI (2',3'-dideoxyinosine), ddC (2',3'-dideoxycytidine), dda (2',3'-dideoxyadenine), Ara A (adenine arabinoside), FdU (5-fluorodeoxyuridine), and IdU (Idoxuridine) are not substrates of hCNT2.³⁷ Species specific differences in interaction with nucleoside analogs between rat and human CNT2 transporters have been observed. For instance, ddI which is not a permeant for the hCNT2, is transported by rCNT2 ($K_m=29.2 \mu\text{M}$).³⁷

Mechanistically, CNT3 differs from CNT1 and CNT2 in two aspects. CNT3 employs a 2:1 Na⁺ nucleoside coupling ratio in contrast to the 1:1 ratio employed by CNT1 and CNT2.^{23,39} Physiologically, this means that CNT3 can concentrate nucleosides 10 times more than CNT1 or CNT2. Hence, CNT3 mediated transport of nucleosides and nucleoside analogs are important even in tissues such as the kidney where lower levels of this transporter are expressed. CNT3 also exhibits a broad selectivity for nucleoside substrates by transporting both purine and pyrimidine nucleosides. Hence CNT3 interacts with a much broader range of therapeutic nucleoside analogs and is expected to play an important role in the absorption, distribution and elimination of nucleoside drugs. hCNT3 is known to transport both purine and pyrimidine nucleosides with high affinity, exhibiting K_m values ranging from 15 μ M for adenosine and cytidine to 53 μ M for inosine.^{23,40} The hCNT3 transporter efficiently transports pyrimidine nucleoside analogs such as 5-fluorouridine, 5-fluoro-2'-deoxyuridine and gemcitabine. It is also known to transport purine nucleoside analogs such as cladribine and fludarabine.²³ Low uptake of nucleoside analogs such as AZT, ddI, and ddC has also been observed.

Although the three concentrative nucleoside transporters, CNT1, CNT2 and CNT3 have been cloned and characterized, the proteins that demonstrate N4-*cit-like*, N5-*cs* or N6-*csg* activities have not yet been identified. The N4-*cit-like* system is selective for pyrimidine nucleosides but also accepts adenosine and guanosine, N5-*cs* system transports adenosine and its analogues, and N6-*csg* activity is guanosine-selective.^{29,31,41-44}

1.2.4 Molecular Determinants of Concentrative Nucleoside Transporter Substrates

Uridine and adenosine are two common permeants of the three major concentrative nucleoside transporters CNT1, CNT2, and CNT3. A number of uridine analogs have been studied to evaluate the transportability profile of these three concentrative nucleoside transporters.⁴⁵⁻⁴⁷

The C^{3'}-OH has been identified to be a critical functional group for high affinity binding of uridine analogs to the CNT1 transporter.⁴⁵ Any modification, such as addition of bulk at this position has resulted in decreased transportability of uridine analogs. The C⁵ and the N³ positions of uridine have also been identified as important regions for hCNT1-mediated transport. The C^{2'}-OH is relatively unimportant for hCNT1-uridine interactions as uridine analogs with modification at this position were both good inhibitors and good permeants. The C^{5'}-OH has also been identified for high affinity hCNT1-uridine interactions but was not essential for transportability.

The C^{3'}-OH and C^{5'}-OH groups have been identified as functional groups important for high-affinity interactions between hCNT2 and uridine analogs.^{46,47} Modifications to these two hydroxyls which may include substitution, removal of the hydroxyl groups or inversion of configuration at the C^{3'}-OH may yield molecules that are either poor permeants or no permeants at all. The N³-H atom is also critical for binding.

The $C^{2'}$ -OH and C^5 positions are also important structural requirements at the hCNT2 transporter. Removal of the $C^{2'}$ -OH group is tolerated but its inversion is not. Also, addition of bulk, such as azido or methyl groups, at the $C^{2'}$ position is not tolerated. Addition of halogens, methyl or ethyl groups to the C^5 position of uridine analogs also leads to loss of affinity for the hCNT2 transporter.

For the interaction of uridine analogs with hCNT3, the $C^{3'}$ -OH group is one of the most important functional groups. Removal or modification of this functional group leads to significant loss of affinity and transport of nucleoside analogs. The $C^{2'}$ -OH and C^5 -OH positions are relatively unimportant for transport and binding. The C^5 and N^3 modifications also cause no substantial changes in hCNT3 binding, identifying them as minor determinants for hCNT3 transportability.

1.2.5 Concentrative Nucleoside Transporter Inhibitors

Understanding the molecular requirements at the concentrative nucleoside transporters can guide the rational design of nucleoside transporter inhibitors to be developed for application in various disease conditions. To date, only a very limited number of potent inhibitors have been identified for these transporters. Knowledge regarding concentrative nucleoside transporter inhibitors is also limited, and potent inhibitors are actively being pursued. The few inhibitors known in the literature are:

- Phloridzin,⁴⁸
- 5'-position modified nucleoside derivatives of adenosine,⁴⁹
- Benzimidazole ribofuranosides,⁵⁰
- 8-position modified purine nucleoside derivatives⁵¹

1.2.5.1 Phloridzin

Phloridzin (**I**), a dihydrochalcone glucoside, is a mild to moderate inhibitor of the three major sodium-dependent NTs (Figure 1.6). It inhibits CNT1 with an IC_{50} of 250 μ M, CNT2 with an IC_{50} of 100 μ M and CNT3 with a K_i of 15 μ M at CNT3.⁴⁸ An addition, phloridzin has also been shown to inhibit concentrative nucleoside transport in rat intestinal epithelium with an IC_{50} of 700 μ M and in renal brush border membranes with an IC_{50} of 60 μ M.⁵²

1.2.5.2 5'-Position Modified Nucleoside Derivatives of Adenosine

The synthesis and CNT2 inhibitory activity of 5'-position modified nucleoside derivatives of adenosine was described in a 2004 Japanese patent⁴⁹ (Figure 1.6). Compound **II**, is representative of this class, and exhibited an IC_{50} of 3.1 μ M against the

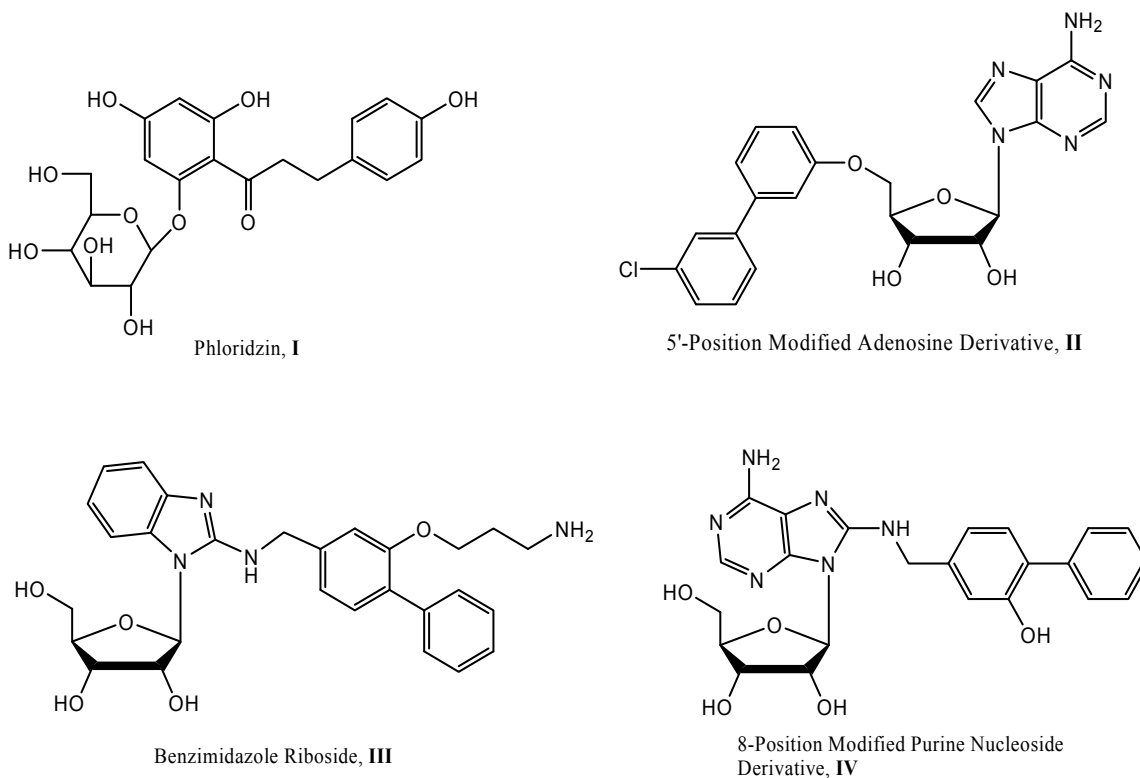


Figure 1.6: CNT inhibitors

CNT2 transporter. The compounds synthesized and tested in this patent have been claimed to be useful for the treatment of hyperuricemia, gout and hyperuric nephropathy.

1.2.5.3 Ribofuranoside Compounds with Benzimidazole Moiety

Another Japanese patent describes the synthesis and CNT2 mediated adenosine uptake inhibition assays for a class of modified nucleoside analogs⁵⁰ (Figure 1.6). These compounds have a ribofuranose moiety as the glycone unit but have a benzimidazole moiety as the aglycone unit. One of the potent compounds from this class is compound **III**. The IC_{50} of compound **III** was found to be 9 nM. These compounds have also been claimed to be useful for hyperuricemia, gout and hyperuric nephropathy.

1.2.5.4 8-Position Modified Purine Nucleoside Derivatives

A class of 8-position modified purine nucleoside derivatives has been described by Tatani *et al.* in a Japanese patent⁵¹ (Figure 1.6). As in the earlier case, these compounds have also been studied as inhibitors of CNT2. Compound **IV**, which is representative of this class of compounds, inhibited the uptake of [¹⁴C]-adenosine mediated by hCNT2 transporter expressed in COS-7 cells with an IC_{50} of 297 nM. These compounds have been claimed to be useful for the treatment or prevention of diseases

attributable to abnormality in plasma uric acid, in particular gout, hyperuricemia, urinary stones or acute hyperuric neuropathy.

1.3 Equilibrative Nucleoside Transporters

The equilibrative nucleoside transporters mediate low affinity, bi-directional facilitated diffusion transport processes and are widely distributed in the body. They belong to the SLC29 family of proteins.⁵³ The general topology of human equilibrative nucleoside transporters (hENTs) consists of 11 transmembrane (TM) domains with a long extracellular loop between transmembrane domains 1 and 2 and a much longer cytoplasmic loop between transmembrane domains 6 and 7.⁵⁴ (Figure 1.7) Of the four identified ENTs, ENT1 and ENT2, have been well characterized, whereas the other two, ENT3 and ENT4 were identified recently and isolated as a result of the completion of the human genome project. Human ENT1 was formerly referred to as the *es* (equilibrative inhibitor-sensitive) nucleoside transporter and ENT2 was referred to as the *ei* (equilibrative inhibitor-insensitive) nucleoside transporter earlier based on their sensitivity to inhibition by *S*⁶-(4-nitrobenzyl) mercaptopurine riboside (NBMPR) (V) and its congeners.⁵⁵ Some of the other potent inhibitors of ENTs include coronary vasodilator drugs such as dipyridamole (VI), draflazine (VII), and dilazep (VIII) (Figure 1.8).

1.3.1 Molecular Characteristics

Human ENT1 (hENT1) is a 456-residue glycoprotein with an intracellular N-terminus and a short extracellular C-terminus.⁵⁷ hENT1 is highly sensitive to inhibition by NBMPR at the nanomolar concentration ($K_i = 0.1-1.0$ nM). It is glycosylated at Asn-48 in the extracellular loop between TMs 1 and 2,⁵⁸ and although glycosylation is not required for transport of nucleosides by hENT1, it may have an effect on the binding affinity of transport inhibitors such as NBMPR.⁵⁸ The hENT1 protein is 78 % identical in sequence to its 457-residue rat homolog (rENT1)⁵⁹ and 79 % identical to the 460-residue mouse homolog (mENT1.1).^{60, 61} Relative to hENT1, rENT1 has been shown to be rather resistant to inhibition by dipyridamole, dilazep and draflazine. Dipyridamole inhibited hENT1 with an IC_{50} value of 190 nM whereas it inhibited rENT1 with an IC_{50} value ≥ 10 μ M when competitive inhibition experiments were conducted using 10 μ M uridine.⁵⁴

The amino terminal half of hENT1 has been identified as the major site of interaction for vasodilator drugs.⁵⁴ Studies have been carried out to identify the amino terminal half of rENT1 as also involved in the transport inhibitory activity of NBMPR. Replacing the amino terminal half of rENT1 with that of the NBMPR insensitive transporter rENT2 rendered rENT1 insensitive to NBMPR.⁶² Transmembrane domains 3-6 have been identified as the NBMPR binding domains within the ENT1 transporter.⁶²

The human ENT2 (hENT2) transporter was cloned from HeLa cells⁶³ and human placenta.⁶⁴ Human ENT2 function is weakly inhibited by NBMPR.⁶⁵ hENT2 is a 456-residue protein that is 46 % identical in amino acid sequence to hENT1. As in the case of

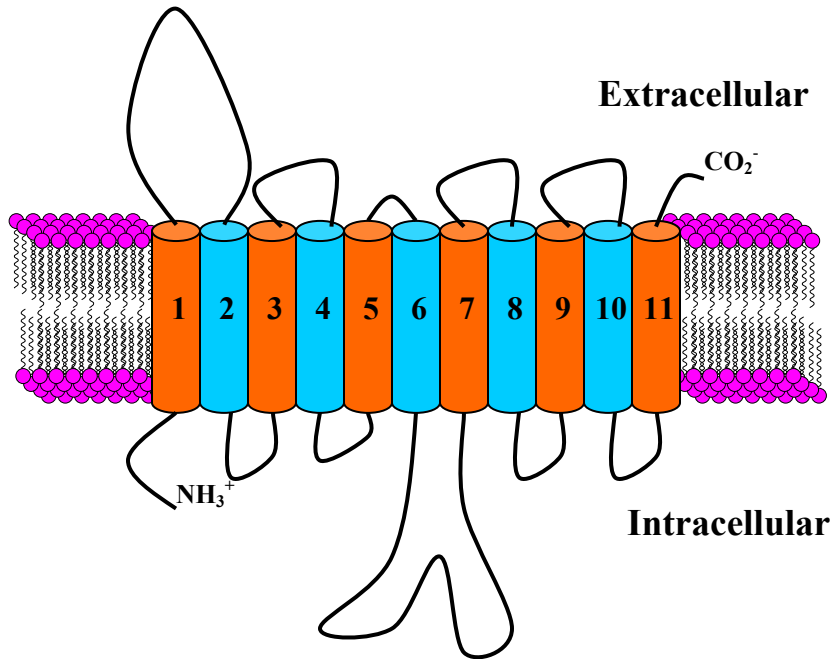
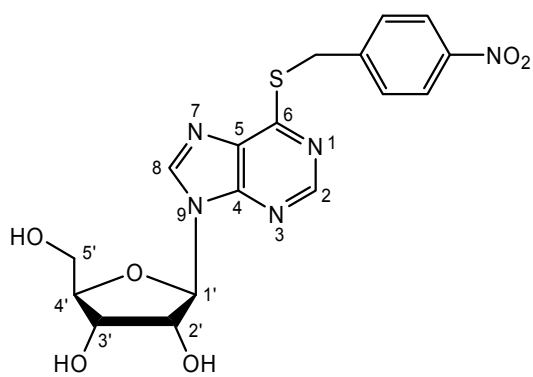
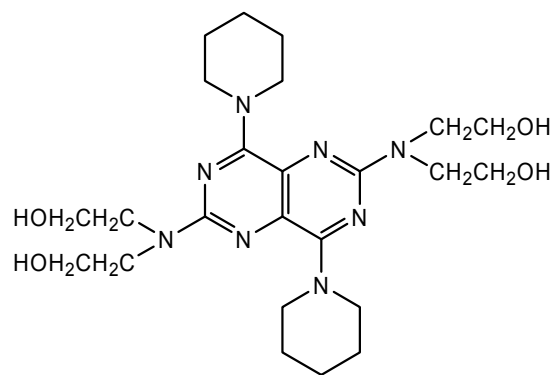


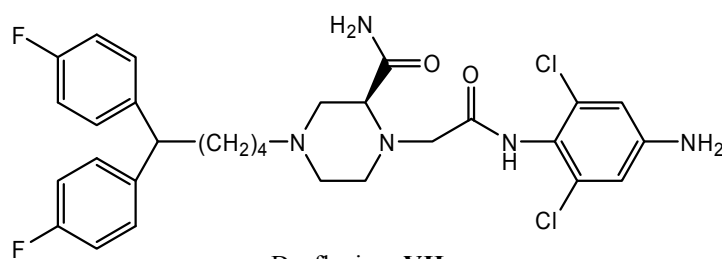
Figure 1.7: Topographical model of an equilibrative nucleoside transporter



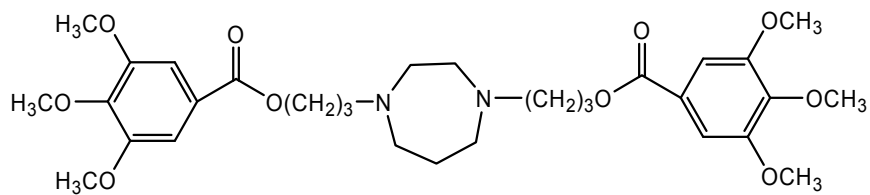
NBMPR, **V**



Dipyridamole, **VI**



Draflazine, **VII**



Dilazep, **VIII**

Figure 1.8: Potent ENT inhibitors

hENT1, it is also predicted to be an 11 transmembrane domain protein. The most homologous regions between hENT1 and hENT2 are the transmembrane segments, whereas the hydrophilic termini and loops are the least homologous. The hENT2 transporter protein is glycosylated at two sites- Asn48 and Asn57.⁶⁶ Glycosylation is required for the efficient targeting of the hENT2 protein to the plasma membrane. However, glycosylation is not known to change the function of hENT2. The rat and mouse orthologs of the ENT2 protein, rENT2 and mENT2, respectively, have also been cloned.^{59, 61}

1.3.2 Tissue Distribution

The hENT1 protein is ubiquitously distributed in a variety of human tissues although its abundance in tissues varies. High expression levels of the hENT1 protein or mRNA have been observed in a number of different tissues such as erythrocytes, placenta, brain, heart, liver, lung and colon.^{67, 68} The co-localization of hENT1 and A₁ receptors suggests an important role of hENT1 in the neuromodulatory actions of adenosine in the human brain⁶⁹. Similarly, abundant expression of the rENT1 protein in cardiac atrial and ventricular cells and the sinoatrial node suggests an important role for the ENT1 transporter in regulating the local concentrations of adenosine in the heart.⁶⁸ hENT2 mRNA is expressed in a wide range of tissues including brain, heart, placenta, thymus, pancreas, prostate and kidney, but is particularly abundant in skeletal muscle.^{63, 67} hENT2 transporter protein is also found in certain tumor tissues obtained from kidney, breast, prostate, colon and stomach.⁶⁷

1.3.3 Transport of Physiologic Nucleosides and Nucleoside Analogs

The hENT1 transporter protein stably expressed in a nucleoside transporter-deficient cell line, PK 15, exhibits a broad substrate specificity for both purine and pyrimidine nucleosides. The K_m values for different nucleosides range from 50 μ M for adenosine to 680 μ M for cytidine.⁷⁰ However, hENT1 is unable to transport nucleobases. The hENT1 protein also interacts with a number of nucleoside analogs used in the treatment of cancer and viral infections. The poor transport of a number of 3'- deoxy nucleosides, such as 2',3'-dideoxycytidine (ddC), 2',3'-dideoxyinosine (ddI) and 3'-azido-3'-deoxythymidine (AZT) routinely used as antiviral agents, indicates that the presence of a 3'-hydroxyl group is important for the recognition of nucleosides as substrates by the hENT1 protein.⁷¹

Similar to the hENT1 nucleoside transporter, hENT2 also transports a broad range of purine and pyrimidine nucleosides. However the apparent affinity of nucleosides towards hENT2 is much lower compared to hENT1, with the only exception being that of inosine.^{63, 64, 70} The hENT2 protein exhibits 7.7 and 19.3 fold lower affinities for guanosine and cytidine, but a 4-fold higher affinity for inosine. hENT2 is also known to transport a number of purine and pyrimidine nucleobases such as adenine, guanine, thymine, uracil and hypoxanthine.⁷² The nucleobases exhibit a lower apparent affinity but

a higher turnover number for transport compared to the corresponding nucleosides.⁷² Thus, at physiological concentrations the efficiencies of nucleoside and nucleobase transport by the ENT2 transporter are similar. In contrast to hENT1, hENT2 plays an important role in the cellular uptake of clinical antiviral agents such as ddC, ddI and AZT.⁷¹

As the hENT2 protein transports dideoxynucleosides and nucleobases that do not bear a ribose moiety, it appears that ENT2 accepts more substrates than ENT1. A number of uridine and cytidine analogs have also been demonstrated to interact with hENT2 when studied as inhibitors of [³H]-uridine uptake in yeast producing the recombinant protein.⁷³ Cytidine exhibits an EC₅₀ of 1.98 mM. Analogs of cytidine that were studied include 2'-deoxycytidine (EC₅₀ = 3.06 mM), 3'-deoxycytidine (EC₅₀ = 2.49 mM), 2', 3'-dideoxycytidine (EC₅₀ = 1.10 mM) and araC (EC₅₀ = 1.20 mM). Similarly, a number of uridine analogs such as 5-fluorouridine, 5-iodouridine, 2'-deoxyuridine, 5-fluoro-2'-deoxyuridine, and 5-bromo-2'-deoxyuridine displayed EC₅₀ values in the 0.21 – 0.47 mM range.⁷³

Human ENT3 is a 475-residue protein displaying 73 % identity to the mouse homologue (mENT3).^{1, 74-76} ENT3 has a characteristic, long (51 aa) hydrophilic N-terminal region preceding the first transmembrane (TM1) domain. The N-terminal region of ENT3 consists of two dileucine motifs characteristic of endosomal and lysosomal targeting motifs. This architectural design distinguishes the ENT3 protein from other members of the equilibrative transporter family.

Indeed, it was demonstrated that hENT3 protein is predominantly localized intracellularly and that mutation of the dileucine motif to alanine triggers the relocation of ENT3 protein to the cell surface.^{74, 75} In comparison to ENT1, the ENT3 transporter is much less susceptible to inhibition by NBMPR and coronary vasodilatory drugs like dipyridamole and dilazep. Human ENT3 demonstrates a broad selectivity for nucleosides, but does not transport hypoxanthine. hENT3 facilitates the transport of several adenosine analogues like CdA and cordycepin (3'-deoxyadenosine). The antiviral purine and pyrimidine nucleoside analogues ddI, ddC and in particular AZT are efficiently transported by this protein.^{74, 75}

Human ENT4 is a 530-residue protein displaying 86 % identity to its 528-residue mouse homologue.⁷⁴ The substrate specificity of hENT4 has not been determined in detail, but among ENT proteins, hENT4 has the lowest affinity for adenosine.⁷⁷ ENT4, is abundant in the heart, in particular in the plasma membranes of ventricular myocytes and vascular endothelial cells and is virtually absent from the sinoatrial and atrioventricular nodes. Originally described as a monoamine/organic cation transporter, it was found that both human and mouse ENT4 exhibited a novel, pH-dependent adenosine transport activity optimal at acidic pH (apparent *K_m* values 0.78 and 0.13 mmol/L, respectively, at pH 5.5) and absent at pH 7.4. In contrast, serotonin transport by ENT4 was relatively insensitive to pH. ENT4-mediated nucleoside transport was adenosine selective, sodium independent and only weakly inhibited by the classical inhibitors of equilibrative nucleoside transport, dipyridamole, dilazep, and nitrobenzylthioinosine.

It is predicted that in addition to playing roles in cardiac serotonin transport, ENT4 contributes to the regulation of extracellular adenosine concentrations, in particular under the acidotic conditions associated with ischemia.⁷⁸

1.3.4 Equilibrative Nucleoside Transporter Inhibitors

There are different classes of compounds significantly active as inhibitors against ENTs. Some of these classes are as follow: NBMPR (V) and derivatives⁷⁹⁻⁸⁵, C⁸-alkylamine substituted purines⁸⁵, pyrimidopyrimidines and pteridines^{86, 87} (e.g. dipyridamole, VI); alkyl, cycloalkyldiamine and piperazine compounds^{88, 89} (e.g. draflazine, VII and dilazep, VIII), Protein kinase inhibitors^{24, 90}, cannabinoids⁹¹ (e.g. THC); adenosine receptor ligands⁹² (e.g. propentofylline); dihydropyridine calcium channel blockers⁹³⁻⁹⁵ (e.g. nimodipine), verapamils⁹², benzodiazepines^{96, 97} (e.g. diazepam), epipodophyllotoxins⁹⁸⁻¹⁰⁰ (e.g. etoposide), thiazolidinediones¹⁰¹ (e.g. troglitazone), xanthine oxidase inhibitors¹⁰², organomercurials^{103, 104} (e.g. *p*-chloromercuriphenyl sulphonate) and some belonging to miscellaneous category. Figure 1.8 lists some of the above mentioned compounds.

1.4 Applications of Nucleoside Transporter Inhibitors

Nucleoside transporters have potential to serve as pharmacological targets in a variety of important disease areas. Nucleoside transport inhibitors can be used in 1) antimetabolite potentiation, 2) adenosine potentiation, and 3) host tissue protection. Each of the three areas of application has been outlined in the following sections.

1.4.1 Antimetabolite Potentiation

1.4.1.1 Cancer Chemotherapy

In the early 1980s it was observed that the cytotoxic effect of *de novo* pathway inhibitors such as 5-fluorouracil and methotrexate on tumor cells were overcome by nucleotide biosynthesis via the salvage pathways.¹⁰⁵ Hence it was thought that combining *de novo* pathway inhibitors with salvage pathway inhibitors can increase effective cell kill. Weber and coworkers first explored this biochemical modulation of antimetabolite chemotherapy by combining them with nucleoside transport inhibitors.^{106, 107} Since then, the therapeutic promise of combining nucleoside transport inhibitors with antimetabolite anticancer agents such as 5-fluorouracil and methotrexate has been demonstrated in several experimental studies. The anticancer activity of lipophilic analogs of cytotoxic nucleosides such as N⁴-hexadecyl-1-β-D-arabinofuranosylcytosine (NHAC) which enter cancer cells by passive diffusion can also be potentiated by nucleoside transport inhibitors. Nucleoside transport inhibitors in this case will suppress competition from

extracellular physiological nucleosides and thus enhance the antitumor activity of NHAC.¹⁰⁸

1.4.1.2 Viral Infections

Nucleobase or nucleoside antimetabolites are commonly used in the treatment of viral infections. In the treatment of HIV infections, AZT and related dideoxynucleoside reverse transcriptase inhibitors were the first agents with clinical utility. Majority of dideoxynucleosides including AZT enter the cell mainly by passive diffusion whereas nucleoside transporters are responsible for the entry of endogenous nucleoside competitors such as thymidine. Hence nucleoside transport inhibitors can shut out the competition from endogenous nucleosides. Studies in this direction have successfully demonstrated the advantages of such a combination therapy.¹⁰⁹

1.4.2 Adenosine Potentiation

1.4.2.1 Cardioprotection

Endogenous adenosine protects the heart against ischemic and reperfusion tissue injury by 1) vasodilatation via adenosine A₂- receptors, causing increased coronary blood flow to increase local oxygen supply, 2) inhibition of catecholamine release and action, thereby preventing cardiac overstimulation, 3) inhibition of neutrophil adherence and release of tissue damaging reactive oxygen metabolites through A_{2a} receptor activation action,¹¹⁰ and 4) preconditioning through A₁ and A₃ receptors.^{111, 112} During cardiac ischemia and reperfusion, the action of adenosine produced locally to protect against tissue injury is short-lived mainly due to uptake into endothelial cells and inactivation by adenosine deaminase. Interaction of adenosine with the A₂ receptor is also known to stimulate its own transport.¹¹³ Hence, nucleoside transport inhibitors can be employed to prevent adenosine uptake by the endothelial cells leading to prolonged local effect of adenosine. The use of nucleoside transport inhibitors in cardioprotection is attractive because the release of adenosine in ischemia is transient and localized in the tissue under ischemic stress. As a result activation of adenosine receptors all over the body of the patient would not occur in this case leading to decreased side effects as compared to adenosine receptor agonists.

1.4.2.2 Ischemic Preconditioning and Heart Transplantation

In preconditioning, the patient is made more resistant to future ischemic injury and adenosine transport inhibitors have been shown to have potential utility in this condition.^{114, 115} During heart transplantation nucleoside transporter inhibitors can potentially improve the long term *ex vivo* storage of hearts.¹¹⁶ Nucleoside transport inhibitors have also been found to be useful in intra-operative myocardial protection.¹¹⁷

1.4.2.3 Neuroprotection and Stroke

The neuroprotective action of extracellular adenosine released during cerebral ischemia is terminated primarily due to its uptake into the surrounding cells via nucleoside transporters. These protective effects of extracellular adenosine can be prolonged by the use of nucleoside transport inhibitors.¹¹⁸ The presence of multiple subtypes of nucleoside transporters in the central nervous system offers the potential for the development of drugs with selectivity for certain areas of the brain. Propentofylline, a xanthine derivative with moderate nucleoside transporter inhibitory activity and good CNS penetration has been shown to prevent ischemia-induced brain damage in Mongolian gerbils and in rats.¹¹⁹ In rat hippocampal slices, propentofylline, NBMPR and other nucleoside transport inhibitors have been shown to increase extracellular adenosine levels. The reduction in neurotransmitter release following adenosine potentiation by nucleoside transport inhibitors has been suggested as a therapeutic strategy in stroke.¹²⁰

1.4.2.4 Anti-inflammatory Effects

During inflammation, adenosine is released and it acts as an endogenous anti-inflammatory agent.¹²¹ Adenosine A_{2a} receptors have an important role in the anti-inflammatory effects of adenosine.¹²² Adenosine broadly inhibits neutrophil functions¹²³ (e.g., oxygen radical production, adhesion to vascular endothelium, injury to endothelial cells, phagocytosis and arachidonic acid release), macrophage functions¹²⁴ (e.g., production of pro-inflammatory cytokines), and endothelial cell activation¹²⁵ (e.g., cytokine release and adhesion molecule expression) leading to its anti-inflammatory effects. However, these effects of adenosine are insufficient because of the rapid uptake and metabolism of adenosine by adjacent cells. Thus nucleoside transport inhibitors can be used to prevent this adenosine reuptake into the surrounding cells and thus bring about adenosine potentiation. The nucleoside transport inhibitor, dipyridamole has been reported to inhibit inflammatory events both *in vitro* and *in vivo*¹²⁶ in models of inflammatory diseases such as glomerulonephritis.¹²⁷

1.4.3 Host Tissue Protection

1.4.3.1 Protection against Nucleoside Anticancer Drugs Toxicity

One of the major drawbacks of current cancer chemotherapy is the immense suffering caused in patients as a result of host tissue toxicity. This not only prevents dose escalation but in many patients also leads to discontinuation of chemotherapy. The combination of nucleoside anticancer agents with nucleoside transport inhibitors has been shown to protect against host tissue toxicity.¹²⁸⁻¹³⁰

1.4.3.2 Antiprotozoal Chemotherapy

Nucleoside transporter inhibitors have been used for host tissue protection during experimental treatment of schistosomiasis,¹³¹⁻¹³³ trypanosomiasis,¹³⁴ and leishmaniasis¹³⁵. However, certain parasites are known to induce the expression of new inhibitor resistant transporters in the infected mammalian host cells which has been best demonstrated in mammalian erythrocytes infected with malarial parasites.¹³⁶ This altered purine nucleoside transport in plasmodium infected erythrocytes has been proposed as a target for developing novel antimalarial therapies. Selectivity can be achieved by combining antimalarial nucleosides with nucleoside transport inhibitors which will protect normal cells but not plasmodium infected cells against the cytotoxic nucleoside analogs.¹³⁷ *Toxoplasma gondii* is another opportunistic obligate intracellular parasite responsible for causing toxoplasmic endocephalitis in AIDS patients. This parasite is dependent entirely on purine and purine nucleoside salvage for its metabolic and growth requirements.^{138, 139} The parasite expresses a single dipyridamole sensitive nucleoside transporter which is not inhibited by NBMPR even at concentrations as high as 15 μ M.¹⁴⁰ Hence there is a possibility of combining adenosine analogs with NBMPR for treatment of *Toxoplasma* infections in AIDS patients.

Chapter 2: Research Objectives

The cellular uptake and efflux of nucleosides are mediated by specialized transmembrane proteins known as NTs. As mentioned in Chapter 1, NTs can be classified into two families, namely, bidirectional sodium-independent equilibrative nucleoside transporters (ENTs) and unidirectional sodium-dependent concentrative nucleoside transporters (CNTs). Different isoforms of each of these classes have been identified, and some have been cloned and extensively characterized. The substances that inhibit nucleoside transporters have potential therapeutic applications in the treatment of various diseases such as cancer, HIV infection, cardiac ischemia, stroke and inflammation. However, the available NT inhibitors are largely unsuitable for clinical development and thus the need for novel inhibitors. ENT 2, 3 and 4 and most CNT family members lack potent inhibitors, which limits their biological characterization and therapeutic targeting. This research was thus conducted to identify novel selective NT inhibitors as biological probes and potential therapeutic lead compounds.

In the absence of a three dimensional structure of any nucleoside transporter or its co-crystal with inhibitors, drug discovery for this class of targets depends on ligand-based approaches. The main reason for studying flavones and related compounds is their structural resemblance to phloridzin, a naturally occurring dihydrochalcone glucoside that has demonstrated low to moderate inhibitory activity against the three major concentrative nucleoside transporters, CNT1, CNT2 and CNT3 (Figure 2.1). Flavones were also suggested as potential nucleoside transporter inhibitors in a nucleoside transporter inhibition pharmacophore analysis study carried out by our laboratory and collaborators.¹⁴¹ In that study, fifteen known inhibitors of equilibrative nucleoside transporters comprising derivatives of NBMPR, pyrimidopyrimidines, pteridines and flazines were used to derive a common feature hypothesis. The generated pharmacophore was used for database searching, which returned hits that included flavone and isoflavone structures suggesting that flavones can be analyzed for nucleoside transporter inhibition. Thus, it was of interest to investigate the inhibitory activity of flavonoids against both the CNT and ENT classes of NTs. Hence, flavones and analogs including coumarins, 4H-benzopyrans and a quinoxaline derivative were tested against hCNT1, hCNT2, hCNT3, hENT1 and hENT2 transport function. The results obtained were used to gain insights into the structure-activity relationships of flavonoids regarding these five nucleoside transporters.

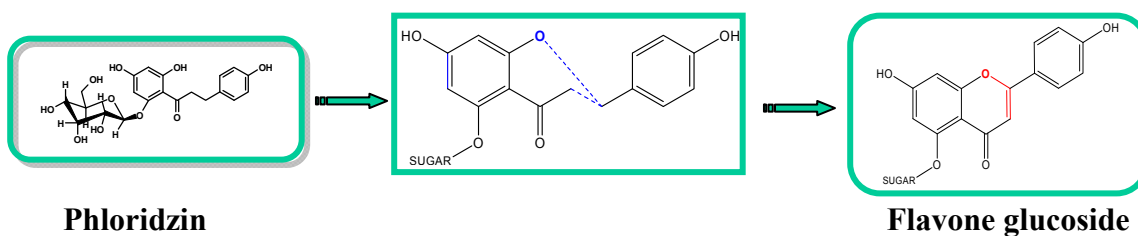


Figure 2.1: Structural resemblance of phloridzin to flavone

The specific aims of this research were: 1) to conduct biological evaluation of a series of flavones and related compounds as concentrative and equilibrative nucleoside transporter inhibitors, 2) to use the biological data for structure-activity relationship information and to build 3D-QSAR models which can be further used for *in silico* drug design of flavonoid-based nucleoside transporter inhibitors. The cumulative data obtained in this manner using flavonoids and related compounds, can be further used for hit identification and lead optimization to obtain new potent and selective nucleoside transporter inhibitors.

Chapter 3: Biological Evaluation and 3D-QSAR Studies of Flavone Analogs for Human Concentrative Nucleoside Transporter Inhibition

3.1 Introduction

In this chapter, the findings on a series of flavone analogues as CNT inhibitors are presented. The compounds were tested against the three cloned human CNT transporters, hCNT1, hCNT2 and hCNT3. The biological activity data were used to derive CoMFA and CoMSIA 3D-QSAR models, which were further used for insights on the influence of physicochemical descriptors and *in silico* activity prediction.

3.2 Uridine Uptake Assay

A uridine uptake assay was used to measure the function of transporters, entails the measurement of the uptake of radiolabeled uridine and inhibition by test compounds. The cell line that was used for the study is the nucleoside transporter deficient PK15NTD cell line stably transfected with hCNT1, hCNT2 or hCNT3 cDNA. The amount of radiolabeled uridine present intracellularly following a two-minute exposure to CNTs, is determined in the absence and presence of varying concentrations of test compounds. After the uptake, the radiolabeled uridine present extracellularly is washed off and then the cells are lysed with an appropriate detergent and the radioactivity is measured. The amount taken up by the cells is highest in the absence of an inhibitor and decreases in the presence of an inhibitor. Thus, by appropriately varying the inhibitor concentrations suitable dose-response curves can be developed and IC_{50} (concentration that causes 50 % inhibition) values can be determined. Using the above assay procedure, compounds used in the study were first screened at a concentration of 10 μ M. Only those compounds showing more than 50 % inhibition at 10 μ M were further analyzed for IC_{50} determination. The IC_{50} values thus obtained were further converted to the corresponding K_i values using the Cheng-Prusoff equation.¹⁴² The K_i values were used to compare the abilities of compounds to inhibit individual CNT transporters, and their affinity as well. Details of the [³H]-uridine uptake assay are provided in the experimental section of this chapter. Phloridzin was used as a standard to compare the inhibitory activities of the rest of the compounds.

3.3 IC_{50} Curves of Active Flavones

The screening (Figure 3.1) and IC_{50} value determination of compounds as hCNT1 and hCNT2 inhibitors was carried out by Dr. Chunmei Wang, who is a postdoctoral fellow in our laboratory. The structures of all ninety five compounds and their IC_{50} values against hCNT1, hCNT2 and hCNT3 are presented in Table 3.1. Figure 3.2 shows the IC_{50} curves for compounds active against hCNT3.

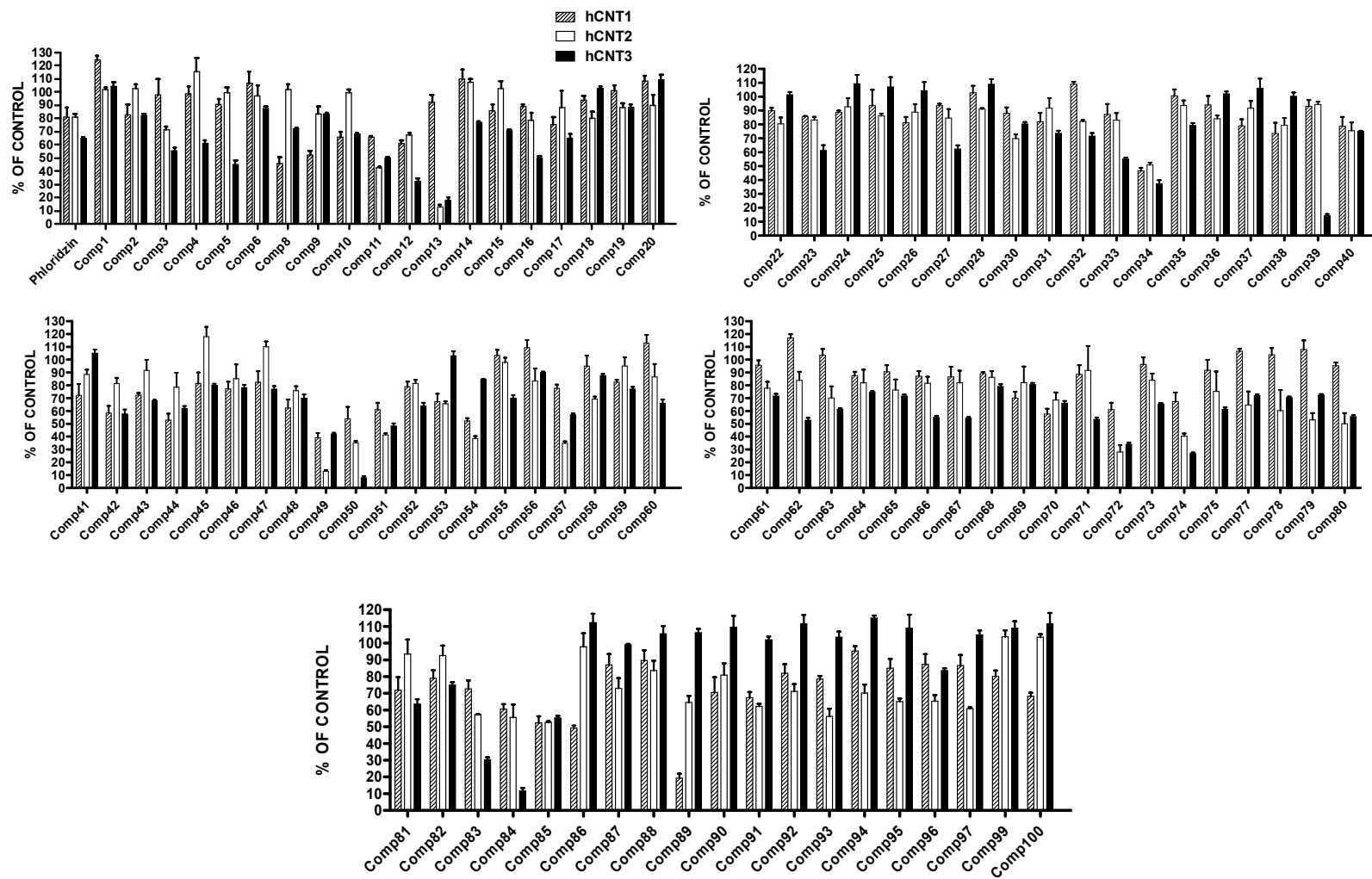
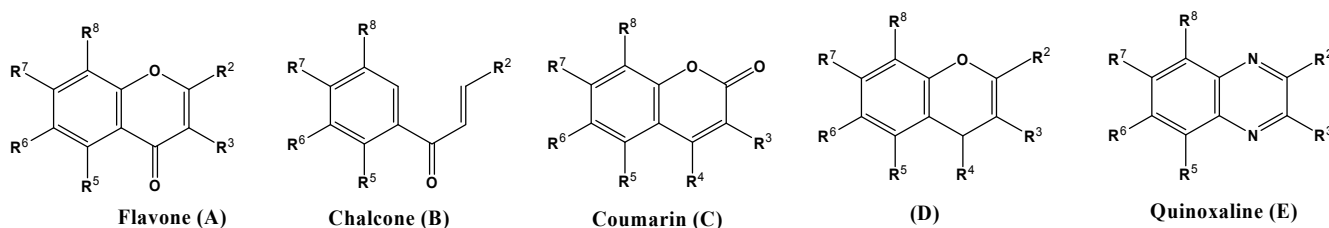


Figure 3.1: Comparison graph of % of inhibition at 10 μM concentration by compounds against hCNT1, hCNT2 and hCNT3

Table 3.1: Compounds evaluated for CNT inhibition with IC₅₀ values



Compound	Type	R ²	R ³	R ⁴	R ⁵	R ⁶	R ⁷	R ⁸	hCNT1 IC ₅₀ (μM)	hCNT2 IC ₅₀ (μM)	hCNT3 IC ₅₀ (μM)
Phloridzin	-	-	-	-	-	-	-	-	247.30 ± 2.10	121.00 ± 1.70	25.13 ± 3.75
1	A	4-bromophenyl	H	C=O	H	Cl	CH ₃	H	-	-	-
2	A	4-hydroxyphenyl	OH	C=O	H	H	H	H	-	-	55.68 ± 4.50
3	A	3,4-dihydroxyphenyl	H	C=O	H	H	OH	H	-	28.84 ± 1.40	11.29 ± 3.79
4	A	Phenyl	OH	C=O	OH	H	H	H	-	-	34.36 ± 1.00
5	A	Phenyl	OH	C=O	H	OH	H	H	-	-	11.00 ± 3.57
6	A	Phenyl	OH	C=O	H	H	OH	H	-	-	104.07 ± 26.81
8	A	4-hydroxyphenyl	H	C=O	H	OH	H	H	-	-	22.26 ± 5.98
9	A	Phenyl	H	C=O	H	OH	OH	H	30.67 ± 1.40	40.43 ± 1.50	71.74 ± 5.83
10	A	2-hydroxyphenyl	H	C=O	H	H	OH	H	-	-	18.07 ± 4.02
11	A	3-hydroxyphenyl	H	C=O	H	H	OH	H	41.69 ± 1.50	13.80 ± 1.40	8.86 ± 3.78
12	A	4-hydroxyphenyl	H	C=O	H	H	OH	H	35.75 ± 1.50	24.40 ± 1.30	4.74 ± 1.13
13	A	Phenyl	H	C=O	H	H	OH	OH	40.43 ± 1.50	3.38 ± 1.10	1.62 ± 0.81
14	A	4-hydroxyphenyl	H	C=O	OH	H	OCH ₃	H	-	-	74.00 ± 6.85
15	A	Phenyl	H	C=O	OH	OH	OCH ₃	H	-	100.00 ± 1.70	26.26 ± 3.60
16	A	3,4,5-trimethoxyphenyl	OH	C=O	H	H	OH	H	-	43.10 ± 1.20	34.34 ± 2.79
17	A	3-hydroxy-4-methoxyphenyl	H	C=O	OH	OCH ₃	OCH ₃	H	-	-	17.15 ± 1.61
18	A	2,3-dimethoxyphenyl	H	C=O	H	H	H	H	-	-	-
19	A	4-methoxyphenyl	OCH ₃	C=O	H	H	H	H	-	-	64.60 ± 2.61
20	A	3,4-dimethoxyphenyl	H	C=O	H	H	H	H	-	-	-
22	A	Phenyl	H	C=O	H	OCH ₃	OCH ₃	H	-	-	176.73 ± 20.97
23	A	3,4-dimethoxyphenyl	OH	C=O	H	H	H	H	-	-	18.07 ± 4.02

Table 3.1: (continued)

Compound	Type	R ²	R ³	R ⁴	R ⁵	R ⁶	R ⁷	R ⁸	hCNT1 IC ₅₀ (μM)	hCNT2 IC ₅₀ (μM)	hCNT3 IC ₅₀ (μM)
24	A	2,3-dimethoxyphenyl	OH	C=O	H	H	H	H	-	-	-
25	A	2,4-dimethoxyphenyl		C=O	H	H	H	H	-	-	-
26	A	2-methoxyphenyl	OH	C=O	H	OCH ₃	H	H	-	-	-
27	A	3-methoxyphenyl	OH	C=O	H	OCH ₃	H	H	-	-	22.92 ± 7.02
28	A	4-methoxyphenyl	OH	C=O	H	OCH ₃	H	H	-	-	-
30	A	3-methoxyphenyl	OH	C=O	H	H	OCH ₃	H	-	-	56.25 ± 8.47
31	A	2,4-dimethoxyphenyl	OH	C=O	H	CH ₃	H	H	-	-	28.15 ± 5.75
32	A	3,4-dimethoxyphenyl	OH	C=O	H	CH ₃	H	H	-	-	32.08 ± 4.49
33	A	3,4-dimethoxyphenyl	H	C=O	OH	OCH ₃	OCH ₃	H	-	-	16.16 ± 3.06
34	A	3,4-dihydroxyphenyl	OH	C=O	H	H	OH	H	26.30 ± 1.20	8.80 ± 1.20	4.25 ± 0.53
35	A	3,4,5-trimethoxyphenyl	H	C=O	OH	OCH ₃	OCH ₃	OCH ₃	-	-	49.83 ± 7.98
36	A	3,4,-dihydroxyphenyl	OH	C=O	OH	H	OH	OH	-	-	-
37	A	3,4,-dihydroxyphenyl	OH	C=O	OH	H	OH	OGlu	-	-	-
38	A	3,4,5-trimethoxyphenyl	H	C=O	OCH ₃	OCH ₃	OCH ₃	H	-	-	-
39	A	Phenyl	H	C=O	H	OH	OCH ₃	H	-	-	0.57 ± 0.20
40	A	4-methoxyphenyl	H	C=O	H	H	OH	H	-	-	27.18 ± 7.25
41	A	3,4,5-trimethoxyphenyl	OH	C=O	H	H	OCH ₃	H	-	-	-
42	A	3,4,5-trimethoxyphenyl	OH	C=O	H	H	H	H	-	-	18.04 ± 2.71
43	B	2-hydroxy-4-methoxyphenyl	-	C=O	H	OCH ₃	H	H	-	-	23.34 ± 5.57
44	B	3,4-Dimethoxy-2-hydroxyphenyl	-	C=O	H	H	H	H	-	-	24.27 ± 3.08
45	B	2-hydroxy-4-methoxyphenyl	-	C=O	H	H	OCH ₃	H	-	-	44.14 ± 8.10
46	B	2-hydroxy-5-methylphenyl	-	C=O	OCH ₃	H	OCH ₃	H	-	-	43.44 ± 9.60
47	B	2-hydroxy-5-methylphenyl	-	C=O	OCH ₃	H	H	OCH ₃	-	-	51.44 ± 4.26
48	A	2-phenyl	H	C=O	OH	OH	OH	H	23.99 ± 2.30	67.22 ± 1.60	29.83 ± 11.98
49	A	3-hydroxyphenyl	H	C=O	H	H	OH	OH	11.75 ± 1.70	1.66 ± 1.10	7.18 ± 1.76
50	A	4-hydroxyphenyl	H	C=O	H	H	OH	OH	29.39 ± 1.70	5.25 ± 1.10	0.68 ± 0.23
51	A	3,4-dihydroxyphenyl	H	C=O	H	H	OH	OH	25.51 ± 1.70	5.62 ± 1.10	8.45 ± 0.22
52	A	Phenyl	H	C=O	OH	OH	H	H	-	-	15.77 ± 3.60
53	A	3-hydroxyphenyl	H	C=O	H	H	OH	H	-	122.10 ± 9.80	-

Table 3.1: (continued)

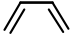


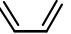


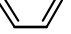

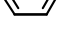

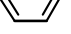


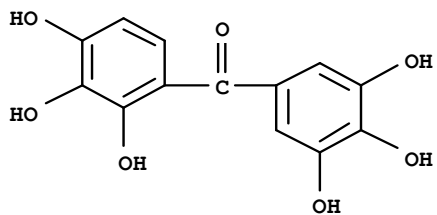
Compound	Type	R ²	R ³	R ⁴	R ⁵	R ⁶	R ⁷	R ⁸	hCNT1 IC ₅₀ (μM)	hCNT2 IC ₅₀ (μM)	hCNT3 IC ₅₀ (μM)
54	A	3,4-dihydroxyphenyl	H	C=O	H	H			231.74 ± 1.90	11.20 ± 1.50	32.50 ± 9.66
55	A	Phenyl	H	C=O	H	H	OCH ₃	OCH ₃	-	-	25.90 ± 3.96
56	A	Phenyl	H	C=O	H	H	OCH ₃	OH	-	-	35.55 ± 2.90
57	A	2-hydroxyphenyl	H	C=O	H	H	OH	OH	16.60 ± 1.50	4.06 ± 1.30	9.51 ± 1.67
58	A	H	4-chloro phenyl	C=O	H	H	OH	CH ₃	-	-	43.63 ± 10.1
59	A	H	phenyl	C=O	H	H	OH	CH ₃	-	-	31.62 ± 7.68
60	A	Phenyl	H	C=O			H	H	-	-	20.33 ± 3.53
61	A	Phenyl	H	C=O	H	H			-	-	32.36 ± 0.42
62	A	3,4-dihydroxyphenyl	H	C=O			H	H	-	-	13.48 ± 2.47
63	A	3,4-dimethoxyphenyl	H	C=O	H	H			-	-	14.69 ± 8.00
64	A	2-hydroxyphenyl	H	C=O	H	H			-	-	30.47 ± 5.10
65	A	2-hydroxyphenyl	H	C=O			H	H	-	-	32.95 ± 5.99
66	A	3-hydroxyphenyl	H	C=O	H	H			-	-	16.39 ± 7.56
67	A	3-hydroxyphenyl	H	C=O			H	H	-	-	16.96 ± 7.07
68	A	4-hydroxyphenyl	H	C=O	H	H			-	-	39.51 ± 1.06
69	A	4-hydroxyphenyl	H	C=O			H	H	-	-	42.00 ± 3.31
70	A	2-phenyl	OCH ₃	C=O	H	H			-	-	20.21 ± 6.90
71	A	4-methoxyphenyl	H	C=O	H	H			-	-	15.87 ± 4.85
72	A	3,4,5-trihydroxyphenyl	H	C=O	OH	H	OH	H	24.73 ± 1.20	15.80 ± 1.40	6.59 ± 1.17
73	A	4-hydroxyphenyl	H	C=O	H	H	OH	OGlu	-	-	26.97 ± 4.74
74	A	H	(1-phenyl-1H- pyrazol-4-yl)	C=O	H	H	OH	OH	27.90 ± 1.80	79.43 ± 3.10	7.42 ± 1.66
75	A	Phenyl	H	C=O	H	H	H	H	-	-	26.06 ± 5.48

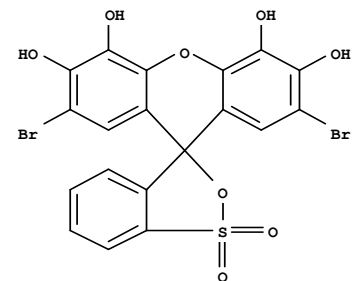
Table 3.1: (continued)

Compound	Type	R ²	R ³	R ⁴	R ⁵	R ⁶	R ⁷	R ⁸	hCNT1 IC ₅₀ (μM)	hCNT2 IC ₅₀ (μM)	hCNT3 IC ₅₀ (μM)
77	A	Phenyl	H	C=O	H	Cl	Cl	H	-	-	34.68 ± 8.56
78	A	H	4-chloro Phenoxy	C=O	H	H	OH	OH	-	-	31.71 ± 5.70
79	A	H	4-Fluoro phenoxy	C=O	H	H	OH	OH	-	-	27.06 ± 1.28
80	A	Methyl	phenyl	C=O	H	H	OH	OH	-	-	22.93 ± 1.46
81	A	H	phenyl	C=O	H	OH	OH	H	34.62 ± 2.10	141.00 ± 2.40	26.25 ± 4.47
82	A	H	phenyl	C=O	H	H	OH	OH	98.23 ± 2.70	126 ± 1.90	55.83 ± 11.99
83	A	H	(4-CH ₃ -2- thiazoyl)	C=O	H	H	OH	OH	51.88 ± 1.90	20.00 ± 1.60	3.02 ± 1.95
84	A	3,4,5-trihydroxyphenyl	OH	C=O	H	H	OH	H	27.12 ± 2.10	13.30 ± 1.30	1.04 ± 0.60
85	A	3,4,5-trihydroxyphenyl	H	C=O	H	H	OH	H	23.99 ± 1.60	8.17 ± 1.20	12.05 ± 1.17
86 ^a	-	-	-	-	-	-	-	-	-	-	-
87 ^b	-	-	-	-	-	-	-	-	-	-	-
88	C	C=O	H	CH ₃	H	H	OH	NO ₂	-	-	-
89	C	C=O	4'-methoxy phenyl	CH ₂	H	H	OH	H	4.44 ± 1.30	-	-
90	C	C=O	Phenyl	CH ₂	H	OCH ₃	H	H	-	-	-
91	C	C=O	Phenyl	CH ₂	H	H	OCH ₃	H	-	-	-
92	C	C=O	H	CH ₂	H	H	OH	OH	-	-	-
93	C	C=O	H	CH- phenyl	H	H	OH	OCH ₃	-	-	-
94	D	2-methyl	H	H	H	H	NH ₂	H	-	-	-
95	C	C=O	Phenyl	OH	OH	H	OH	H	-	-	-
96	D	2-NH ₂	CN	Pyridin -4-yl	H	H	OH	H	-	-	54.65 ± 2.03
97	D	H	Phenoxy	H	H	H	OH	OH	-	-	-
99	D	2-methyl	4'-nitro phenoxy	H	H	H	OCH ₃	CH ₃	-	-	-
100	E	2-Phenyl	H	N	H	OCH ₃	OCH ₃	H	-	-	-

Table 3.1: (continued)



^aCompound 86 (2,3,4,3',4',5'-hexahydroxybenzophenone)



^bCompound 87 (Bromopyrogallol red)

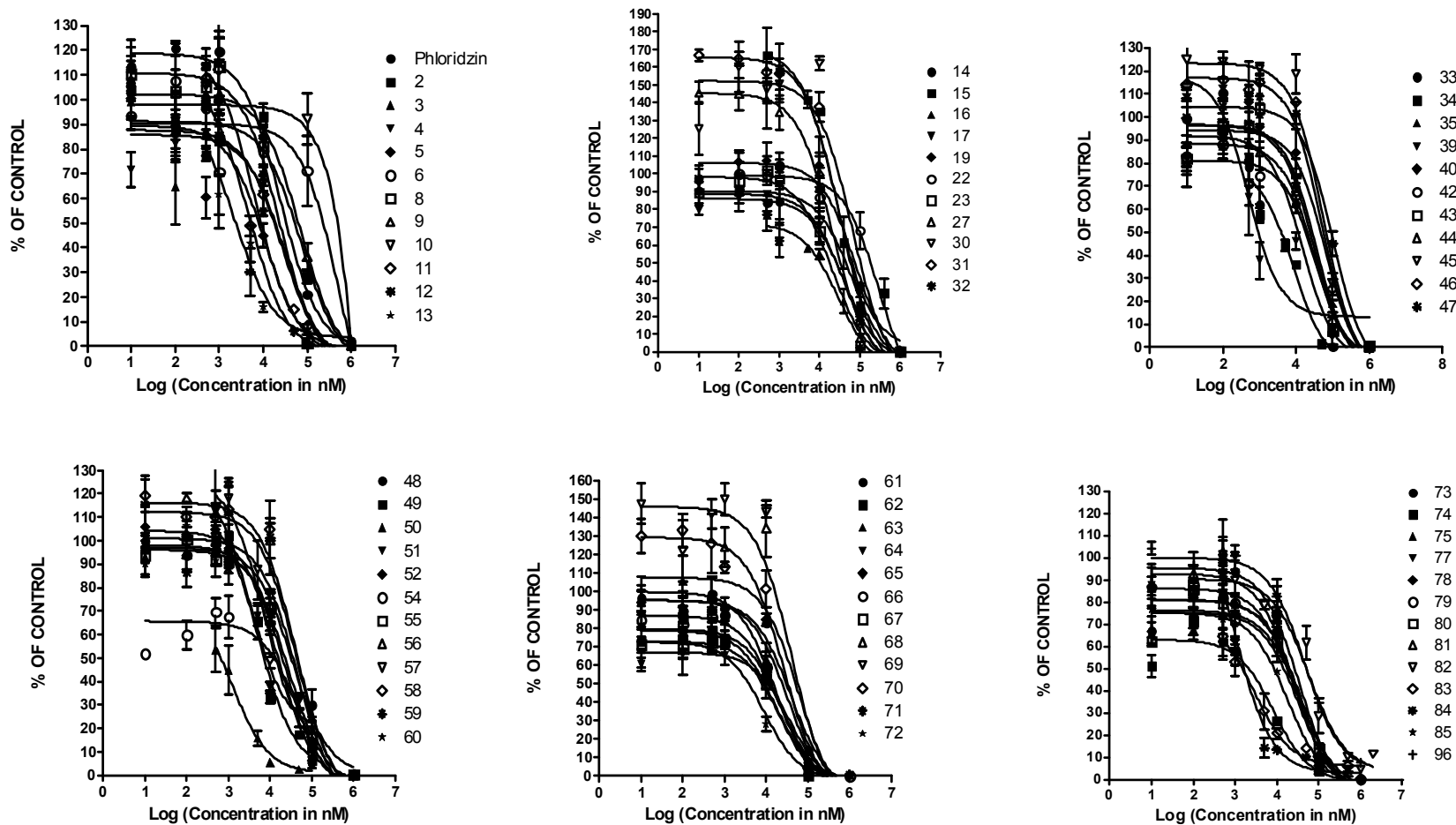


Figure 3.2: IC₅₀ curves of active compounds for CNT3 inhibition

3.4 Materials and Methods

All compounds listed in Table 3.1 were initially screened for CNT1, CNT2 and CNT3 nucleoside transporter inhibitory activities. Compounds showing more than 50 % inhibition in preliminary screening were evaluated to determine the IC_{50} values. The biological activity data was used to carry out 3D-QSAR analyses. The structures of the compounds and activity values (IC_{50} values) are shown in Table 3.1. The IC_{50} values were transformed into K_i values and the pK_i values were used as the dependent variable in CoMFA¹⁴³ and CoMSIA¹⁴⁴ analysis.

3.5 Molecular Modeling

Three-dimensional structure building and all modeling operations were performed using SYBYL 7.3 (Tripos Associates Inc.)¹⁴⁵ on a Silicon Graphics Octane workstation. MOPAC charges were assigned to all molecules. Energy minimization was performed using the Tripos force field with a distance-dependent dielectric and the BFGS algorithm, with a convergence criterion of 0.01 kcal/(mole* Å). Compounds in the data set were aligned using the MATCH module in SYBYL. Match alignment for CoMFA and CoMSIA studies was performed with the core of the flavone molecule as shown in Figure 3.3 as the template. Figure 3.4 shows the overlay of all the compounds used in the study aligned to the template.

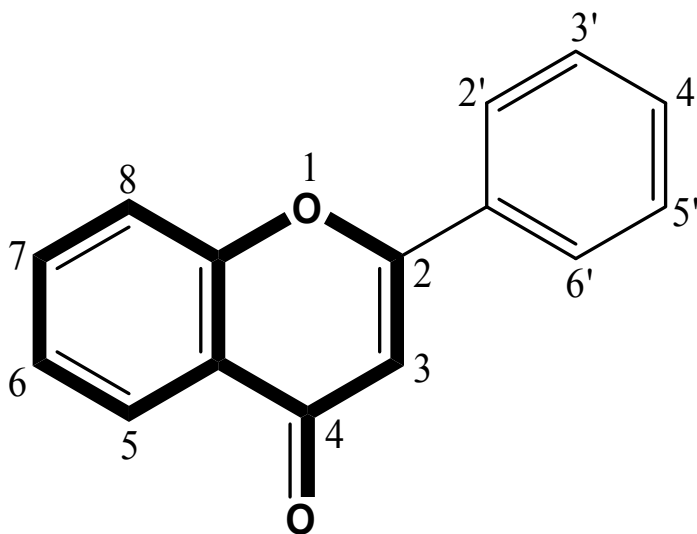


Figure 3.3: Atoms used in MATCH alignment shown in bold face

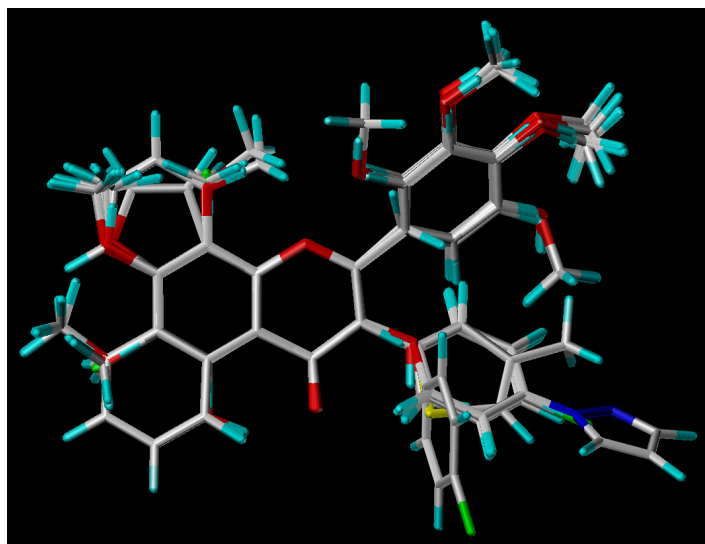


Figure 3.4: Atom-by-atom compound superposition used for 3D-QSAR analysis

For the molecules, red indicates oxygen, yellow refers to sulfur, grey indicates carbon, green indicates fluorine or chlorine and cyan indicates hydrogen.

3.6 CoMFA and CoMSIA Models

CoMFA and CoMSIA 3D-QSAR studies were undertaken to determine the effects of steric, electrostatic, hydrophobic, and hydrogen bonding properties of the compounds on different hCNT nucleoside transporter inhibitory activities, and to obtain reliable models for predicting the activity of compounds that belong to the same structural class. CoMFA and CoMSIA descriptor fields were derived by placing the molecules in a three dimensional cubic lattice with a spacing of 2 Å and extending 4 Å units beyond the aligned molecules in all directions. CoMFA descriptors were calculated using an sp^3 carbon probe atom with a van der Waals radius of 1.52 Å and a charge of +1 with a distance dependent dielectric to generate steric (Lennard-Jones 6-12 potential) fields and electrostatic (Coulombic potential) fields at each lattice point. An energy cutoff of 30 kcal/mole was applied. The CoMFA steric and electrostatic fields were scaled by the CoMFA-STD method in SYBYL. CoMSIA similarity index descriptors were calculated using a similar lattice box as in CoMFA. CoMSIA descriptors, namely, steric, electrostatic, hydrophobic, hydrogen bond donor and hydrogen bond acceptor were derived according to Klebe *et. al.*^{144, 147} using a sp^3 carbon probe atom with +1 charge and a van der Waals radius of 1.4 Å.¹⁴⁶

The PLS statistics obtained from CoMSIA analysis are shown in Table 3.2 and results obtained from PLS regression analysis, using CoMFA steric and electrostatic descriptors as independent variables are presented in Table 3.3. The stability of the CoMFA and CoMSIA models was evaluated by performing group cross-validation (30 runs), randomization (20 runs) and bootstrapping (20 runs). The results of these validations are shown in Table 3.4.

Table 3.2: PLS statistics of CoMFA and CoMSIA 3D-QSAR models for CNT

	hCNT1		hCNT2		hCNT3	
PLS statistics	CoMFA	CoMSIA	CoMFA	CoMSIA	CoMFA	CoMSIA
Q^2 (LOO)	0.525	0.547	0.583	0.613	0.517	0.493
R^2	0.984	0.997	0.840	0.863	0.910	0.919
S	0.037	0.020	0.247	0.224	0.141	0.107
F	99.22	294.01	29.67	37.69	50.26	66.26
PLS components	5	6	3	3	7	6
Total no. of compounds used for analysis	18		22		64	
No. of outliers	4	5	1	None	12	12
Outlier Compounds	13,54,74,81	9,54,74,81,84	16	None	16,17,39,50,58,6,63,71,77,80,82,9	16,19,39,4,50,6,63,71,73,80,82,9
No. of compounds in training set	N/A	N/A	N/A	N/A	43	42
No. of compounds in test set	N/A	N/A	N/A	N/A	9	10
Test set compounds	N/A	N/A	N/A	N/A	2,3,10,32,49,54,64,70,81	12,22,33,48,56,61,68,75,8,84

q^2 = cross validated correlation coefficient; s = standard error; r^2 = non-validated correlation coefficient; F = F-test value.

Table 3.3: Field contribution by CoMFA and CoMSIA descriptors for CNT

Descriptor	hCNT1		hCNT2		hCNT3	
	CoMFA	CoMSIA	CoMFA	CoMSIA	CoMFA	CoMSIA
Steric	0.564	0.074	0.503	0.071	0.417	0.064
Electrostatic	0.436	0.710	0.497	0.327	0.583	0.432
Hydrophobic	-----	0.210	-----	0.149	-----	0.162
Donor	-----	-----	-----	0.312	-----	0.232
Acceptor	-----	-----	-----	0.140	-----	0.110

Table 3.4: Results of group cross validation, randomization and bootstrapping for CNT

Method	hCNT1		hCNT2		hCNT3	
	CoMFA	CoMSIA	CoMFA	CoMSIA	CoMFA	CoMSIA
Group validation q^2 (30 groups and 30 runs)	0.525 ± 0.030	0.547 ± 0.029	0.583 ± 0.015	0.623 ± 0.009	0.513 ± 0.023	0.495 ± 0.012
Randomization q^2 (20 runs)	- 0.371	- 0.075	- 0.150	- 0.107	- 0.005	- 0.034
Bootstrapping (20 runs) 1. r^2	0.984 ± 0.007	0.999 ± 0.001	0.917 ± 0.009	0.920 ± 0.016	0.945 ± 0.028	0.961 ± 0.013
2. SD	0.018 ± 0.002	0.011 ± 0.014	0.040 ± 0.012	0.028 ± 0.005	0.112 ± 0.077	0.073 ± 0.043

q^2 = cross validated correlation coefficient; r^2 = non-validated correlation coefficient, SD = standard deviation.

3.7 Results of 3D-QSAR Analyses

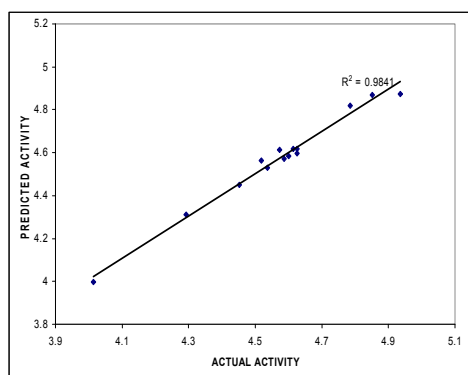
The results of the 3D-QSAR analyses are presented in the form of PLS statistics, fitted and prediction curves and contour isopleths. On the basis of the values of different statistical quantities, the QSAR results' validity and predictive capacity was judged.

The QSAR models were generated on different molecules listed in Table 3.1 for each nucleoside transporter. The CoMFA and CoMSIA models generated on the molecules show a correlation coefficient (r^2) of **0.984** and **0.997** (CNT1), **0.840** and **0.863** (CNT2) and **0.910** and **0.919** (CNT3) with cross-validated r^2 (q^2) of **0.525** and **0.547** (CNT1), **0.583** and **0.613** (CNT2) and **0.517** and **0.493** (CNT3), respectively. The 3D-QSAR models for CNT1 and CNT2 could not be validated by dividing data set into training and test set due to small number of compounds in both cases. Also, only three descriptors were considered for CoMSIA analysis of hCNT1 to obtain good PLS statistics. Hence, the CNT1 and CNT2 models need refinement by testing more flavones. The 3D-QSAR models for CNT3 were externally validated against a **test set of 9 and 10 molecules** and predictive R^2 (R^2 pred) recorded as **0.596** (CoMFA) and **0.569** (CoMSIA), respectively indicate fairly well significance of models for prediction.

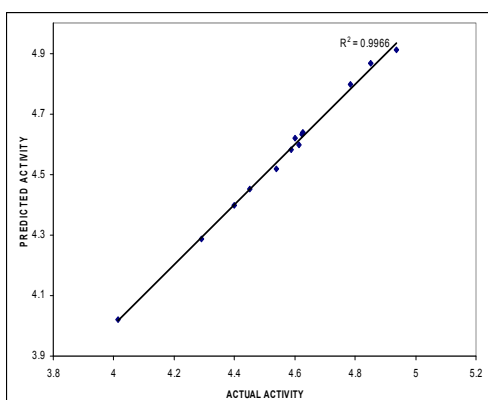
All the CoMFA and CoMSIA models have fairly reasonable cross validated q^2 and non-validated r^2 values as presented in Table 3.2. All of the models describing hCNT1, 2 and 3 inhibition are statistically acceptable ($q^2 > \sim 0.5$). The non-validated r^2 values of the CoMSIA models are similar to those of the CoMFA models for all the three transporters. However, if the q^2 values are compared, the CoMFA model appears to be better than the CoMSIA model for hCNT1 and hCNT3, whereas the CoMSIA model appears better than the CoMFA model for hCNT2.

The outliers were decided on the basis of q^2 by leave-one-out cross-validation. In generating the model for hCNT-3, the most active compounds 39 and 50 behaved as outliers, which indicate a possibility of different binding site or binding mode compared to the other compounds. It may also be due to an inadequacy of the modeling methods. Some of the possible reasons for the outlier status are: i) different binding site or binding mode compared to the rest of the compounds, ii) inability to align correctly with the training set, iii) inaccurate activity data, iv) physiochemical properties falling far outside the range of the rest of the training set compounds, and v) other processes not accounted for such as metabolism or transport.

The compounds belonging to the test set were selected to get a good R^2 predictivity. The prediction curves for both CoMFA and CoMSIA, as shown in Figures 3.5 to 3.8, are the graphs of the predicted activity vs. actual activity. The graphs show a good scatter of compounds around the regression line, which indicates good fitting of the data. The predictive abilities of the models were evaluated against 9 and 10 test compounds for CoMFA and CoMSIA, respectively and the values are listed in Table 3.5 were used to calculate the R^2_{pred} (correlation coefficient for predictive ability). From Table 3.6, it can be seen that the predictive ability of the CoMFA model is slightly better than the CoMSIA model.

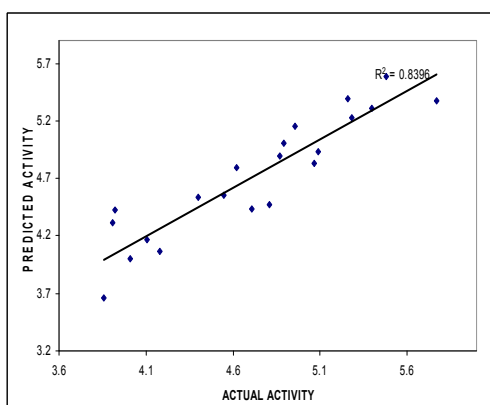


CoMFA

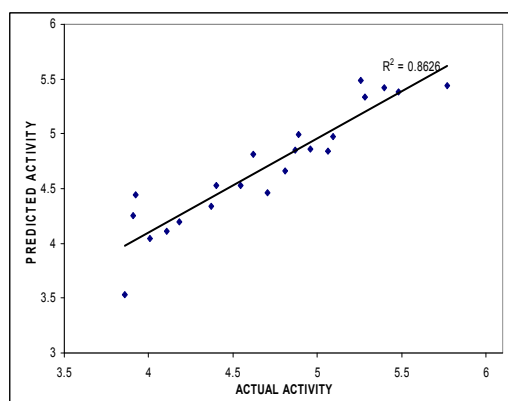


CoMSIA

Figure 3.5: Prediction curves for CoMFA and CoMSIA models for hCNT1 inhibition

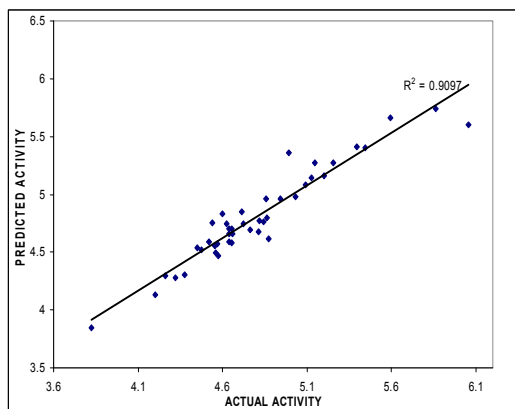


CoMFA

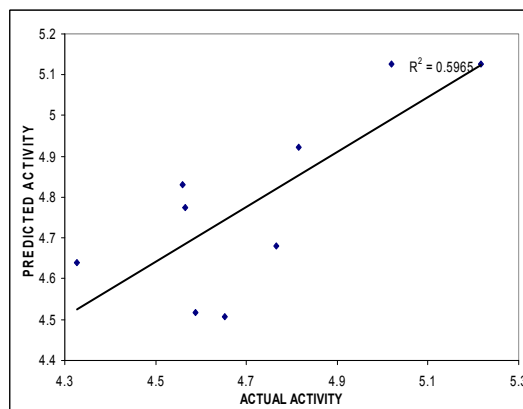


CoMSIA

Figure 3.6: Prediction curves for CoMFA and CoMSIA models for hCNT2 inhibition

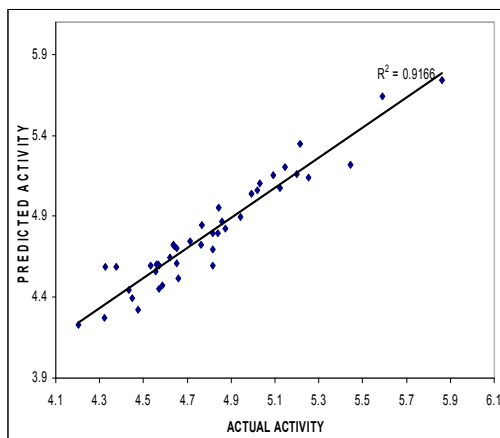


Training Set

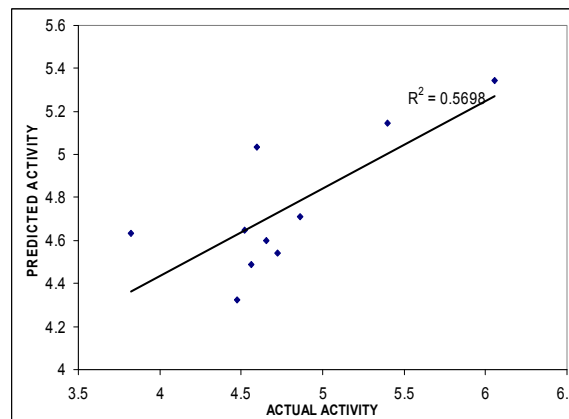


Test Set

Figure 3.7: Prediction curves for CoMFA training set and test set for hCNT3 inhibition



Training Set



Test Set

Figure 3.8: Prediction curves for CoMSIA training set and test set for hCNT3 inhibition

Table 3.5: Residuals of predictions of test set by CoMFA and CoMSIA models for hCNT3 inhibition

Compound number	Actual p <i>K</i> _i	Predicted CoMFA p <i>K</i> _i	CoMFA Residuals	Compound number	Actual p <i>K</i> _i	Predicted CoMSIA p <i>K</i> _i	CoMSIA Residuals
2	4.32	4.63	-0.31	12	5.39	5.14	0.24
3	5.01	5.12	-0.10	22	3.82	4.63	-0.80 ^a
10	4.81	4.92	-0.10	33	4.86	4.70	0.15
32	4.56	4.77	-0.20	48	4.59	5.03	-0.43
49	5.21	5.12	-0.08	56	4.52	4.64	-0.12
54	4.56	4.82	-0.26	61	4.56	4.48	0.07
64	4.58	4.51	0.07	68	4.47	4.32	0.15
70	4.76	4.68	0.08	75	4.65	4.60	0.05
81	4.65	4.50	0.14	8	4.72	4.54	0.18
-----	-----	-----	-----	84	6.05	5.34	0.71 ^a

^aThe residual values greater than 0.5 is responsible for the low predictivity of the respective models.

Table 3.6: Predictive R² values of test set by CoMFA and CoMSIA models for hCNT3 inhibition

	hCNT3 CoMFA	hCNT3 CoMSIA
R ² _{predictivity}	0.596	0.569

R²_{predictivity} = Correlation coefficient for predictive ability

3.8 PLS Contour Maps

Contour maps were generated by plotting the coefficients from CoMFA and CoMSIA QSAR models, which indicate regions in 3D space around the molecules where changes in the particular physicochemical properties are predicted to increase or decrease potency. The steric and electrostatic contours for CoMFA and CoMSIA models, and hydrophobic and hydrogen bond contours for the CoMSIA model for hCNT transporter inhibition, projected onto compound **49**, are shown in Figures 3.9 to 3.11.

Steric and electrostatic contours: Green contours indicate sterically favored regions whereas yellow contours denote sterically unfavorable regions. Blue contours identify regions that favor electropositive substituents and red regions favor electronegative substituents.

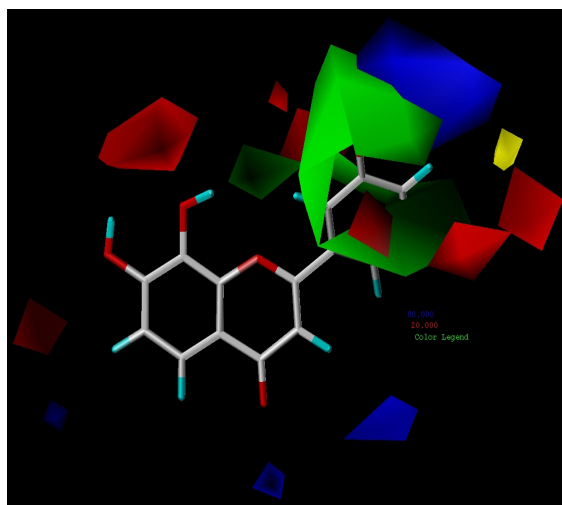
Hydrophobic, hydrogen bond donor and acceptor contours: Yellow contours indicate regions where hydrophobic groups are favored whereas white contours denote regions that disfavor hydrophobic groups. For the CNT1 CoMSIA model, color coding for a hydrophobic substituent favored region is orange. The cyan and purple contours indicate favorable and unfavorable regions for hydrogen bond donors, respectively. The magenta and red contours identify favorable and unfavorable positions for hydrogen bond acceptors, respectively.

3.8.1 PLS Contour Interpretation for CNT1 CoMFA

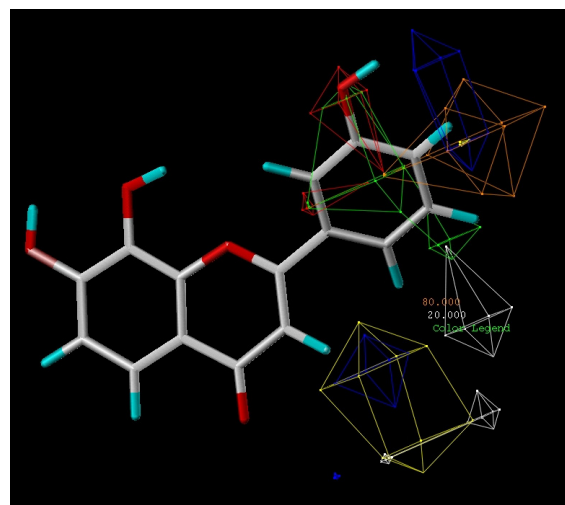
A distinct green contour near the 2-position phenyl ring indicates that sterically bulky substituents are favoured in this region. Red contours around the phenyl ring at the 5'-position indicate a favorable region for electronegative substituents. A red contour near position 8 also shows another region that favors electronegative substituents. A large blue contour near the 3'- of 2-position phenyl ring shows region that favors electropositive groups and small blue contours near 3- and 4- positions of the flavone indicate a region which can tolerate electropositive substituents (Figure 3.9A).

3.8.2 PLS Contour Interpretation for CNT1 CoMSIA

A green contour covering the 2-position phenyl ring indicates sterically favored region. Also, an orange contour covering the same part of molecule depicts a region that favors hydrophobic groups. The 4'-position is occupied by a blue contour suggesting an electrostatically favored part. A white contour near the 5'- and 6'- positions map hydrophobically unfavorable regions. A large yellow contour near the 3-position surrounding a blue contour in it indicates that this region is unfavorable for hydrophobic substituents and the blue contour suggests that electropositive groups are favored here (Figure 3.9B).

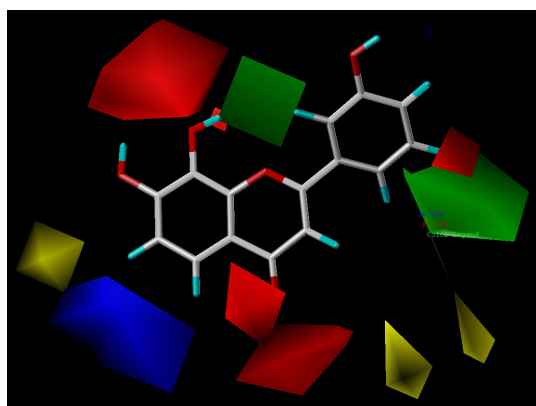


(A)

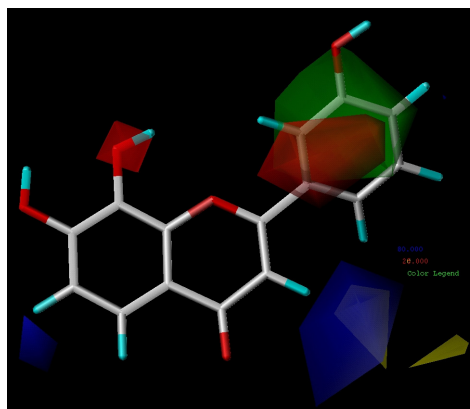


(B)

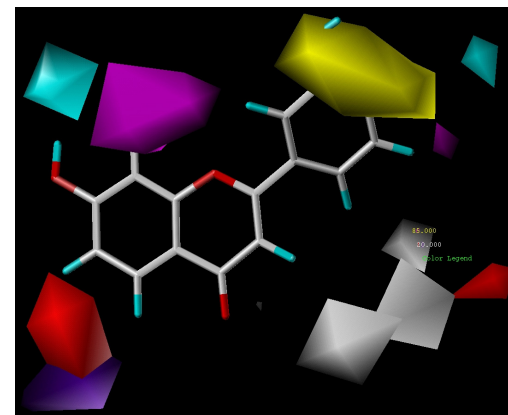
Figure 3.9: PLS contours from CoMFA steric and electrostatic (A) and CoMSIA steric, electrostatic and hydrophobic (B) descriptors for hCNT1 inhibition



(A)

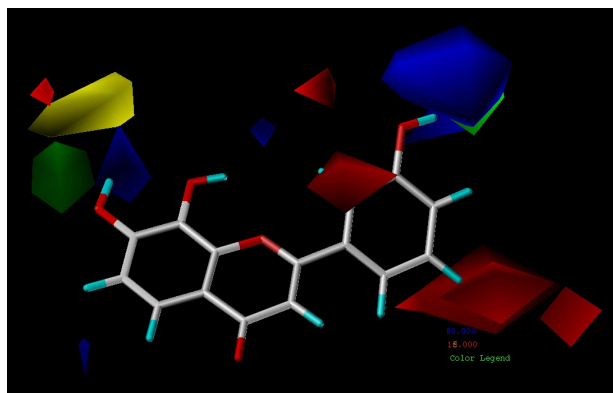


(B)

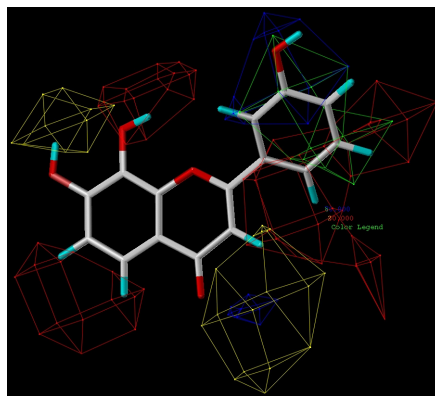


(C)

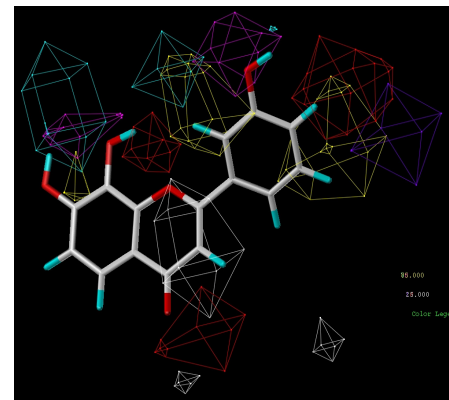
Figure 3.10: PLS contours from CoMFA steric and electrostatic (A), CoMSIA steric and electrostatic (B) and CoMSIA hydrophobic and hydrogen bond donor and acceptor (C) descriptors for hCNT2 inhibition



(A)



(B)



(C)

Figure 3.11: PLS contours from CoMFA steric and electrostatic (A), CoMSIA steric and electrostatic (B) and CoMSIA hydrophobic and hydrogen bond donor and acceptor (C) descriptors for hCNT3 inhibition

3.8.3 PLS Contour Interpretation for CNT2 CoMFA

The 2-position phenyl ring is sterically favored as shown by the presence of two green contours around it. Position 8 is strongly recommended for electronegative substituents due to the presence of a large red contour. Positions 5 and 6 are favorable towards electropositive substituents, whereas position 4 is favorable for electronegative substituents. The region between positions 6 and 7, and the region around position 3 are strictly unfavorable for sterically bulky groups (Figure 3.10A).

3.8.4 PLS Contour Interpretation for CNT2 CoMSIA

A large green contour over the 2-position phenyl ring indicates a sterically favored region. A red contour at the same position shows that an electronegative group is favored as well. Position 3 shows a blue contour covering a yellow one indicating that it is an electropositive favored region but no tolerance for sterically bulky groups. A red contour at the 8- and blue at 6-positions indicate electrostatically disfavored and favored regions, respectively (Figure 3.10B).

A large yellow contour at the 2' and 3' positions of the 2-phenyl ring indicates a strong propensity for hydrophobic groups. A white contour near position 3 shows a part of the molecule that disfavors hydrophobic groups. A cyan contour near position 7 and a magenta near position 8 show regions favored for H-bond donor and H-bond acceptor groups, respectively. The occurrence of red and purple contours near positions 5 and 6 denote that this part of the molecule is neither favored for H-bond donor nor for acceptor groups (Figure 3.10C).

3.8.5 PLS Contour Interpretation for CNT3 CoMFA

A green contour overlapped by a blue one near the 3'-position of the 2-phenyl ring indicates that the position favors sterically bulky and electropositive groups. Two distinct red contours near the 2'- and 5'- positions show positions suitable for electronegative groups. The blue contour at position 7 shows that electropositive groups are predicted to increase activity at that location. The same position is partly favoured and and partly disfavored for sterically bulky groups as well (Figure 3.11A).

3.8.6 PLS Contour Interpretation for CNT3 CoMSIA

The red contours between positions 5 and 6, at position 8 and near the 5' and 6' positions indicate electronegative substituent favored regions. A large green contour over the 2-phenyl ring and the yellow contour near position 3 indicate sterically favored and disfavored regions, respectively. Both the 3- and 3'- positions are prefer electropositive substituents (Figure 3.11B).

The yellow contours at the positions 2' and 5' signify favorable positions for hydrophobic groups. A hydrophobic disfavored region at position 3 is indicated by the white contour. A cyan contour at position 7 shows a strong propensity for H-bond donor property; and the red contour at position 4 indicates an unfavorable position for H-bond acceptors. Purple and red contours near positions 4' and 5' indicate no tolerance for both H-bond donor or acceptor. Magenta contours near positions 2' and 8 indicate region favorable for H-bond acceptors (Figure 3.11C).

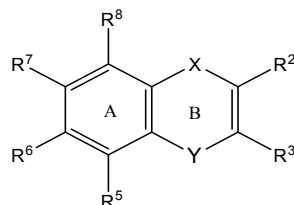
In general, the active sites of the transporters can be outlined with the help of the isopleths obtained from 3D-QSAR analyses. For all the CNTs, (i) position 2 should be occupied by sterically bulky and a hydrophobic group to obtain compounds with increased activity, (ii) positions 7 and 8 should be substituted with H-bond donor and H-bond acceptor groups, respectively (iii) position 3 is unfavorable to hydrophobic and bulky substituents, (iv) positions 2' and 5' favor electronegative groups and (v) position 3 favors electropositive, whereas position 4 favors electronegative groups.

The differentiating features for these three CNTs are, 1) CNT1 can tolerate more sterically bulky group compared to the other two CNTs, 2) activity is significantly influenced by the presence or absence of H-bond donor and acceptor at positions 7 and 8 for CNT2 and CNT3 inhibition, 3) substitutions at positions 5 and 6 do not significantly influence CNT1 inhibition but the inhibitory activity on CNT2 and CNT3 can be modified by the presence of appropriate electrostatic modifying functional groups as shown by different electrostatic contours.

3.9 Activity Prediction of *In silico* Designed Compounds Using 3D-QSAR Models for hCNT3

One of the best uses of 3D-QSAR models is their use for prediction of designed molecules which have not been synthesized or tested yet for the desired biological activity. The models derived for hCNT3 inhibition were validated for predictive ability by dividing the data set into training and test sets and the highest R^2 -predictivity was ~0.6 for CoMFA compared to 0.569 for CoMSIA. These models were used to predict the activities of 58 *in silico* designed molecules which are listed in Table 3.7. The predicted activities were compared with the potent inhibitors compound, **50** ($pK_i = 6.237$) and compound **84** ($pK_i = 6.056$). Some compounds from Table 3.7 such as **Pred 2**, **Pred 16**, **Pred 19**, **Pred 20** and **Pred 21** showed the highest predicted activities and it was distinctly noticed that these compounds have $-NH_2$ substitution as the R^3 group, suggesting the importance of H-bond donor at this position (Figure 3.12). These compounds were searched for their availability using SciFinder search module and it was found that none of these good predicted compounds are available commercially yet, in turn suggesting their novelty. These compounds can be synthesized and biologically evaluated.

Table 3.7: Predicted activities for *in silico* designed compounds for hCNT3-inhibition



Compound	X	R ²	R ³	Y	R ⁵	R ⁶	R ⁷	R ⁸	hCNT3 pK _i (μM)	
									CoMFA	CoMSIA
Pred 1	NH	3-hydroxyphenyl	N	CH ₂	H	H	OH	OH	5.0894	5.4002
Pred 2	O	3-hydroxyphenyl	NH ₂	C=O	H	H	OH	OH	5.2408	5.9004
Pred 3	O	3-hydroxyphenyl	CN	C=O	H	H	OH	OH	5.4583	5.5355
Pred 4	O	3-hydroxyphenyl	H	C=O	H	H	OH	Acetyl	5.2366	5.2125
Pred 5	O	3-hydroxyphenyl	H	C=O	H	H	OH	N ₃	5.3650	5.1107
Pred 6	O	3-hydroxyphenyl	H	C=O	H	H	OH	Br	5.2089	4.9560
Pred 7	O	3-hydroxyphenyl	H	C=O	H	H	OH	Cl	5.2617	5.0409
Pred 8	O	3-hydroxyphenyl	H	C=O	H	H	OH	CN	5.2691	5.1720
Pred 9	O	3-hydroxyphenyl	H	C=O	H	H	OH	F	5.1534	5.0479
Pred 10	O	3-hydroxyphenyl	H	C=O	H	H	OH	Formyl	5.2695	5.0802
Pred 11	O	3-hydroxyphenyl	H	C=O	H	H	OH	I	5.1486	4.8534
Pred 12	O	3-hydroxyphenyl	H	C=O	H	H	OH	NO ₂	5.5612	5.5916
Pred 13	O	3-hydroxyphenyl	H	CH ₂	H	H	OH	OH	5.5351	5.5770
Pred 14	O	3-hydroxyphenyl	H	CH ₂	H	CH ₃	OH	OH	5.5928	5.5767
Pred 15	O	3-hydroxyphenyl	H	C=O	H	Tetrahydro isoquinolino		H	5.1472	5.3560
Pred 16	O	3-hydroxyphenyl	NH ₂	CH ₂	H	H	OH	OH	5.5568	6.0750
Pred 17	O	3-hydroxyphenyl	H	C=O	H	H	NH ₂	OH	5.0259	5.5197
Pred 18	O	3-hydroxyphenyl	H	CH ₂	H	OCH ₃	OH	OH	5.4888	5.6436

Table 3.7: (continued)

Compound	X	R ²	R ³	Y	R ⁵	R ⁶	R ⁷	R ⁸	hCNT3 pK _i (μM)	
									CoMFA	CoMSIA
Pred 19	O	3-hydroxyphenyl	NH ₂	CH ₂	H	CN	OH	OH	5.5568	6.1241
Pred 20	O	3-hydroxyphenyl	NH ₂	CH ₂	H	CN	OH	NO ₂	5.9676	6.3450
Pred 21	O	Tetrazoyl	NH ₂	CH ₂	H	CN	OH	NO ₂	5.2610	5.8926
Pred 22	O	3-hydroxyphenyl	H	3 membered B ring	H	H	OH	OH	5.2425	5.3099
Pred 23	NH	3-hydroxyphenyl	H	3 membered B ring	H	H	OH	OH	5.0969	5.5006
Pred 24	NH	3-hydroxyphenyl	H	C=O	H	H	OH	OH	5.1599	5.4527
Pred 25	O	3-hydroxyphenyl	N	C=O	H	H	OH	OH	5.1265	5.3518
Pred 26	CH ₂	3,4,5-trimethoxyphenyl	H	CH ₂	H	H	OH	H	5.4952	4.8389
Pred 27	CH ₂	3,4,5-trimethoxyphenyl	OH	C=O	H	H	OH	H	5.3633	4.9562
Pred 28	CH ₂	3,4,5-trimethoxyphenyl	OH	CH ₂	H	H	OH	H	5.6982	5.1398
Pred 29	NH	3,4,5-trimethoxyphenyl	OH	C=O	H	H	OH	H	5.2473	5.1803
Pred 30	NH	3,4,5-trimethoxyphenyl	NH ₂	C=O	H	H	OH	H	5.2020	5.2744
Pred 31	O	2-NH ₂ ,3,4,5-trimethoxyphenyl	OH	C=O	H	H	OH	H	5.3347	5.2910
Pred 32	O	2-OH,3,4,5-trimethoxyphenyl	OH	C=O	H	H	OH	H	5.2122	5.1918
Pred 33	O	3,4,5-trimethoxyphenyl	OCH ₃	C=O	H	H	OH	H	5.0896	5.1326
Pred 34	O	3,4,5-trimethoxyphenyl	OH	CH ₂	H	H	OH	H	5.3347	5.2425
Pred 35	O	3,4,5-trimethoxyphenyl	OH	C=O	OH	H	OH	H	5.1796	5.1052
Pred 36	O	3,4,5-trimethoxyphenyl	OH	C=O	H	CN	OH	H	4.9763	5.1815
Pred 37	O	3,4,5-trimethoxyphenyl	OH	C=O	H	NH ₂	OH	H	5.2424	5.0991
Pred 38	O	3,4,5-trimethoxyphenyl	OH	C=O	H	OH	OH	H	5.2910	5.1160
Pred 39	O	3,4,5-trimethoxyphenyl	OH	C=O	H	H	CN	H	5.3218	4.8213
Pred 40	O	3,4,5-trimethoxyphenyl	OH	C=O	H	H	CN	NH ₂	5.2755	5.2923
Pred 41	O	3,4,5-trimethoxyphenyl	OH	C=O	H	H	SH	H	5.1556	4.8635
Pred 42	O	3,4,5-trimethoxyphenyl	OH	C=O	H	H	N ₃	H	5.0955	4.8090

Table 3.7: (continued)

Compound	X	R ²	R ³	Y	R ⁵	R ⁶	R ⁷	R ⁸	hCNT3 pK _i (μM)	
									CoMFA	CoMSIA
Pred 43	O	3,4,5-trimethoxyphenyl	OH	C=O	H	H	NH ₂	H	5.1002	5.2004
Pred 44	O	3,4,5-trimethoxyphenyl	OH	C=O	H	H	NO ₂	H	5.6695	4.7746
Pred 45	O	3,4,5-trimethoxyphenyl	H	C=O	H	H	OH	H	5.0245	4.7465
Pred 46	O	3,4,5-triethoxyphenyl	OH	C=O	H	H	OH	H	5.3961	4.9736
Pred 47	CH ₂	3,4,5-trimethoxyphenyl	OCH ₃	CH ₂	OCH ₃	OCH ₃	OCH ₃	H	4.1784	4.9407
Pred 48	O	3,4-methylenedioxy-5-methoxy phenyl	OH	C=O	H	H	OH	H	4.1996	5.0094
Pred 49	O	3,4,5-trimethoxyphenyl	OCH ₃	C=O	OCH ₃	OCH ₃	OCH ₃	H	3.8809	4.7287
Pred 50	O	3,4,5-trimethoxyphenyl	H	C=O	OCH ₃	OCH ₃	OCH ₃	H	4.0213	4.6782
Pred 51	O	3,4,5-trimethoxyphenyl	OH	C=O	OCH ₃	OCH ₃	OCH ₃	H	3.9378	4.9402
Pred 52	O	3,4,5-trimethoxyphenyl	H	C=O	H	H	OCH ₃	OCH ₃	4.7539	4.4927
Pred 53	O	Phenyl	NH ₂	C=O	H	OH	OCH ₃	H	4.3038	5.008
Pred 54	O	Phenyl	OH	C=O	H	OH	OCH ₃	H	4.4621	4.7291
Pred 55	O	4-hydroxy phenyl	NH ₂	C=O	H	H	OH	OH	4.6009	5.0547
Pred 56	O	4-hydroxy phenyl	OH	C=O	H	H	OH	OH	5.1213	5.2011
Pred 57	O	3,4,5-trihydroxyphenyl	NH ₂	C=O	H	H	OH	H	4.8295	5.6005
Compound XI	O	3,4,5-trimethoxyphenyl	-----	-----	H	H	OCH ₃	OCH ₃	4.7762	4.5118

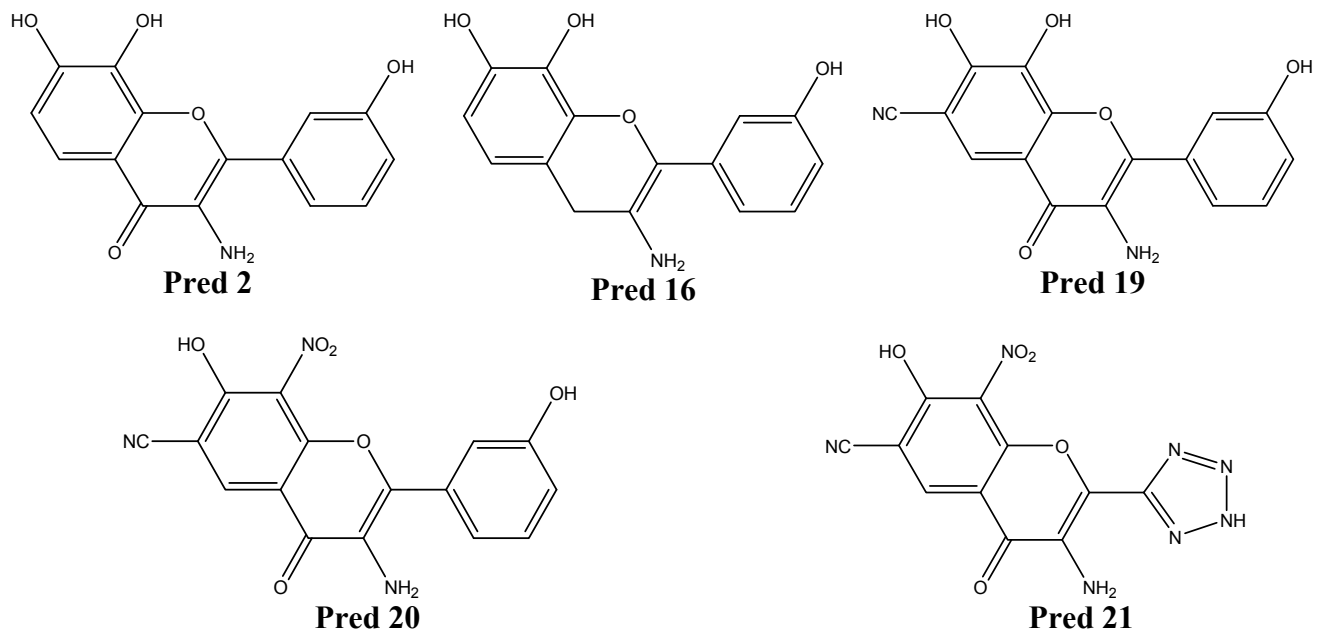


Figure 3.12: *In silico* compounds with high predicted hCNT3 inhibitory activity

3.10 Discussion

The highlights of the SAR are: 1) hCNT3 is the most sensitive to inhibition by flavones followed by hCNT2 and then hCNT1. 2) Compound **49** is the most active flavone against CNT1 and CNT2 (IC₅₀ values of 11.75 μM and 1.66 μM, respectively), whereas, compound **39** is most active for CNT3 (IC₅₀ of 0.57 μM). But, compound **39** does not obey the general trend followed by other active flavones, i.e. the presence of 7-OH. Thus, it is thought to possibly act via a different binding mode. 3) The other highly active inhibitors for CNT3 are compounds **50** (IC₅₀ of 0.68 μM) and **84** (IC₅₀ of 1.04 μM). 4) In general, the 7,8-dihydroxy moiety is a key structural feature particularly for inhibition of hCNT2 and hCNT3 by flavones (compounds **13**, **49**, **50**, **51**, **57**). 5) 3'-Hydroxy and 4'-hydroxy substitutions are also favorable structural features for higher inhibitory activity (compounds **49**, **50**). 6) Methoxy substitution on the 2-phenyl ring is detrimental for all three hCNTs (compounds **16**, **18-33**, **35**). 7) The 7,8-dihydroxy substitution is much better than 7,8-dimethoxy substitution (compare compounds **13** and **55**). 8) Interestingly, 7,8-dihydroxy substitution in isoflavones does not improve activity (compounds **78-80**, **82**, **83**). 9) Compounds with 3',4',5'-trihydroxy substitution are better inhibitors (compounds **72**, **84**, **85**) than those with 3',4',5'-trimethoxy substitution (compare with compound **35**). 10) Compounds **9**, **48**, and **81** with 6,7-dihydroxy substitution are slightly more selective for hCNT1. 11) All of the chalcones are only moderately active against hCNT3 (compounds **43-47**), but inactive against hCNT1 or hCNT2. 12) Compound **49** is the most selective compound against hCNT2 (7.07 folds and 4.32 folds compared to hCNT1 and hCNT3, respectively); other selective compounds are compounds **54**, **57** and **85** (20.69 folds, 4.08 folds and 2.93 folds compared to hCNT1 and 2.90 folds, 2.34 folds and 1.47 folds compared to hCNT3 for compounds **54**, **57** and **85**, respectively). 13) Compounds **12** and **83** are selective inhibitors of hCNT3 (7.54 folds and 17.17 folds compared to their inhibition of hCNT1 and 5.14 folds and 6.62 folds compared to hCNT2, for compounds **12** and **83**, respectively). 14) Naphthoflavones containing 3'-OH or 3',4'-dihydroxyphenyl moiety (compounds **62**, **66**, **67**) are more active than those having 2'-OH or 4'-OH substitution (compounds **64**, **65**, **68**, **69**). 15) In general, 3',4'-dihydroxy substitution is favored in the naphthoflavone class, but compound **63** is an exception, which has 3',4'-dimethoxy substitution.

Taking into consideration, the contributions made by different descriptors for all the CNTs, it can be said that, in the case of CoMFA, the **steric descriptor** contributes to greater extent than the **electrostatic descriptor** for hCNT1 and hCNT2, whereas for hCNT3, the reverse is true. For the CoMSIA analyses, the **electrostatic descriptor** contributes the most among all the CoMSIA descriptors for all the transporters. The **hydrogen bond donor descriptor** is the next most important descriptor in the case of hCNT2 and hCNT3 followed by hydrophobic descriptors and then the **H-bond acceptor descriptor**.

The QSAR models derived for hCNT3 were utilized for prediction of in silico designed compounds some of which showed high predicted activities. These compounds (**Pred 2**, **Pred 16**, **Pred 19**, **Pred 20**, **Pred 21**) can be acquired and assayed to examine

the validity of these predictions and the additional information can be utilized to explore more molecules for the possibility of finding better hCNT3 inhibitors.

3.11 Conclusion

In this study, an attempt has been made to rationalize the binding data of new selective inhibitors of all the three cloned hCNT transporters and to understand the structural features important for selective and potent inhibitory activity at each transporter. The obtained CoMFA and CoMSIA contours can be used to assist the design of selective compounds. These models correlate structural features with inhibitory activities against CNTs and bring valuable information regarding the relevant characteristics of flavonoids tested and the active sites; but this information might not hold true for flavones with more diverse functionalities. The new compounds designed and predicted *in silico* to have high activity may be useful in finding new leads for hCNT3 inhibition.

3.12 Experimental Section: [³H]-Uridine Uptake Assay

The ability of the compounds to inhibit uptake of nucleosides CNTs was determined by studying the inhibition of uptake of radiolabeled uridine. Uptake experiments were performed on a nucleoside transporter deficient, PK15NTD cell line, stably expressing the cloned hCNT 1, 2 or 3 nucleoside transporter. Cells were maintained in Eagles minimum essential medium/Earles's balanced salt solution (1:1) with 0.1mM non-essential amino acids, 1mM sodium pyruvate, 5% Fetal bovine serum, penicillin/streptomycin (50,000 units/litre, 50 mg/litre) at 37° C with 5% CO₂ and 95% air. The Na buffer was HEPES Ringers solution containing (in mM): 135.0 NaCl, 5.0 KCl, 3.3 NaH₂PO₄, 0.8 Na₂HPO₄, 1.0 CaCl₂, 1.0 MgCl₂, 10.0 glucose, and 5.0 HEPES (pH 7.4). Na free buffer contained (in mM): 140.0 N-methyl-D-glucamine (NMDG), 5.0 HEPES, 5.0 KH₂PO₄, 1.0 CaCl₂, 1.0 MgCl₂, and 10.0 glucose (pH 7.4). The cells were seeded into a 48 well plate and grown until confluent. The cells were washed three times in Na-free buffer solution followed by the addition of varying concentrations of the inhibitors (1 nM – 200 μM) and [³H] uridine (0.2 μM). The [³H] uridine uptake was measured for 2 minutes. Following a two-minute exposure the action of radiolabelled uridine was terminated by rapidly washing the cells thrice with ice cold PBS (pH 7.4). Cells were solubilized overnight in 300 μl 5% Triton X-100, and radioactivity was measured by β-counter. The PRISM program was used (GraphPad, San Diego, CA) to derive concentration dependent curves to obtain IC₅₀ values which were finally used to calculate inhibition constants (K_i).

Chapter 4: Biological Evaluation and 3D-QSAR Studies of Flavones Analogs for Human Equilibrative Nucleoside Transporter Inhibition

4.1 Introduction

In this chapter, QSAR studies have been applied to the modeling of the ENT1 and ENT2 inhibitory activities of flavonoids. In our current work, we carried out 3D-QSAR studies to establish correlations between structural properties of 95 flavones, chalcones and analogous compounds such as coumarins and a quinoxaline derivative and their inhibitory activities against ENT1 and ENT2. 3D-QSAR analyses were performed using comparative molecular field analysis (CoMFA) and comparative molecular similarity indices analysis (CoMSIA). The models derived were used to predict the activities of designed flavones. Based on the SAR, a new lead compound **XI** was designed; but a mixture of compounds **XII** and **XIII** was obtained after an attempted synthesis of this compound. The mixture was evaluated as such, against hENT1, hENT2 and hCNT3 transporters.

4.2 Biological Evaluation: Uridine Uptake Assay

The procedure followed for the assay is same as that mention in Chapter 3. The cell line that was used for the study is the nucleoside transporter deficient PK15NTD cell line stably transfected with cDNA of hENT1 or hENT2. The amount of radiolabeled uridine present intracellularly following a five or two minutes exposure of [³H]-uridine to ENT1 (0.3 μM) or ENT2 (0.2 μM), respectively, is determined in the absence and presence of varying concentrations of an inhibitor (1 nM – 200 μM). Details of the [³H] uridine uptake assay are provided in the experimental section in Chapter 3. All compounds used in the study were first screened at a concentration of 10 μM. Only those compounds showing more than 50% inhibition at 10 μM were further tested for IC₅₀ determination. Figure 4.1 shows the comparison graph of ENT and ENT2 inhibition by the compounds. S⁶-(4-Nitrobenzyl) mercaptopurine riboside (NBMPR, **V**) and dipyridamole (**VI**) were used as standards to compare the inhibitory activities of the compounds.

The results obtained from [³H]-nucleoside uptake assays were entered into the PRISM program (GraphPad, San Diego, CA) to plot concentration-dependent inhibition curves (Figures 4.2 and 4.3). From these curves, the IC₅₀ values (Table 4.1) were computed and used to calculate inhibition constant (*K_i*) values using Equation 4.1.

$$K_i = IC_{50}/(1+[L]/K_L) \quad (\text{Eq. 4.1})$$

where, [L] and *K_L* are the concentration and the *K_m* value of [³H] uridine, respectively. The *K_i* values were used to compare the abilities of the compounds to inhibit [³H]-uridine uptake.

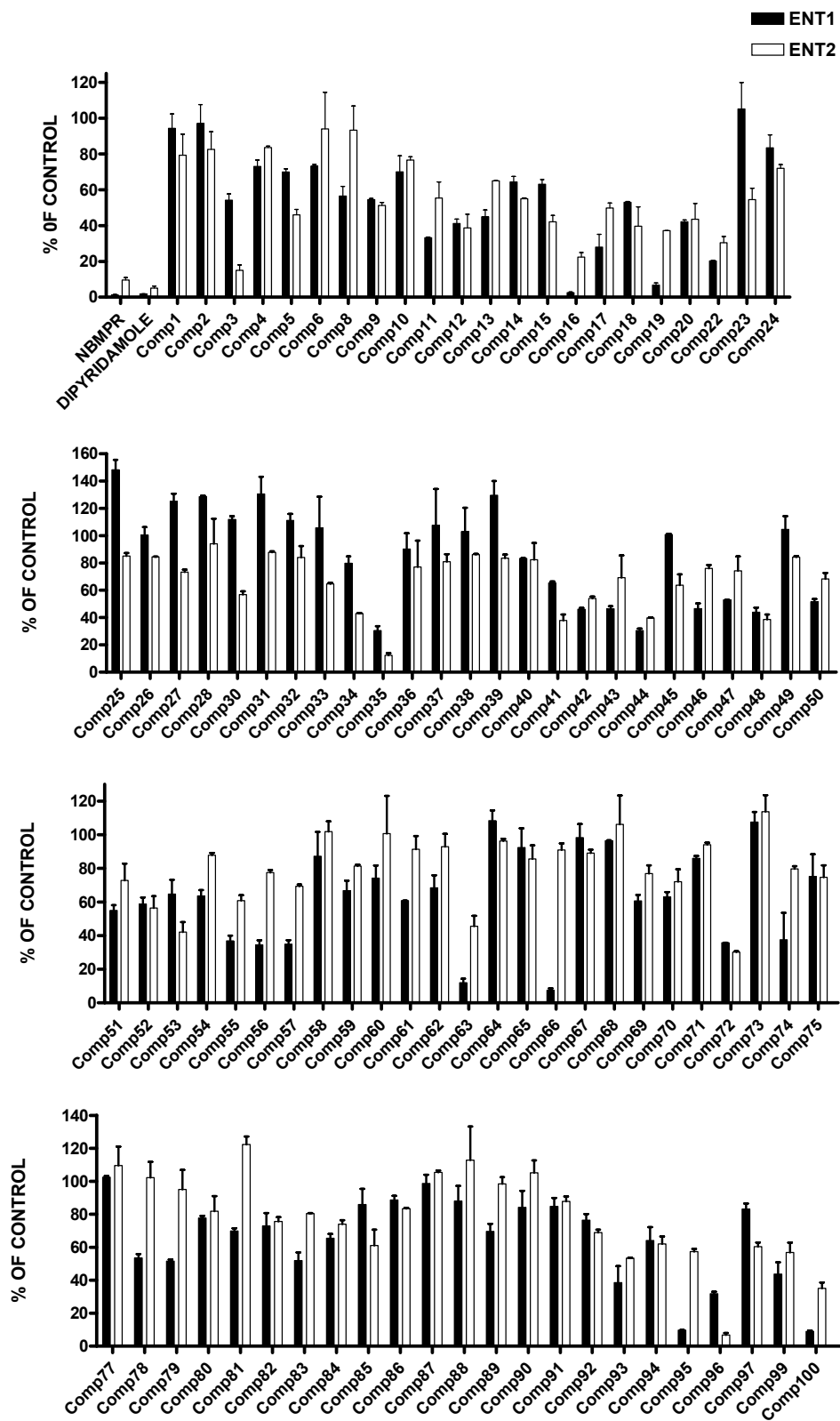


Figure 4.1: Comparison graph of % of inhibition at 10 μ M

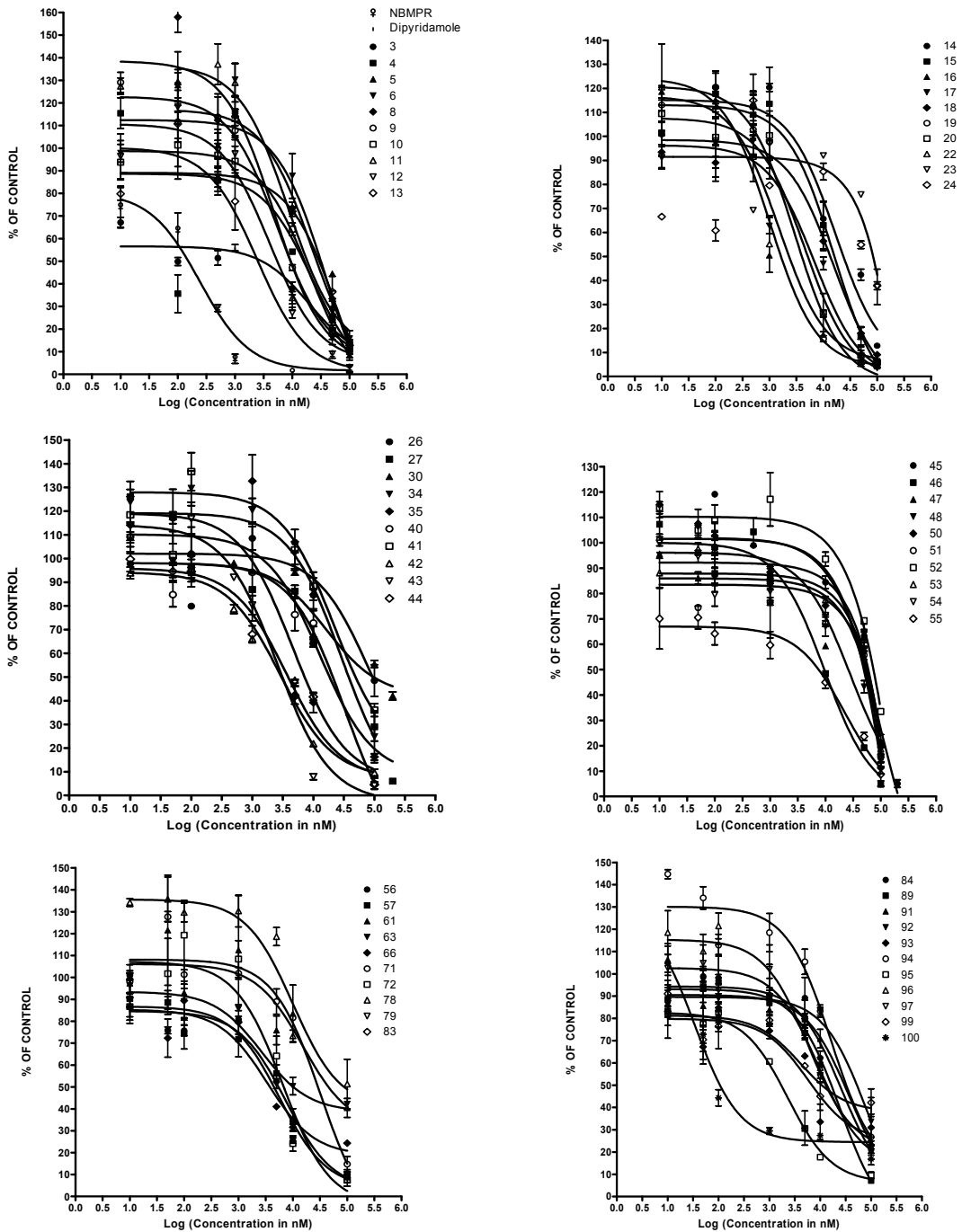


Figure 4.2: IC₅₀ curves of compounds in study for ENT1 inhibition

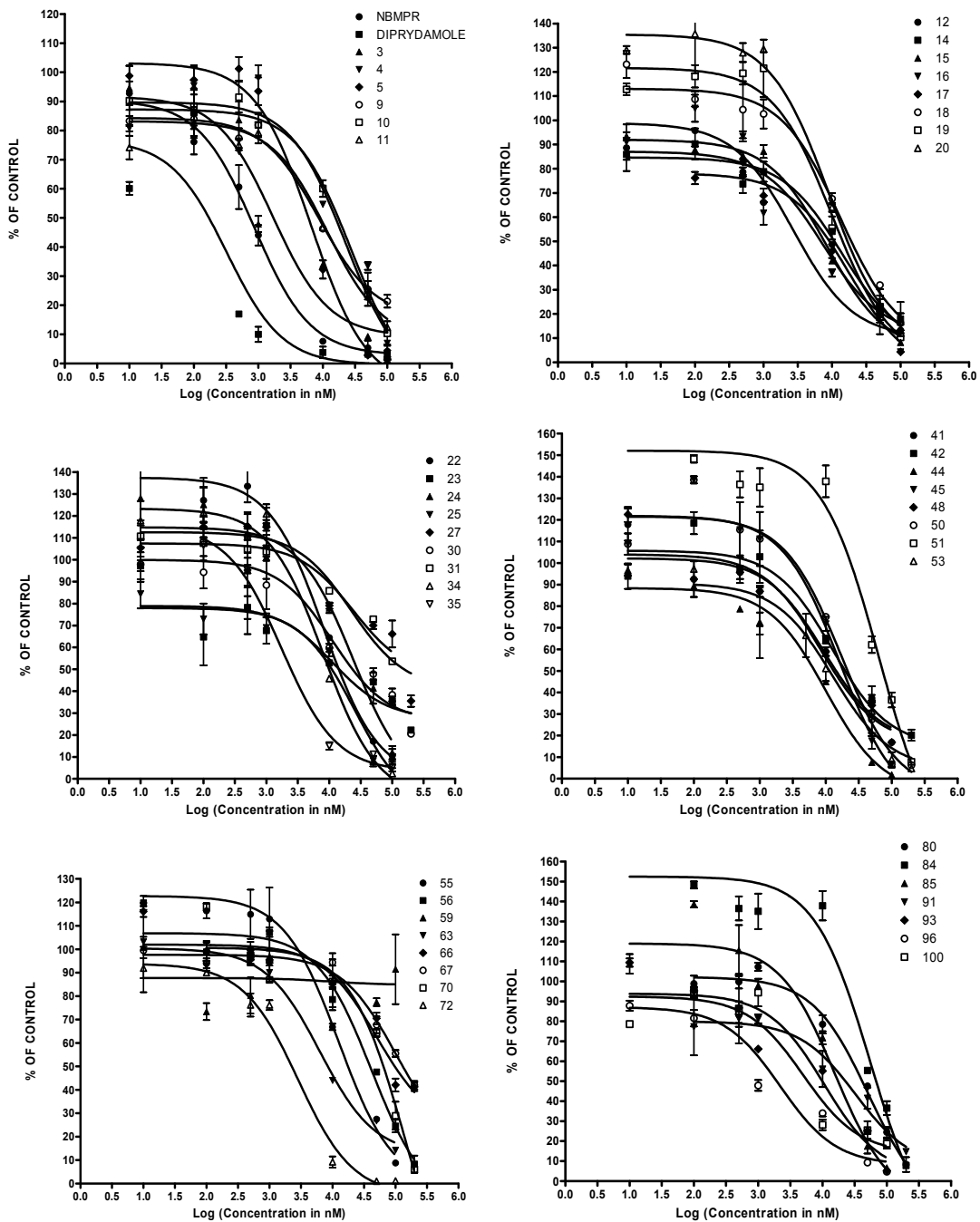
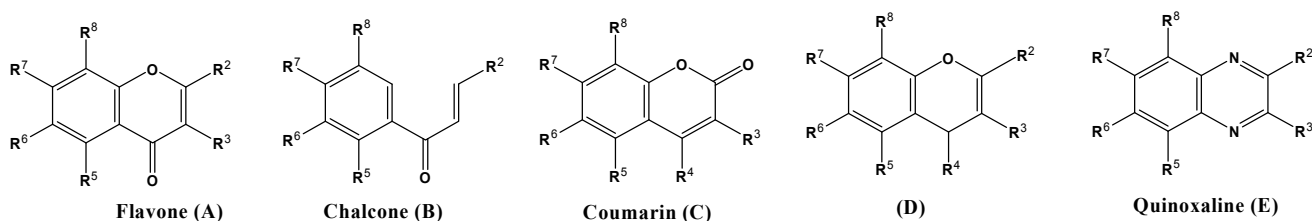


Figure 4.3: IC₅₀ curves of compounds in study for ENT2 inhibition

Table 4.1: Compounds evaluated for ENT inhibition with IC₅₀ values



Compound	Type	R ²	R ³	R ⁴	R ⁵	R ⁶	R ⁷	R ⁸	hENT1 IC ₅₀ (μM)	hENT2 IC ₅₀ (μM)	SI ^a
V	-	-	-	-	-	-	-	-	0.0006 ± 0.0004	0.87 ± 0.01	-
VI	-	-	-	-	-	-	-	-	0.015 ± 0.001	0.32 ± 0.03	-
1	A	4-bromophenyl	H	C=O	H	Cl	CH ₃	H	-	-	-
2	A	4-hydroxyphenyl	OH	C=O	H	H	H	H	-	-	-
3	A	3,4-dihydroxyphenyl	H	C=O	H	H	OH	H	14.08 ± 2.63	1.81 ± 0.46	7.77
4	A	Phenyl	OH	C=O	OH	H	H	H	28.45 ± 2.78	28.19 ± 4.23	1.00
5	A	Phenyl	OH	C=O	H	OH	H	H	22.18 ± 1.78	6.66 ± 2.02	3.33
6	A	Phenyl	OH	C=O	H	H	OH	H	50.31 ± 4.02	-	-
8	A	4-hydroxyphenyl	H	C=O	H	OH	H	H	12.59 ± 2.33	-	-
9	A	Phenyl	H	C=O	H	OH	OH	H	5.58 ± 1.03	8.83 ± 1.37	0.63
10	A	2-hydroxyphenyl	H	C=O	H	H	OH	H	20.10 ± 4.18	27.30 ± 17.60	0.73
11	A	3-hydroxyphenyl	H	C=O	H	H	OH	H	4.84 ± 0.24	11.96 ± 2.21	0.40
12	A	4-hydroxyphenyl	H	C=O	H	H	OH	H	4.00 ± 0.51	7.20 ± 1.36	0.55
13	A	Phenyl	H	C=O	H	H	OH	OH	8.72 ± 1.44	-	-
14	A	4-hydroxyphenyl	H	C=O	OH	H	OCH ₃	H	17.04 ± 1.79	14.01 ± 10.26	1.21
15	A	Phenyl	H	C=O	OH	OH	OCH ₃	H	16.72 ± 5.09	8.49 ± 0.53	1.96
16	A	3,4,5-trimethoxyphenyl	OH	C=O	H	H	OH	H	1.02 ± 0.09	2.81 ± 0.71	0.36
17	A	3-hydroxy-4-methoxyphenyl	H	C=O	OH	OCH ₃	OCH ₃	H	7.27 ± 3.18	14.76 ± 1.79	0.49
18	A	2,3-dimethoxyphenyl	H	C=O	H	H	H	H	16.87 ± 7.27	13.58 ± 2.73	1.27
19	A	4-methoxyphenyl	OCH ₃	C=O	H	H	H	H	2.98 ± 1.17	9.98 ± 2.69	0.29
20	A	3,4-dimethoxyphenyl	H	C=O	H	H	H	H	4.98 ± 1.96	10.77 ± 4.71	0.46
22	A	Phenyl	H	C=O	H	OCH ₃	OCH ₃	H	1.62 ± 0.77	7.65 ± 2.21	0.14
23	A	3,4-dimethoxyphenyl	OH	C=O	H	H	H	H	112.31 ± 7.97	11.45 ± 2.09	9.80

Table 4.1: (continued)

Compound	Type	R ²	R ³	R ⁴	R ⁵	R ⁶	R ⁷	R ⁸	hENT1 IC ₅₀ (μM)	hENT2 IC ₅₀ (μM)	SI ^a
24	A	2,3-dimethoxyphenyl	OH	C=O	H	H	H	H	24.47 ± 5.71	22.42 ± 5.91	1.09
25	A	2,4-dimethoxyphenyl		C=O	H	H	H	H	-	27.24 ± 9.62	-
26	A	2-methoxyphenyl	OH	C=O	H	OCH ₃	H	H	76.30 ± 3.07	-	-
27	A	3-methoxyphenyl	OH	C=O	H	OCH ₃	H	H	137.55 ± 16.70	22.66 ± 5.09	6.07
28	A	4-methoxyphenyl	OH	C=O	H	OCH ₃	H	H	-	-	-
30	A	3-methoxyphenyl	OH	C=O	H	H	OCH ₃	H	104.33 ± 12.02	11.44 ± 1.51	9.11
31	A	2,4-dimethoxyphenyl	OH	C=O	H	CH ₃	H	H	-	26.09 ± 6.56	-
32	A	3,4-dimethoxyphenyl	OH	C=O	H	CH ₃	H	H	-	-	-
33	A	3,4-dimethoxyphenyl	H	C=O	OH	OCH ₃	OCH ₃	H	-	-	-
34	A	3,4-dihydroxyphenyl	OH	C=O	H	H	OH	H	28.92 ± 1.26	8.11 ± 1.90	3.56
35	A	3,4,5-trimethoxyphenyl	H	C=O	OH	OCH ₃	OCH ₃	OCH ₃	4.65 ± 0.82	1.77 ± 0.64	2.62
36	A	3,4,-dihydroxyphenyl	OH	C=O	OH	H	OH	OH	-	-	-
37	A	3,4,-dihydroxyphenyl	OH	C=O	OH	H	OH	OGlu	-	-	-
38	A	3,4,5-trimethoxyphenyl	H	C=O	OCH ₃	OCH ₃	OCH ₃	H	-	-	-
39	A	Phenyl	H	C=O	H	OH	OCH ₃	H	-	-	-
40	A	4-methoxyphenyl	H	C=O	H	H	OH	H	32.83 ± 4.39	-	-
41	A	3,4,5-trimethoxyphenyl	OH	C=O	H	H	OCH ₃	H	19.05 ± 0.91	9.51 ± 2.14	2.00
42	A	3,4,5-trimethoxyphenyl	OH	C=O	H	H	H	H	7.17 ± 1.51	12.49 ± 1.97	0.57
43	B	2-hydroxy-4-methoxyphenyl	-	C=O	H	OCH ₃	H	H	5.71 ± 0.45	-	-
44	B	3,4-Dimethoxy-2-hydroxyphenyl	-	C=O	H	H	H	H	3.64 ± 0.39	9.98 ± 1.34	0.36
45	B	2-hydroxy-4-methoxyphenyl	-	C=O	H	H	OCH ₃	H	101.93 ± 6.76	16.82 ± 4.38	6.06
46	B	2-hydroxy-5-methylphenyl	-	C=O	OCH ₃	H	OCH ₃	H	9.71 ± 0.23	-	-
47	B	2-hydroxy-5-methylphenyl	-	C=O	OCH ₃	H	H	OCH ₃	11.85 ± 0.62	-	-
48	A	2-phenyl	H	C=O	OH	OH	OH	H	7.01 ± 1.33	8.22 ± 2.09	0.85
49	A	3-hydroxyphenyl	H	C=O	H	H	OH	OH	-	-	-
50	A	4-hydroxyphenyl	H	C=O	H	H	OH	OH	10.61 ± 0.49	17.79 ± 3.57	0.59
51	A	3,4-dihydroxyphenyl	H	C=O	H	H	OH	OH	13.71 ± 1.12	63.94 ± 11.05	0.21
52	A	Phenyl	H	C=O	OH	OH	H	H	14.88 ± 1.43	-	-
53	A	3-hydroxyphenyl	H	C=O	H	H	OH	H	20.04 ± 0.37	7.23 ± 1.89	2.77

Table 4.1: (continued)





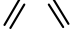

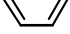

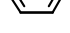

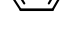
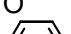

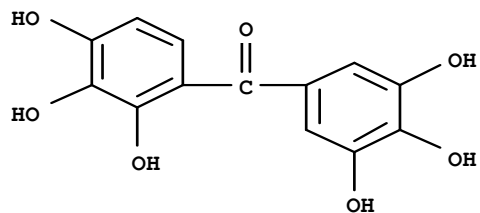
Compound	Type	R ²	R ³	R ⁴	R ⁵	R ⁶	R ⁷	R ⁸	hENT1 IC ₅₀ (μM)	hENT2 IC ₅₀ (μM)	SI ^a
54	A	3,4-dihydroxyphenyl	H	C=O	H	H			20.28 ± 0.78	-	-
55	A	Phenyl	H	C=O	H	H	OCH ₃	OCH ₃	6.24 ± 0.21	12.98 ± 1.86	0.48
56	A	Phenyl	H	C=O	H	H	OCH ₃	OH	5.68 ± 0.36	41.71 ± 2.09	0.13
57	A	2-hydroxyphenyl	H	C=O	H	H	OH	OH	7.40 ± 0.24	-	-
58	A	H	4-chloro phenyl	C=O	H	H	OH	CH ₃	-	-	-
59	A	H	phenyl	C=O	H	H	OH	CH ₃	-	-	-
60	A	Phenyl	H	C=O			H	H	-	-	-
61	A	Phenyl	H	C=O	H	H			15.36 ± 1.69	-	-
62	A	3,4-dihydroxyphenyl	H	C=O			H	H	-	-	-
63	A	3,4-dimethoxyphenyl	H	C=O	H	H			2.65 ± 0.36	6.29 ± 0.87	0.42
64	A	2-hydroxyphenyl	H	C=O	H	H			-	-	-
65	A	2-hydroxyphenyl	H	C=O			H	H	-	-	-
66	A	3-hydroxyphenyl	H	C=O	H	H			3.32 ± 0.26	50.82 ± 7.13	0.06
67	A	3-hydroxyphenyl	H	C=O			H	H	-	100.23 ± 10.19	-
68	A	4-hydroxyphenyl	H	C=O	H	H			-	-	-
69	A	4-hydroxyphenyl	H	C=O			H	H	-	-	-
70	A	2-phenyl	OCH ₃	C=O	H	H			-	129.59 ± 13.85	-
71	A	4-methoxyphenyl	H	C=O	H	H			32.71 ± 1.89	-	-
72	A	3,4,5-trihydroxyphenyl	H	C=O	OH	H	OH	H	6.46 ± 0.31	2.95 ± 0.79	2.18
73	A	4-hydroxyphenyl	H	C=O	H	H	OH	OGlu	-	-	-
74	A	H	(1-phenyl-1H- pyrazol-4-yl)	C=O	H	H	OH	OH	-	-	-
75	A	Phenyl	H	C=O	H	H	H	H	-	-	-
77	A	Phenyl	H	C=O	H	Cl	Cl	H	-	-	-

Table 4.1: (continued)

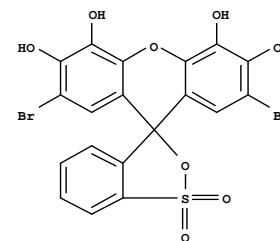
Compound	Type	R ²	R ³	R ⁴	R ⁵	R ⁶	R ⁷	R ⁸	hENT1 IC ₅₀ (μM)	hENT2 IC ₅₀ (μM)	SI ^a
78	A	H	4-chloro Phenoxy	C=O	H	H	OH	OH	10.08 ± 0.17	-	-
79	A	H	4-Fluoro phenoxy phenyl	C=O	H	H	OH	OH	11.38 ± 0.88	-	-
80	A	Methyl	phenyl	C=O	H	H	OH	OH	-	52.54 ± 3.66	-
81	A	H	phenyl	C=O	H	OH	OH	H	-	-	-
82	A	H	phenyl	C=O	H	H	OH	OH	-	-	-
83	A	H	(4-CH ₃ -2- thiazoyl)	C=O	H	H	OH	OH	10.80 ± 0.83	-	-
84	A	3,4,5-trihydroxyphenyl	OH	C=O	H	H	OH	H	26.81 ± 2.14	55.09 ± 8.62	0.48
85	A	3,4,5-trihydroxyphenyl	H	C=O	H	H	OH	H	-	16.14 ± 5.10	-
86 ^b	-	-	-	-	-	-	-	-	-	-	-
87 ^c	-	-	-	-	-	-	-	-	-	-	-
88	C	C=O	H	CH ₃	H	H	OH	NO ₂	-	-	-
89	C	C=O	4'-methoxy phenyl	CH ₂	H	H	OH	H	25.07 ± 4.46	-	-
90	C	C=O	Phenyl	CH ₂	H	OCH ₃	H	H	-	-	-
91	C	C=O	Phenyl	CH ₂	H	H	OCH ₃	H	38.27 ± 0.13	49.43 ± 26.09	0.77
92	C	C=O	H	CH ₂	H		OH	OH	83.79 ± 4.57	-	-
93	C	C=O	H	CH- phenyl	H	OH	OCH ₃	H	5.92 ± 1.73	10.81 ± 1.41	0.54
94	D	2-methyl	H	H	H	H	NH ₂	H	16.30 ± 0.59	-	-
95	C	C=O	Phenyl	OH	OH	H	OH	H	2.24 ± 0.66	-	-
96	D	2-NH ₂	CN	Pyridin -4-yl	H	H	OH	H	5.68 ± 0.46	1.77 ± 0.15	3.20
97	D	H	Phenoxy	H	H	H	OH	OH	46.47 ± 3.20	-	-
99	D	2-methyl	4'-nitro phenoxy	H	H	H	OCH ₃	CH ₃	9.08 ± 0.35	-	-
100	E	2-Phenyl	H	N	H	OCH ₃	OCH ₃	H	0.13 ± 0.03	4.89 ± 0.44	0.02

^aENT2 selectivity index (ENT1_{IC50} / ENT2_{IC50})

Table 4.1: (continued)



^bCompound 86 (2,3,4,3',4',5'-hexahydroxybenzophenone)



^cCompound 87 (Bromopyrogallol red)

4.3 3-D QSAR Analyses

Quantitative structure activity relationship (QSAR) is a statistical process by which the physicochemical properties and/or structural descriptors of a molecule are correlated with its biological activity. Classical QSAR techniques usually consider the 2D structures of the molecules. The orientation of various moieties on the molecule and their interrelationship with each other and with interaction sites on the receptor contribute to the biological activity. Hence, QSAR methods based on the 3D structures would provide more detailed information regarding the drug receptor interaction than 2D-QSAR methods. In this chapter, we report a comprehensive 3D-QSAR study on a series of 95 flavones, chalcones and coumarin derivatives.

4.3.1 Materials and Methods

The biological activity data obtained for the SAR study was used to carry out 3D-QSAR analyses. The structures of the compounds and activity values (IC_{50} values) are shown in Table 4.1. The IC_{50} values were transformed into K_i and then to pK_i values, which were used as the dependent variable in CoMFA¹⁴³ and CoMSIA¹⁴⁴ analyses.

4.3.2 Molecular Modeling

Three-dimensional structure building and all modeling operations were performed using SYBYL 7.3 (Tripos Associates Inc.)¹⁴⁵ running on a Silicon Graphics Octane workstation. MOPAC charges were assigned to all molecules. Energy minimization was performed using the Tripos force field with a distance dependent dielectric and the BFGS algorithm, with a convergence criterion of 0.01 kcal/(mole* Å). Compounds in the data set were aligned using the MATCH module in SYBYL. Reference atoms selected for alignment are shown in Figure 4.4, and molecular alignment is shown in Figure 4.5.

4.3.3 CoMFA and CoMSIA Models

3D-QSAR analyses were performed in a stepwise manner. The 95 compounds were aligned to the common alignment template. For deriving the CoMFA and CoMSIA descriptor fields, the molecules were placed in a three dimensional cubic lattice with a spacing of 2 Å, and extending 4 Å units beyond the aligned molecules in all directions. CoMFA descriptors were calculated using an sp^3 carbon probe atom with a van der Waals radius of 1.52 Å and a charge of +1 with a distance dependent dielectric to generate steric (Lennard-Jones 6-12 potential) field energies and electrostatic (Coulombic potential) fields with a distance-dependent dielectric at each lattice point. An energy cutoff of 30 kcal/mole was applied. The CoMFA steric and electrostatic fields were scaled by the CoMFA-STD method in SYBYL. CoMSIA similarity index descriptors were calculated using a similar lattice box as in CoMFA. CoMSIA similarity index descriptors were

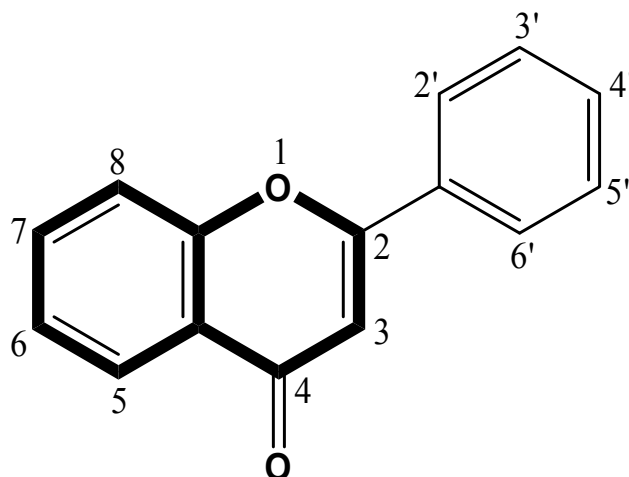


Figure 4.4: Atoms used in MATCH alignment shown in bold face

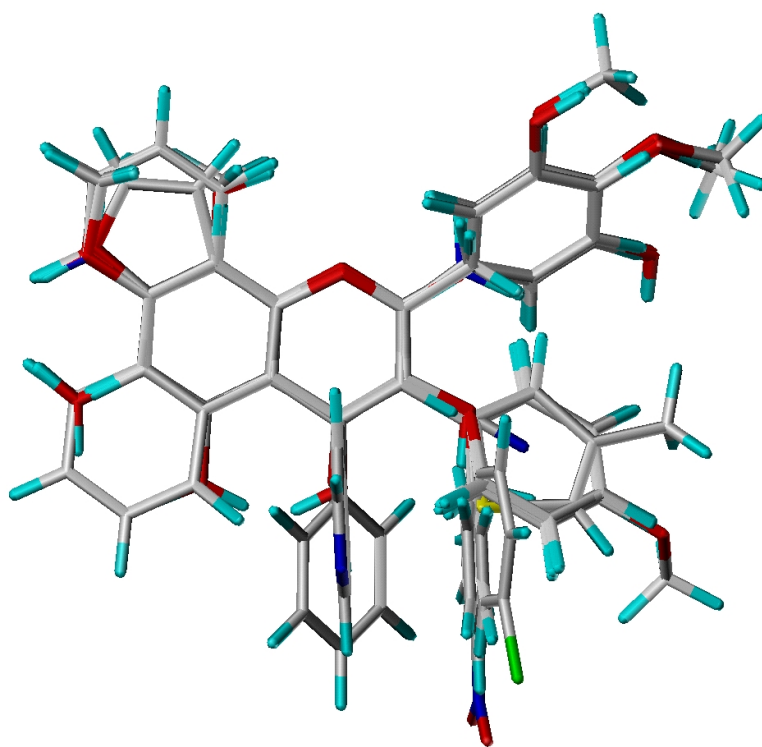


Figure 4.5: Atom-by-atom superposition used for 3D-QSAR analysis

For atom colors, red indicates oxygen, yellow refers to sulfur, white indicates carbon, green indicates fluorine or chlorine and cyan indicates hydrogen.

derived according to Klebe *et al.*¹⁴⁴ The CoMSIA descriptors, namely, steric, electrostatic, hydrophobic, hydrogen bond donor, and hydrogen bond acceptor, were generated using a sp³ carbon probe atom with +1 charge and a van der Waals radius of 1.4 Å. The value of the attenuation factor (α) was set to 0.3. CoMSIA steric indices are related to the third power of the atomic radii, the electrostatic descriptors are derived from atomic partial charges, the hydrophobic fields are derived from atom-based parameters developed by Viswanadhan *et al.*¹⁴⁶, and hydrogen bond donor and acceptor indices are obtained from a rule-based method based on experimental data.

Using CoMFA and CoMSIA descriptors as independent variables and p*K*_i values as dependent variables, partial least squares (PLS) regression analyses were carried out, using the QSAR module of the SYBYL package with default parameters. Leave-one-out (LOO) cross-validation was used to evaluate the predictive ability of the models. The cross-validated coefficient, q^2 , was calculated using Equation 4.2.

$$q^2 = 1 - \frac{\sum(Y_{\text{predicted}} - Y_{\text{actual}})^2}{\sum(Y_{\text{observed}} - Y_{\text{mean}})^2} \quad (\text{Eq. 4.2})$$

where $Y_{\text{predicted}}$, Y_{actual} , and Y_{mean} are predicted, actual and mean values of the target property (p*K*_i), respectively. $\sum(Y_{\text{predicted}} - Y_{\text{actual}})^2$ is the predictive sum of squares (PRESS). The optimum number of components used to derive the final regression models was the one that corresponds to the lowest PRESS value. In addition to the q^2 , the corresponding PRESS, the conventional correlation coefficient (r^2) and its standard error (s) were also calculated.

4.3.4 Results of 3D-QSAR Analyses

CoMFA and CoMSIA 3D-QSAR studies were undertaken to determine the effects of steric, electrostatic, hydrophobic, and hydrogen bonding properties of the compounds on different hENT nucleoside transporter inhibitory activity, and to obtain reliable models for predicting the activity of compounds. The results obtained from PLS regression analysis, using CoMFA steric and electrostatic descriptors as independent variables are shown in Tables 4.2 and 4.3, respectively. Similarly, PLS statistics obtained from CoMSIA analysis are also shown in the same tables. The stability of the models was evaluated by performing group cross-validation (30 runs), and bootstrapping (20 runs). To eliminate the possibility of chance correlation, PLS analysis was carried out using scrambled activity data (20 runs) i.e. randomization was done. The results of these validations are shown in Table 4.4. CoMFA and CoMSIA coefficient contour maps were generated by interpolation of the pair-wise products between the PLS coefficients and the standard deviations of the corresponding CoMFA and CoMSIA descriptor values.

Both the CoMFA and CoMSIA models have fairly good cross validated q^2 and non-validated r^2 values as shown in Table 4.2. The non-validated r^2 value of the CoMSIA model is similar to that of the CoMFA model of both transporters. However, if the q^2

Table 4.2: PLS statistics of CoMFA and CoMSIA 3D-QSAR models for ENT

Transporter Type	hENT1		hENT2	
	CoMFA	CoMSIA	CoMFA	CoMSIA
PLS statistics				
q^2 (LOO)	0.585	0.523	0.510	0.565
r^2	0.937	0.928	0.870	0.957
<i>S</i>	0.120	0.129	0.177	0.107
F	92.36	75.386	51.875	96.971
PLS components	6	6	4	6
Total no. of compounds used for analysis	61		45	
No. of outliers	12	14	5	8
Outlier Compounds	10,19,27,30,35,41,45,51,54,96,97,100	10,22,23,35,40,41,45,54,71,91,95,96,97,100	17,18,19,27,84	17,19,22,27,51,53,84,85
No. of compounds in training set	44	42	36	33
No. of compounds in test set	5	5	4	4
Test set compounds	4,11,61,89,99	4,11,17,46,99	4,14,41,56	4,12,55,100

q^2 = cross validated correlation coefficient; *s* = standard error; r^2 = non-validated correlation coefficient; F = F-test value.

Table 4.3: Field contribution by CoMFA and CoMSIA descriptors for ENT

Descriptor	hENT1		hENT2	
	CoMFA	CoMSIA	CoMFA	CoMSIA
Steric	0.402	0.113	0.315	0.092
Electrostatic	0.598	0.322	0.685	0.404
Hydrophobic	-----	0.144	-----	0.175
Donor	-----	0.251	-----	0.204
Acceptor	-----	0.169	-----	0.125

Table 4.4: Results of group cross validation, randomization and bootstrapping for ENT

Method	hENT1		hENT2	
	CoMFA	CoMSIA	CoMFA	CoMSIA
Group validation q^2 (30 groups and 30 runs)	0.556 ± 0.019	0.518 ± 0.025	0.507 ± 0.056	0.554 ± 0.023
Randomization q^2 (20 runs)	- 0.155	- 0.223	- 0.109	- 0.068
Bootstrapping (20 runs) 1. r^2	0.945 ± 0.021	0.956 ± 0.012	0.909 ± 0.038	0.978 ± 0.013
2. SD	0.110 ± 0.063	0.103 ± 0.062	0.149 ± 0.087	0.077 ± 0.058

q^2 = cross validated correlation coefficient; r^2 = non-validated correlation coefficient; SD = standard deviation.

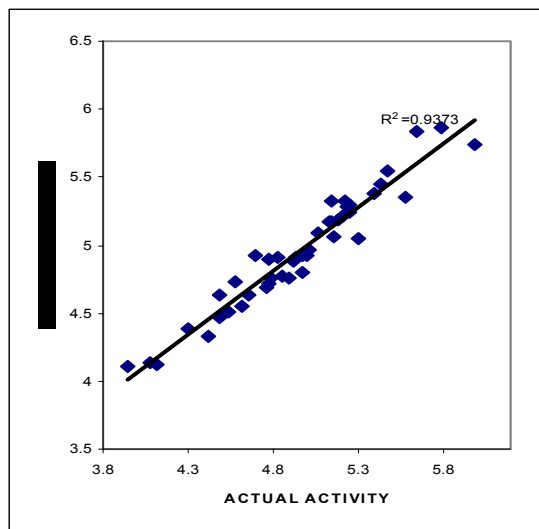
values are compared, the hENT1 CoMFA and hENT2 CoMSIA models appear to be better than the remaining two models. Outliers were decided on the basis of q^2 by the leave-one-out method to arrive at a value more than or equal to 0.5. Also, other methods such as factor analysis and region focusing were applied to obtain significant PLS statistics. From Table 4.2, it can be seen that some of the compounds are common outliers in all the four models. The possible reasons for compounds to be outliers are given in Chapter 3 such as, improper alignment, inappropriate activity data, metabolism, etc. Compounds belonging to the test set were picked selectively to cover a wide range of activity. The prediction curves for both CoMFA and CoMSIA, as shown in Figures 4.6, 4.7, 4.8, and 4.9, are the graphs of the predicted activity vs. actual activity. All graphs show well-scattered compounds around the regression line, which indicates that the models are good. The predicted activities with residuals are shown in Table 4.5.

The derived models were further evaluated by using them to predict the activities of external test compounds **101**, **102**, **104**, **105**, **113**, **114** and **115**, all of which belong to flavone class and were not used to derive the forementioned models. Table 4.6 shows their predicted activities with residuals, while the $R^2_{\text{predictivity}}$ for the models are listed in Table 4.7. The prediction curves are presented in Figures 4.10 and 4.11.

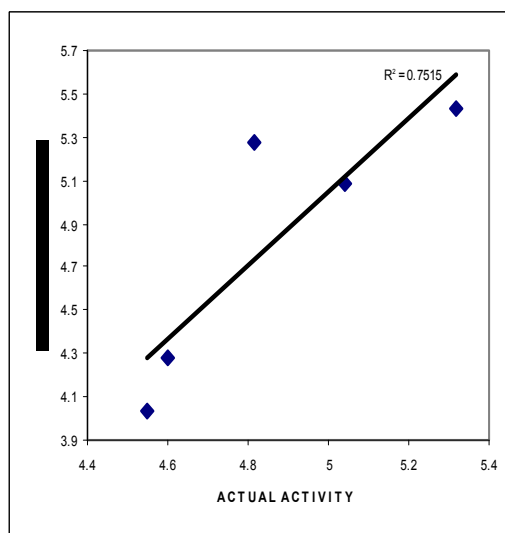
From Table 4.7, it can be seen that all models can predict fairly well, and the predictive ability of the CoMFA model for ENT2 is the best. One residual value in Tables 4.5 and 4.6 is more than 0.5 log in the CoMFA models of ENT1 and ENT2, respectively, which is the cause of the lower R^2_{pred} for those models. Since the number of compounds included in the test set is low, the R^2_{pred} values are probably too optimistic. Similarly, the results from Table 4.7 can be summarized by stating that all the models have fairly good predictive abilities for external test compounds, which signifies the importance and validity of models generated for future use in prediction of activities of various molecules belonging to the same or similar chemical class as the flavones.

4.3.5 PLS Contour Maps

Contour maps were generated by plotting the coefficients from CoMFA and CoMSIA QSAR models, which indicate regions in 3D space around the molecules where changes in the particular physicochemical properties are predicted to increase or decrease potency. The steric and electrostatic contours for the CoMFA and CoMSIA models, and hydrophobic and hydrogen bond contours for the CoMSIA model for hENT transporter inhibition, projected onto compound **16**, are shown in Figures 4.12 and 4.13, respectively. General color coding for the contour maps are as follows: 1) steric and electrostatic contours: green contours indicate sterically favored regions whereas the yellow contours denote sterically unfavorable regions. The blue contours identify regions that favor electropositive substituents and the red regions favor electronegative substituents. 2) Hydrophobic, hydrogen bond donor and hydrogen bond acceptor contours: yellow contours indicate regions where hydrophobic groups are favored whereas the white contours denote regions that disfavor hydrophobic groups. The cyan and purple contours indicate favorable and unfavorable regions for hydrogen bond donors, respectively. The

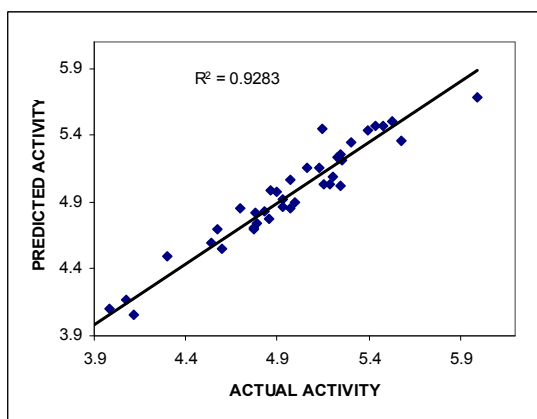


CoMFA Training

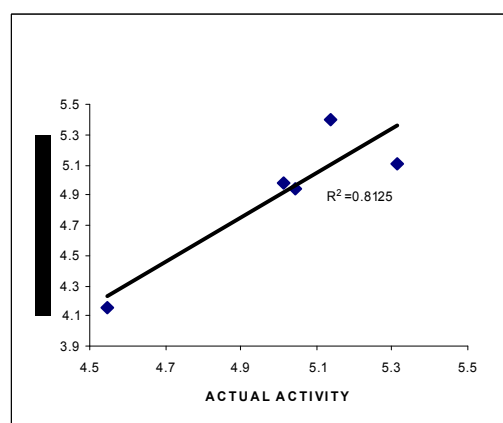


CoMFA Test

Figure 4.6: Predicted vs actual pK_i graphs for CoMFA training set and test set for hENT1 inhibition



CoMSIA Training



CoMSIA Test

Figure 4.7: Predicted vs actual pK_i graphs for CoMSIA training set and test set for hENT1 inhibition

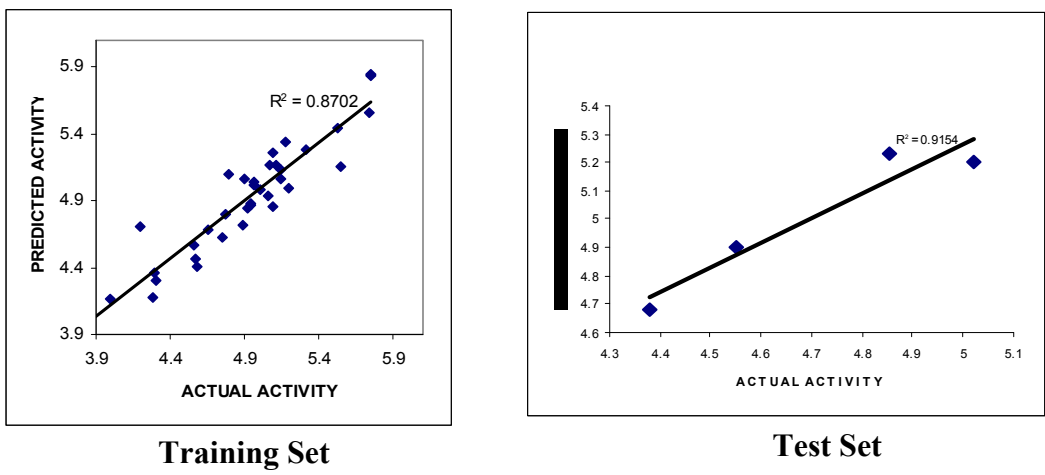


Figure 4.8: Predicted vs actual pK_i graphs for CoMFA training set and test set for hENT2 inhibition

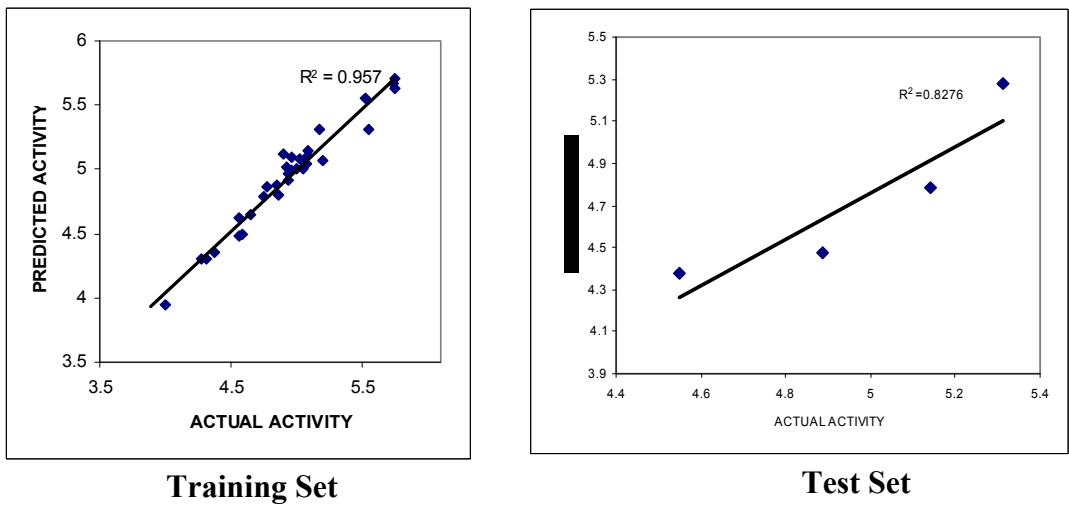


Figure 4.9: Predicted vs actual pK_i graphs for CoMSIA training set and test set for hENT2 inhibition

Table 4.5: Residuals of predictions of internal test set by CoMFA and CoMSIA models for hENT1 and hENT2 inhibition**ENT1**

Compound number	Actual pK_i	Predicted CoMFA pK_i	CoMFA Residuals	Compound number	Actual pK_i	Predicted CoMSIA pK_i	CoMSIA Residuals
61	4.81	5.28	-0.46	4	4.54	4.14	0.39
89	4.60	4.27	0.32	99	5.04	4.93	0.10
11	5.31	5.43	-0.12	11	5.31	5.10	0.20
4	4.54	4.03	0.51 ^a	17	5.13	5.39	-0.25
99	5.04	5.08	-0.04	46	5.01	4.97	0.03

ENT2

Compound number	Actual pK_i	Predicted CoMFA pK_i	CoMFA Residuals	Compound number	Actual pK_i	Predicted CoMSIA pK_i	CoMSIA Residuals
41	5.02	5.20	-0.18	4	4.55	4.37	0.17
56	4.38	4.68	-0.30	12	5.14	4.78	0.35
4	4.55	4.90	-0.35	100	5.31	5.27	0.03
14	4.85	5.22	-0.37	55	4.88	4.47	0.41

^aThe residual values greater than 0.5 is responsible for the low predictivity of the respective models.

Table 4.6: Residuals of predictions of external test set by CoMFA and CoMSIA models for hENT1 and hENT2 inhibition

ENT1							
Compound number	Actual pK_i	Predicted CoMFA pK_i	CoMFA Residuals	Compound number	Actual pK_i	Predicted CoMSIA pK_i	CoMSIA Residuals
101	6.01	5.90	0.11	101	6.01	6.40	-0.38
102	5.71	5.48	0.22	102	5.71	5.35	0.35
104	5.56	5.54	0.02	103	5.56	5.42	0.13
105	5.29	5.22	0.06	105	5.29	5.39	-0.09
113	5.63	5.56	0.06	113	5.63	5.46	0.16
114	5.56	5.32	0.24	114	5.56	5.35	0.20
115	5.38	5.01	0.36	115	5.38	5.22	0.15

ENT2							
Compound Number	Actual pK_i	Predicted CoMFA pK_i	CoMFA Residuals	Compound number	Actual pK_i	Predicted CoMSIA pK_i	CoMSIA Residuals
101	5.11	5.14	-0.02	101	5.11	5.33	-0.21
102	4.94	5.01	-0.07	102	4.94	5.05	-0.10
103	5.02	5.18	-0.15	103	5.02	5.38	-0.35
104	4.83	4.17	0.65 ^a	105	4.83	4.78	0.04
113	5.28	5.23	0.04	113	5.28	5.27	0.01
114	5.24	5.23	0.01	114	5.24	5.45	-0.21
115	5.16	5.11	0.05	115	5.16	5.16	-0.18

^aThe residual values greater than 0.5 is responsible for the low predictivity of the respective models.

Table 4.7: R^2 predictivity of the internal and external test sets by CoMFA and CoMSIA models for hENT1 and hENT2 inhibition

	hENT1		hENT2	
	CoMFA	CoMSIA	CoMFA	CoMSIA
R^2 predictivity for Internal Test set	0.75	0.81	0.91	0.82
R^2 predictivity for External Test set	0.81	0.67	0.63	0.65

R^2 predictivity = Correlation coefficient for predictive ability

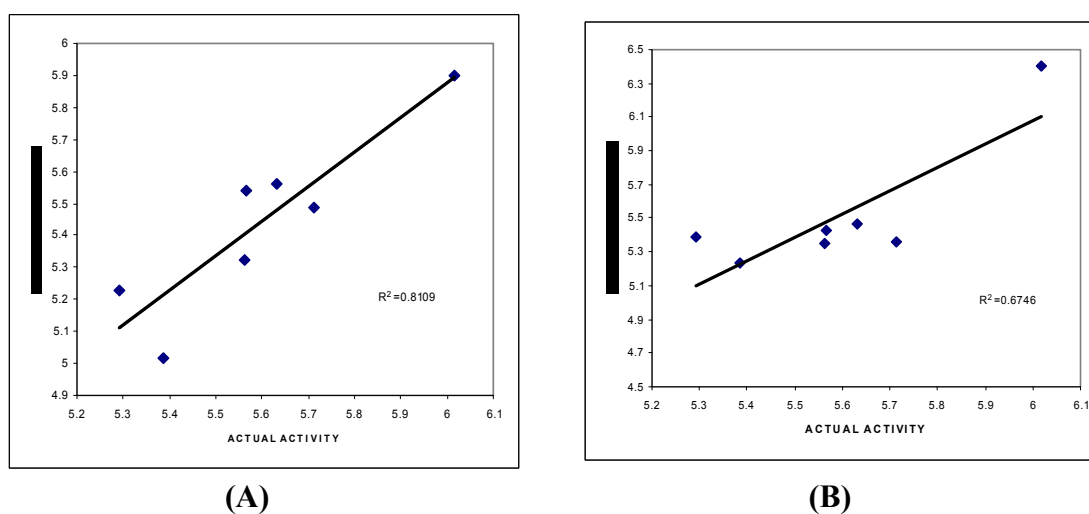


Figure 4.10: Predicted vs actual pK_i graphs for external test set for hENT1 inhibition (A) CoMFA and (B) CoMSIA

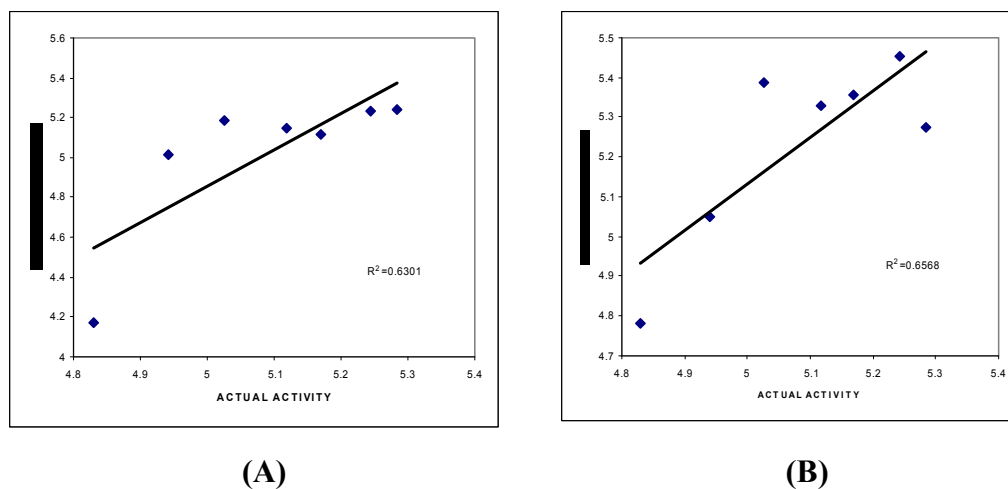


Figure 4.11: Predicted vs actual pK_i graphs for external test set for hENT2 inhibition (A) CoMFA and (B) CoMSIA

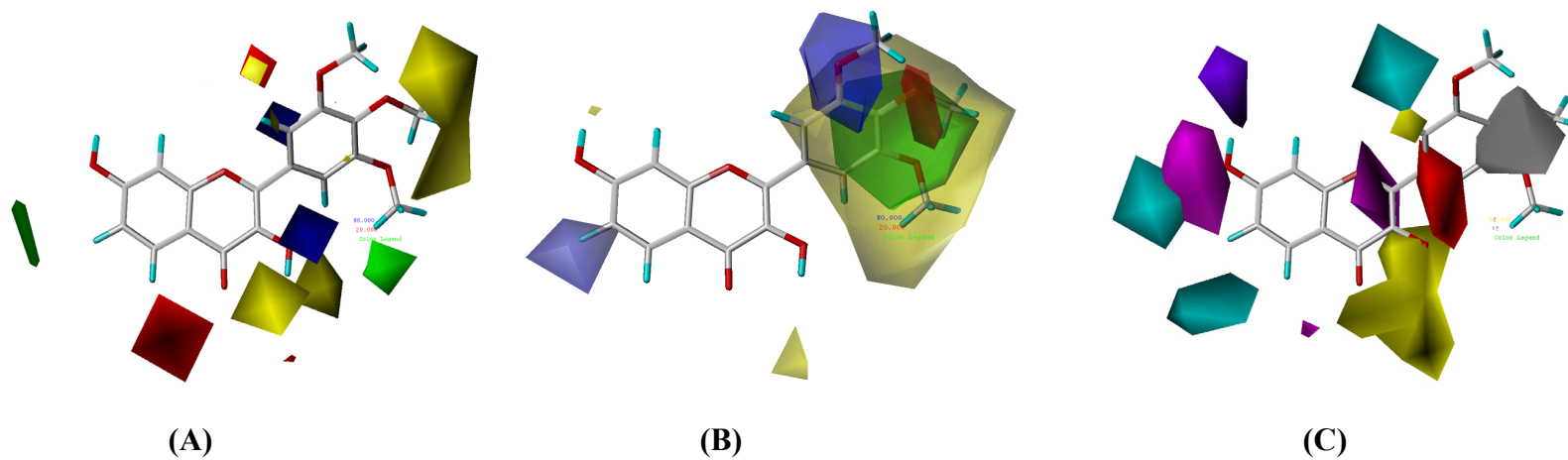


Figure 4.12: PLS contours from CoMFA steric and electrostatic (A), CoMSIA steric and electrostatic (B) and CoMSIA hydrophobic and hydrogen bond donor and acceptor (C) descriptors for hENT1 transporter inhibitors

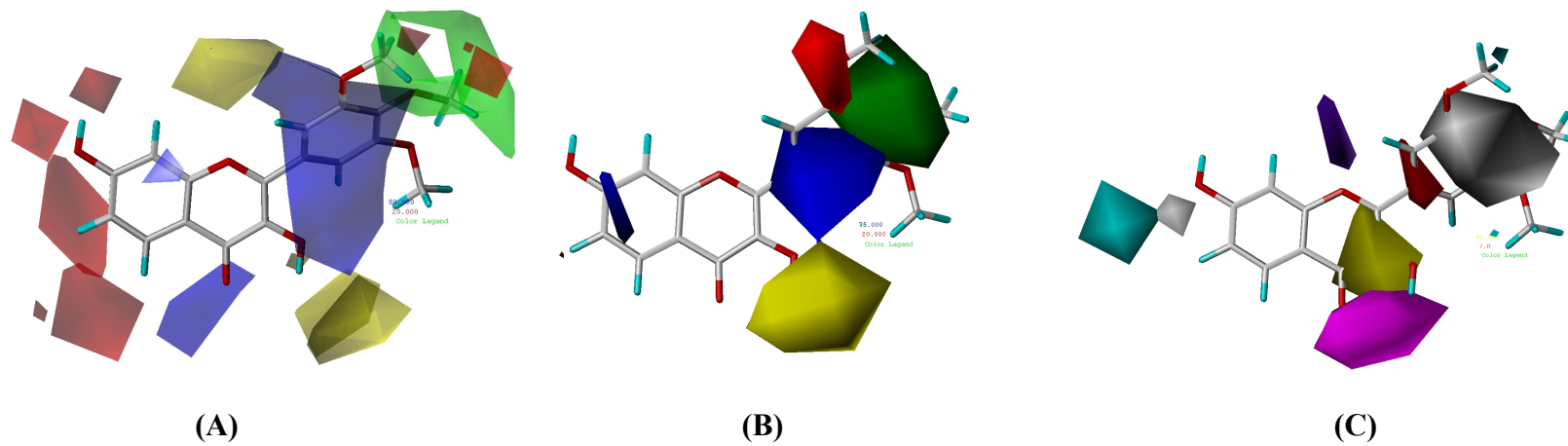


Figure 4.13: PLS contours from CoMFA steric and electrostatic (A), CoMSIA steric and electrostatic (B) and CoMSIA hydrophobic and hydrogen bond donor and acceptor (C) descriptors for hENT2 transporter inhibitors

magenta and red contours identify favorable and unfavorable positions for hydrogen bond acceptors, respectively.

4.3.5.1 PLS Contour Interpretation for ENT1 CoMFA

The extended yellow contour surrounding the 4'-position suggests that groups large groups are not tolerated at this region. The green contours near the 5'-position and between positions 6 and 7 indicate room for bulky groups. There is also a large yellow contour near the 3-position, marking a sterically unfavorable region. Two small blue contours at 3- and in between 2'- and 3'- positions show a possible site for occupancy by electropositive groups. Red contours at the 5-position and near the 3'-position suggest favourable regions for electronegative substituents (Figure 4.12A).

4.3.5.2 PLS Contour Interpretation for ENT1 CoMSIA

A green contour surrounded by a large yellow one at 3'-, 4'-, and 5'-positions suggest that methoxy is an optimum group for inhibitory activity and groups larger than that are not tolerated. A large red contour occupying 4'-position indicates that an electronegative group is favored there. Positions 3' and 6 blue contours indicate electropositively favored regions (Figure 4.12B).

A large yellow contour at the 3- and 4- positions indicates a strong positive contribution by a hydrophobic group. The white contour near positions 4'- and 5'- shows that this part of the molecule disfavors hydrophobic groups. A cyan contour near the 2'-, 5-, 6-, and 7- positions, and a magenta contour near the 7- and 1- position oxygens depict regions favoring H-bond donor and H-bond acceptor substituents, respectively. The red and purple contours near positions 1' and 6' and between positions 7 and 8, respectively, denote parts of the molecule that neither favor H-bond donor nor H-bond acceptor groups, respectively (Figure 4.12C).

4.3.5.3 PLS Contour Interpretation for ENT2 CoMFA

A green contour near the 3'- and 4'- positions of the 2-phenyl ring indicates that the positions are favorable to sterically bulky groups. Four distinct red contours occur near positions 5, 6, 7 and 8, showing that electronegative groups are favored. Blue contours at position 4 and over the entire 2-phenyl ring, indicate that electropositive groups are favored in that region. Positions 1 and 3' do not tolerate bulky groups (Figure 4.13A).

4.3.5.4 PLS Contour Interpretation for ENT2 CoMSIA

A red contour at the 3'-position indicates an area that favors electronegative groups. A large green contour on the 2-phenyl ring and a yellow one near position 3 indicate sterically favored and disfavored regions, respectively. A large blue contour occupying half of the 2-phenyl ring at positions 1', 5' and 6' suggests positions which favor electropositive substituents (Figure 4.13B).

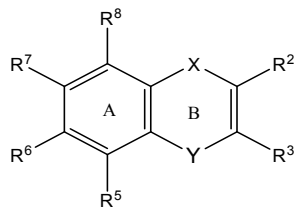
The yellow contour shielding positions 2 and 3 signifies favorable positions for hydrophobic groups. A hydrophobically unfavorable region around positions 3', 4' and 5' is indicated by a white contour, one of which also appears between the 6- and 7-positions. A cyan contour at the 7-position shows a region that favors H-bond donors. A purple contour near position 1 indicates no room for a H-bond acceptor. A magenta contour occurring near positions 3 and 4 predicts favorable sites for H-bond acceptors (Figure 4.13C).

To put the significance of the PLS contour maps (isopleths) for equilibrative nucleoside transporters in general terms, for both ENT1 and ENT2, (i) substitution at positions 3', 4' and 5' of the 2-phenyl ring with methoxy groups increases activity, (ii) position 7 favors H-bond donor groups in both transporters but in the case of ENT1, position 7 is also suitable for H-bond acceptors and (iii) CoMSIA contours of both ENTs suggest that position 3 can tolerate hydrophobic substituents very well and that the *meta* and *para* positions of the 2-phenyl ring should not be substituted with group bulkier than a methoxy group. With regard to differences between the two transporters, the flavone 4-position prefers electronegative substituents for ENT1 inhibition, whereas electropositive or H-bond acceptor groups are preferred for ENT2 inhibition as seen from CoMFA and CoMSIA contours.

4.4 Activity Prediction of *In silico* Designed Compounds Using 3D-QSAR Models for hENT

The 3D-QSAR models were used to predict the activity of *in silico* designed molecules, before testing them to have an idea of how active the compounds will be with a particular structural modification. Since all the models obtained have been validated with both internal and external test sets, these models were used to predict the activities for designed molecules listed in Table 4.8. Looking at Table 4.8, it can be seen that some of the designed molecules are predicted to be more or equally active on specified nucleoside transporters. Comparing the predicted activities with already tested compounds with high ENT1 inhibitory activity, i.e., compound **16** ($pK_i = 5.9897$), compound **95** ($pK_i = 5.6494$) and compound **100** ($pK_i = 6.8794$), the compounds whose activities have been highlighted (**Pred 14**, **Pred 25**, **Pred 26**, **Pred 28**, **Pred 29**, **Pred 31**, **Pred 32**, **Pred 34**, **Pred 37**, **Pred 43** and **Pred 46**) potentially serve as new lead compounds. Similarly, designed compounds designated as **Pred 25**, **Pred 37** and **Pred 43** were compared with flavones with high activity such as compound **35** ($pK_i = 5.7523$) and

Table 4.8: Predicted activities for *in silico* designed compounds



Compound	X	R ²	R ³	Y	R ⁵	R ⁶	R ⁷	R ⁸	hENT1		hENT2	
									p <i>K</i> _i (μM)		p <i>K</i> _i (μM)	
									CoMFA	CoMSIA	CoMFA	CoMSIA
Pred 1	O	3-hydroxyphenyl	NH ₂	C=O	H	H	OH	OH	4.9667	4.4316	4.6229	4.9167
Pred 2	O	3-hydroxyphenyl	CN	C=O	H	H	OH	OH	5.1387	4.7842	4.7141	4.8779
Pred 3	O	3-hydroxyphenyl	H	C=O	H	H	OH	Acetyl	5.4279	5.2625	4.7352	5.0758
Pred 4	O	3-hydroxyphenyl	H	C=O	H	H	OH	N ₃	5.4430	5.1467	4.5908	5.0876
Pred 5	O	3-hydroxyphenyl	H	C=O	H	H	OH	Br	5.5202	5.0942	4.5894	4.9482
Pred 6	O	3-hydroxyphenyl	H	C=O	H	H	OH	Cl	5.5435	5.0951	4.6194	5.0499
Pred 7	O	3-hydroxyphenyl	H	C=O	H	H	OH	CN	5.5743	5.1164	4.6451	5.1280
Pred 8	O	3-hydroxyphenyl	H	C=O	H	H	OH	F	5.5001	5.1182	4.7125	5.0579
Pred 9	O	3-hydroxyphenyl	H	C=O	H	H	OH	Formyl	5.4590	5.1034	4.6204	5.0973
Pred 10	O	3-hydroxyphenyl	H	C=O	H	H	OH	I	5.5002	5.1064	4.5704	4.8531
Pred 11	O	3-hydroxyphenyl	H	C=O	H	H	OH	NO ₂	5.5812	5.2895	4.7178	5.2978
Pred 12	O	3-hydroxyphenyl	H	CH ₂	H	H	OH	OH	4.8592	4.7553	4.7470	4.8403
Pred 13	O	3-hydroxyphenyl	H	CH ₂	H	CH ₃	OH	OH	5.0886	4.7025	4.7809	4.8471
Pred 14	O	3-hydroxyphenyl	H	C=O	H	Tetrahydro isoquinolino		H	5.8309	4.4444	4.6323	4.8206
Pred 15	O	3-hydroxyphenyl	NH ₂	CH ₂	H	H	OH	OH	4.4106	4.2022	4.7928	4.7836
Pred 16	O	3-hydroxyphenyl	H	C=O	H	H	NH ₂	OH	5.4354	4.6931	4.6446	5.0729
Pred 17	O	3-hydroxyphenyl	H	CH ₂	H	OCH ₃	OH	OH	4.8773	4.6013	4.9241	5.1276
Pred 18	O	3-hydroxyphenyl	NH ₂	CH ₂	H	CN	OH	OH	4.5074	4.1678	5.0637	5.1274
Pred 19	O	3-hydroxyphenyl	NH ₂	CH ₂	H	CN	OH	NO ₂	4.4495	4.4736	5.1039	5.3695
Pred 20	O	Tetrazoyl	NH ₂	CH ₂	H	CN	OH	NO ₂	4.2530	4.3421	5.2108	5.1041
Pred 21	O	3-hydroxyphenyl	H	3 membered B ring	H	H	OH	OH	4.5342	4.6524	4.7528	4.9934

Table 4.8: (continued)

Compound	X	R ²	R ³	Y	R ⁵	R ⁶	R ⁷	R ⁸	hENT1		hENT2	
									p <i>K</i> _i (μM)		p <i>K</i> _i (μM)	
									CoMFA	CoMSIA	CoMFA	CoMSIA
Pred 22	NH	3-hydroxyphenyl	H	3 membered B ring	H	H	OH	OH	4.6021	4.8101	4.8324	4.9177
Pred 23	NH	3-hydroxyphenyl	H	C=O	H	H	OH	OH	5.0512	5.1034	4.8772	4.9778
Pred 24	O	3-hydroxyphenyl	N	C=O	H	H	OH	OH	4.9682	4.6162	4.6105	5.0451
Pred 25	CH ₂	3,4,5-trimethoxyphenyl	OH	CH ₂	H	H	OH	H	5.4600	5.9839	5.5281	5.3388
Pred 26	CH ₂	3,4,5-trimethoxyphenyl	OH	C=O	H	H	OH	H	5.4379	5.7053	5.3607	5.3246
Pred 27	CH ₂	3,4,5-trimethoxyphenyl	OH	CH ₂	H	H	OH	H	4.9457	5.5269	5.4529	5.1983
Pred 28	NH	3,4,5-trimethoxyphenyl	OH	C=O	H	H	OH	H	5.4361	5.7499	5.2474	5.1903
Pred 29	NH	3,4,5-trimethoxyphenyl	NH ₂	C=O	H	H	OH	H	5.5229	5.7347	5.2428	5.2174
Pred 30	O	2-NH ₂ ,3,4,5-trimethoxyphenyl	OH	C=O	H	H	OH	H	5.3903	5.6328	5.0574	5.1852
Pred 31	O	2-OH,3,4,5-trimethoxyphenyl	OH	C=O	H	H	OH	H	5.3475	5.7214	5.0870	5.2855
Pred 32	O	3,4,5-trimethoxyphenyl	OCH ₃	C=O	H	H	OH	H	5.3662	6.1082	4.9755	4.9879
Pred 33	O	3,4,5-trimethoxyphenyl	OH	CH ₂	H	H	OH	H	4.9818	5.3326	5.3137	5.3486
Pred 34	O	3,4,5-trimethoxyphenyl	OH	C=O	OH	H	OH	H	5.4954	5.6471	5.1075	5.3724
Pred 35	O	3,4,5-trimethoxyphenyl	OH	C=O	H	CN	OH	H	5.5242	5.5786	5.2953	5.4462
Pred 36	O	3,4,5-trimethoxyphenyl	OH	C=O	H	NH ₂	OH	H	5.5806	5.6177	5.0666	5.5122
Pred 37	O	3,4,5-trimethoxyphenyl	OH	C=O	H	OH	OH	H	5.4493	5.6917	5.1946	5.5770
Pred 38	O	3,4,5-trimethoxyphenyl	OH	C=O	H	H	CN	H	5.2615	5.6259	5.1275	5.2233
Pred 39	O	3,4,5-trimethoxyphenyl	OH	C=O	H	H	CN	NH ₂	5.3981	5.3858	5.0530	5.0679
Pred 40	O	3,4,5-trimethoxyphenyl	OH	C=O	H	H	SH	H	5.3780	5.3874	5.0659	5.0677
Pred 41	O	3,4,5-trimethoxyphenyl	OH	C=O	H	H	N ₃	H	5.2917	5.4933	5.1282	5.1297
Pred 42	O	3,4,5-trimethoxyphenyl	OH	C=O	H	H	NH ₂	H	4.8180	5.2448	5.1041	5.4818
Pred 43	O	3,4,5-trimethoxyphenyl	OH	C=O	H	H	NO ₂	H	4.8579	5.7248	5.0449	5.7607
Pred 44	O	3,4,5-trimethoxyphenyl	H	C=O	H	H	OH	H	5.8899	6.0929	5.2056	5.4481
Pred 45	O	3,4,5-triethoxyphenyl	OH	C=O	H	H	OH	H	4.8010	5.4859	5.1398	5.4732
Pred 46	CH ₂	3,4,5-trimethoxyphenyl	OCH ₃	CH ₂	OCH ₃	OCH ₃	OCH ₃	H	3.8673	4.9775	5.0926	4.7774
Pred 47	O	3,4-methylenedioxy-5-methoxy phenyl	OH	C=O	H	H	OH	H	4.4506	4.6531	5.1749	5.2832
Pred 48	O	3,4,5-trimethoxyphenyl	OCH ₃	C=O	OCH ₃	OCH ₃	OCH ₃	H	4.6644	4.9352	5.3064	5.0092

Table 4.8: (continued)

Compound	X	R ²	R ³	Y	R ⁵	R ⁶	R ⁷	R ⁸	hENT1 p <i>K</i> _i (μM)		hENT2 p <i>K</i> _i (μM)	
									CoMFA	CoMSIA	CoMFA	CoMSIA
Pred 49	O	3,4,5-trimethoxyphenyl	H	C=O	OCH ₃	OCH ₃	OCH ₃	H	3.8986	4.7961	5.2973	5.2324
Pred 50	O	3,4,5-trimethoxyphenyl	OH	C=O	OCH ₃	OCH ₃	OCH ₃	H	4.5602	4.7015	5.2820	5.1549
Pred 51	O	3,4,5-trimethoxyphenyl	H	C=O	H	H	OCH ₃	OCH ₃	5.9877	6.1593	5.1374	5.2996
Compound XI	O	3,4,5-trimethoxyphenyl	-----	-----	H	H	OCH ₃	OCH ₃	4.5792	5.6280	5.4714	5.2555

compound **96** ($pK_i = 5.7523$) for ENT2 inhibition, and can be evaluated for identification of new ENT2 inhibitor leads. **Pred 51** has the highest predicted activity. Only one of these compounds, **Pred 34** was found to be commercially available. Hence, synthesis of rest of these novel compounds and biological evaluation of all of them are the major goals for future work (Figure 4.14). Also, compound **XI** (mentioned in section 4.6) was predicted *in silico*, but predicted activity values may not be reliable due to significant difference in the structure of compound **XI** and the series of flavones used to derive the 3D-QSAR models.

4.5 Evaluation of Related Analogs

Based on the general SAR of flavones tested for the above analyses, some more flavones and analogs were further tested on both ENT1 and ENT2. Table 4.9 shows the list of those extra set of compounds with their IC_{50} values. The structures of these compounds are shown in Figure 4.15. The screening graphs and IC_{50} curves are shown in Figure 4.16. From these results, it can be clearly seen that compound **101** is highly active against ENT1 whereas, compound **111** is selectively potent against ENT2.

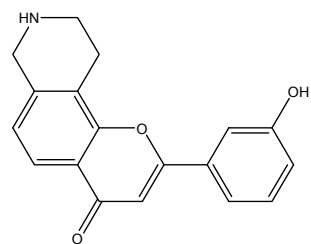
4.6 Synthesis and Testing of a New Lead as an Equilibrative Nucleoside Transporter Specific Inhibitor

An analysis of SAR for ENT1 and ENT2 inhibition showed that the compounds with methoxy substitution at positions 7, 8, 3', 4' and 5', consistently showed high potency (compounds **3**, **16**, **22**, **35**). This information was used to design compound **XI**, which is less constrained compared to the flavones to find out minimum structural features required for ENT inhibitory activity (Figure 4.17). Figure 4.18 shows the synthetic route followed to prepare compound **XI**; but this reaction resulted in C-alkylation instead of O-alkylation, thus, giving compounds **XII** and **XIII**. Due to structural isomerism (same molecular weight) and same Rf values, the mixture could not be separated into two different compounds.

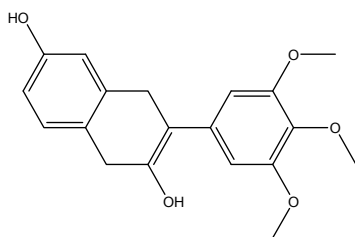
Thus, the mixture of compounds **XII** and **XIII** was evaluated at 10 μ M concentration against hENT1, hENT2 and hCNT3 transporter cell-lines to find out the effect of these novel molecules. Interestingly, the mixture showed substantial inhibitory activity against ENT1, but low activity against ENT2, and no significant activity against hCNT3. This further provides insight into the differences among ENT1, ENT2 and CNT3 inhibitor pharmacophores. Figure 4.19 shows the comparison graph.

4.7 Discussion

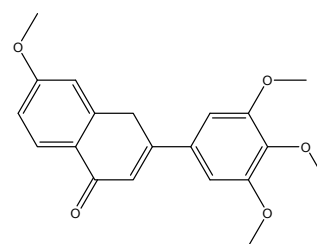
All flavone analogs screened against concentrative nucleoside transporters were tested against ENT1 and ENT2 using a [3 H]-uridine uptake assay. NBMPR and dipyrindamole were used as positive controls with respect to which the biological activities



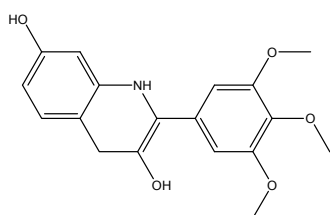
Pred 14



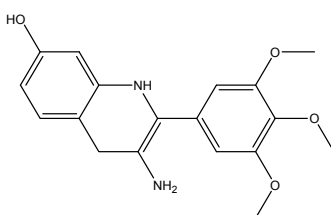
Pred 25



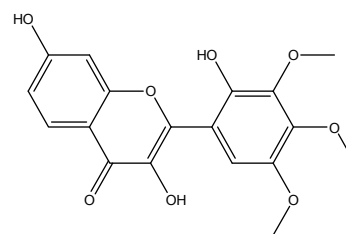
Pred 26



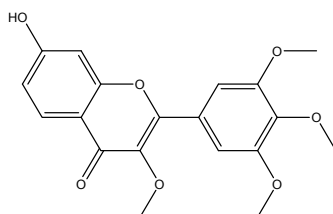
Pred 28



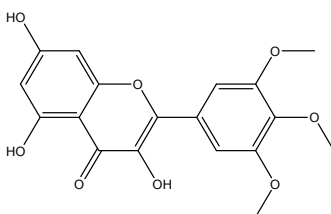
Pred 29



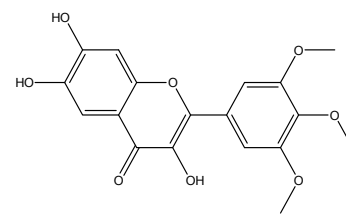
Pred 31



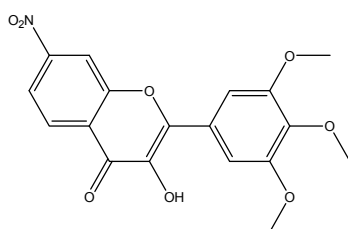
Pred 32



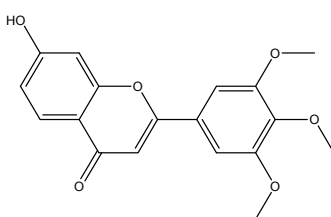
Pred 34



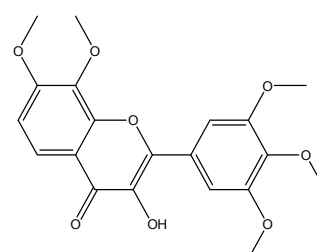
Pred 37



Pred 43



Pred 44



Pred 51

Figure 4.14: *In silico* compounds with high inhibitory activity against ENT1 and ENT2

Table 4.9: Biological activity data of compounds 101 to 115^{ab}

Compound No.	Name	hENT1 IC ₅₀ (μM)	hENT2 IC ₅₀ (μM)
101	3'-benzyloxy-5,6,7,4'-tetramethoxy flavone	0.96	7.62
102	5,6,7,3',4'-pentamethoxyflavone (Sinensetin)	1.93	11.46
104	3',4',5,6,7,8-hexamethoxyflavone (Nobiletin)	2.72	9.43
105	6,7,3',4'-tetramethoxyflavone	5.10	14.77
106	3,7-dihydroxy-3',4'-dimethoxyflavone	---	---
107	3-Amino-1-pyridine-4-yl-1H-benzo(F)chromene-2-carbonitrile	2.10	5.02
108	4H-1-Benzopyran-3-carbonitrile-2-amino-7-hydroxy-4-phenyl	8.41	4.37
109	4H-1-Benzopyran-3-carbonitrile-2-amino-7-hydroxy-4-(3-nitrophenyl)-	8.59	3.49
110	Acetamide, N-[4-(3-carbonitrile-2-amino-7-hydroxy-4H-1-benzopyran-4-yl) phenyl]	7.82	6.08
111	4H-1-Benzopyran-3-carbonitrile-2-amino-7-hydroxy-4-(3-cyclohexen-1-yl)	9.38	1.90
112	4H-1-Benzopyran-3-carbonitrile-2-amino-4-phenyl-7-(phenylamino)	13.56	4.73
113	4H-1-Benzopyran-4-one, 6-hydroxy-2-(3,4,5-trimethoxyphenyl)-	2.34	5.20
114	4H-1-Benzopyran-4-one, 2-(3,4-dimethoxyphenyl)-3-methoxy-	2.74	5.70
115	4H-1-Benzopyran-4-one, 2-(3,4-dimethoxyphenyl)-6-methoxy-	4.11	6.77

^aTested as inhibitors of [³H]-uridine uptake by hENT1 or hENT2

^bThe structures of these compounds are shown in Figure 4.15.

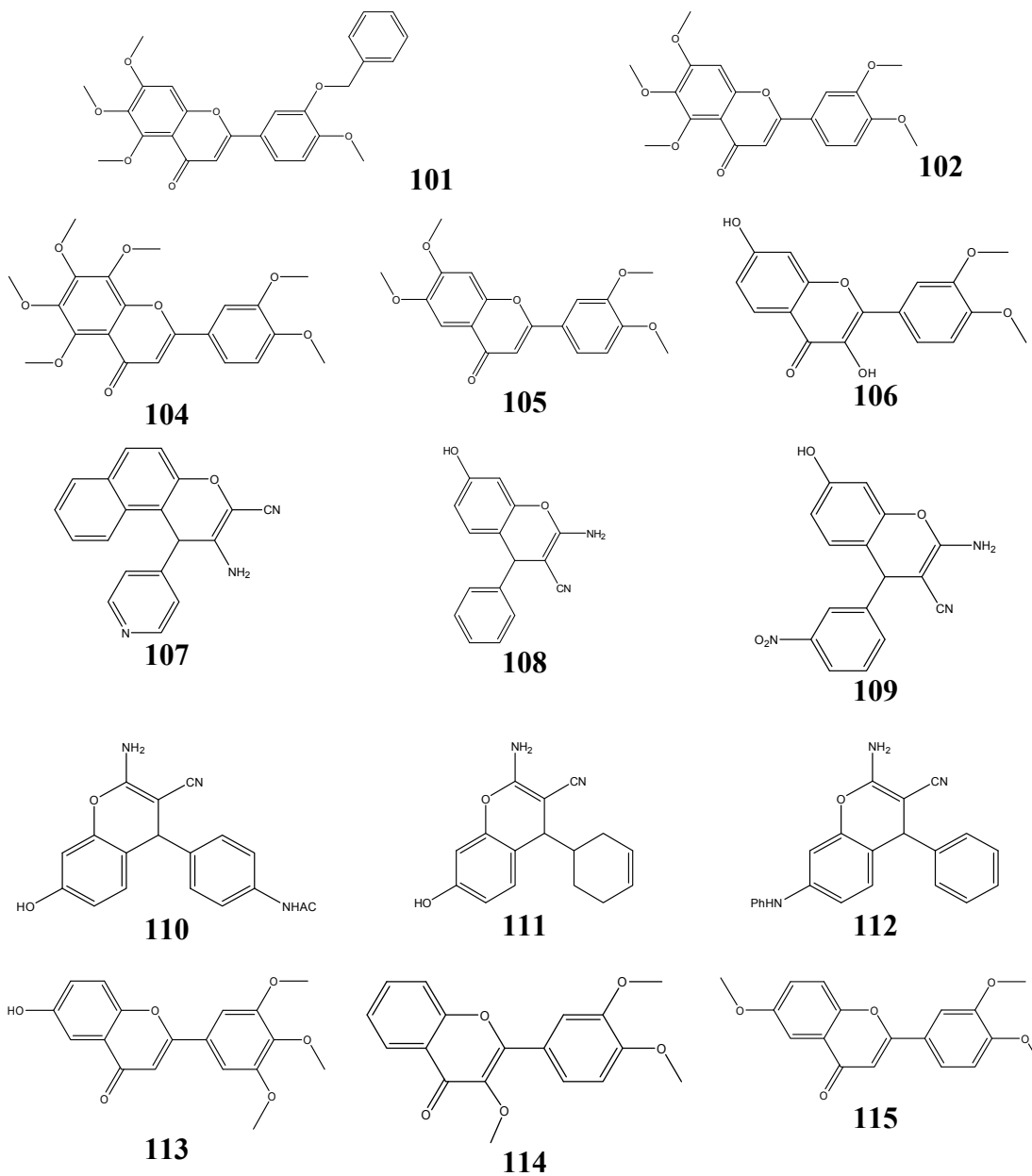


Figure 4.15: Structures of compounds 101 to 115

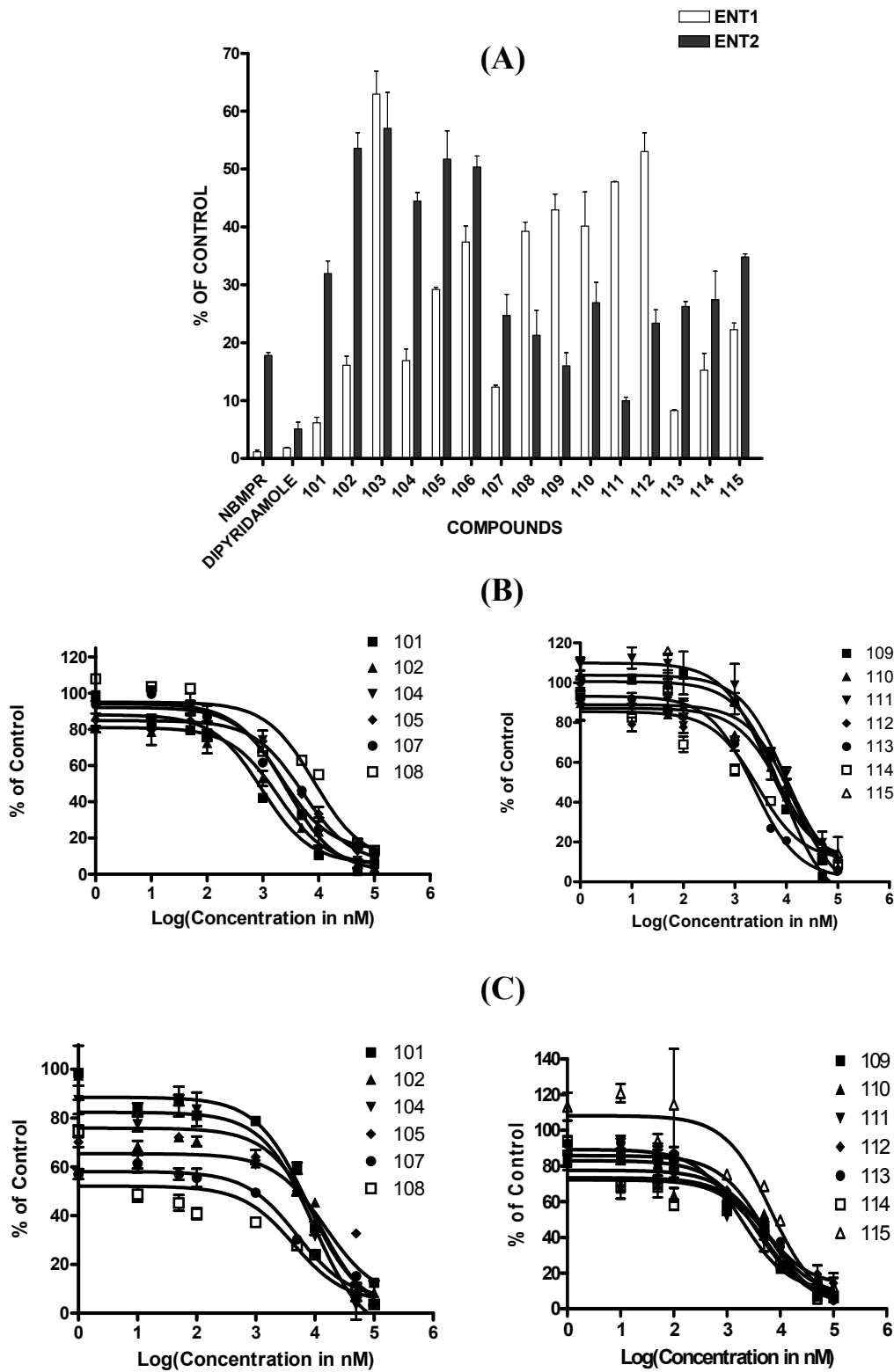


Figure 4.16: (A) Screening at 10 μ M on ENT1 and ENT2, (B) IC₅₀ curves for ENT1 and (C) IC₅₀ curves for ENT2

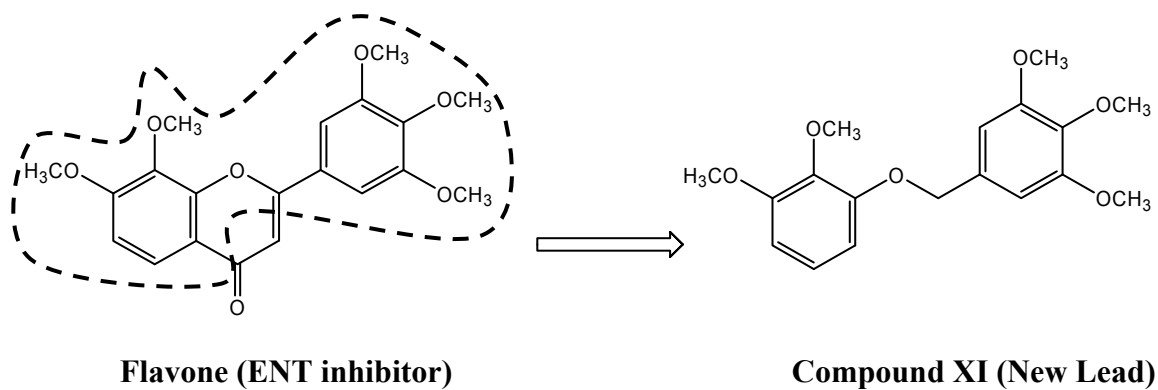


Figure 4.17: Structural similarity between active flavones and compound XI

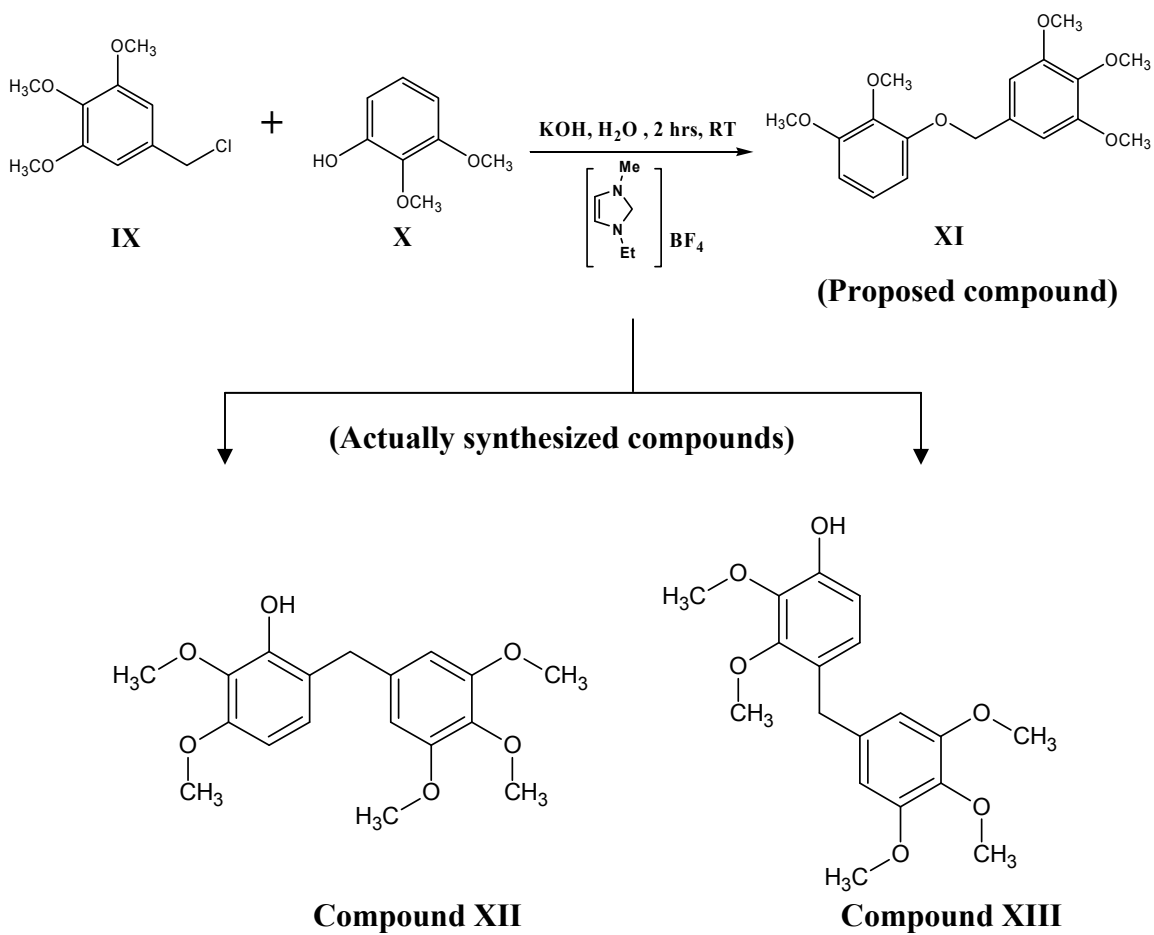


Figure 4.18: Synthetic scheme

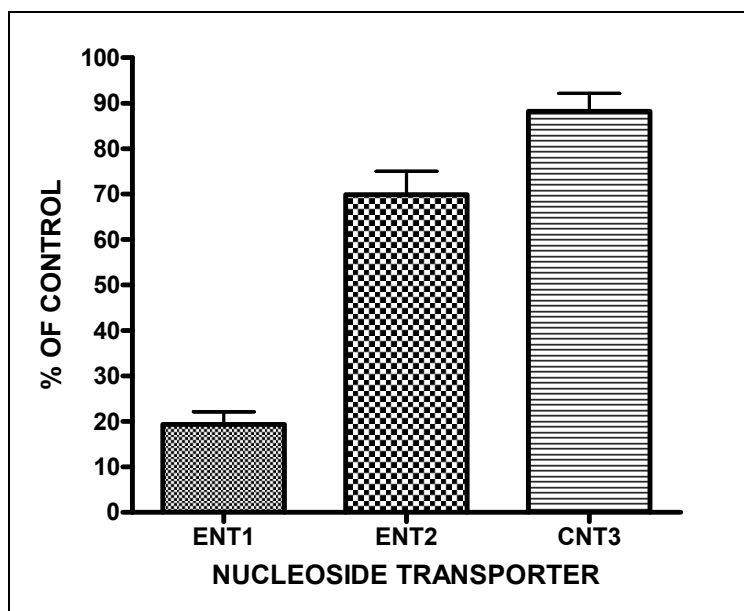


Figure 4.19: Comparison graph of mixture of compound XII and XIII screening

of compounds in the study were compared. None of the flavones tested was found to be as potent as the standards against ENTs. From the SAR established from the available biological activity data, the following points highlight some of the important features that determine the inhibitory activity of flavones. ENT1 transporter shows a higher sensitivity to flavones than ENT2, since a greater number of flavones are active against ENT1. For ENT1 inhibition, compound **95** (IC_{50} of 2.24 μ M) is the most specific inhibitor. Compound **100** (IC_{50} of 0.13 μ M) is the most potent ENT1 inhibitor and belongs to the quinoxaline class. A 3,7-dihydroxy substitution with 3', 4', 5'-trimethoxy substitution was a favorable structural feature for ENT1 inhibition. The most potent flavone is compound **16**, with an IC_{50} of 1.02 μ M. Also, compound **66** ($SI = 15$) is significantly selective for ENT1 inhibition. Compounds **16** ($SI = 2.75$), **19** ($SI = 3.34$), **22** ($SI = 4.72$), **51** ($SI = 4.66$), **56** ($SI = 7.34$), and **93** ($SI = 1.82$) also exhibit low selectivity for ENT1 inhibition. Comparing compound **66** and **70**, it is clear that the 7,8-furano- substituent is worst for ENT1 inhibition compared to 7,8-naphtho- compound. Also, naphthoflavones with only 2'-OH or 4'-OH are not active against ENT1 (compound **64** and **68**), but need to be un-substituted or have 3',4'-dihydroxy, 3'-OH or 4'-methoxy substitution to exhibit inhibitory activity against ENT1 (compounds **61**, **63**, **66**, **71**). The information obtained from compounds that are exclusively active against ENT1, i.e. flavone compounds **6**, **8**, **52**, **54**, **57**, **61**, and **71**, suggests that a 2-phenyl group with 3- and 4- positions occupied by hydrophobic and H-bond acceptor type substituents, and 7- and 8- positions substituted with methoxy groups or hydroxyl groups are essential structural features. Active coumarin compounds **89**, **91**, **92**, and **95** suggest that the 3-position phenyl ring enhances activity in this series, since compounds **91** and **95** are more active than **92**. Also, a comparison of **91** and **95** shows the favorability of 4- and 5-OH groups to inhibitory activity. Isoflavones **78**, **79**, **83**, **97**, and **99**, which are active against only ENT1, strongly suggest that bulk is well tolerated at position 3 by the ENT1 transporter.

All the chalcones are active against ENT1, with the most active chalcone being compound **44** (IC_{50} of 3.64 μ M). Compound **101** in the later studied series is the best ENT1 inhibitor with an IC_{50} value of 0.96 μ M, which suggests that groups with more bulk than $-OCH_3$ group are well tolerated at the 3'-position. Also, 3',4',6,7-tetramethoxy substitution is favorable for ENT1 inhibition (compounds **101,102, 104, 105**).

The most active inhibitors of ENT2 are compound **35** (a flavone, IC_{50} of 1.77 μ M) and compound **96** (4-pyridinyl-4H-chromene derivative, IC_{50} of 1.77 μ M). These two compounds are chemically different structures. They may or may not bind at the same site. Compound **3** is another flavone that is a potent ENT2 inhibitor (IC_{50} of 1.81 μ M). Compound **30** is the most selective (**SI = 9.11**), though it is not the potent one. Other compounds with some selectivity for ENT2 inhibition are: **3** (**SI = 7.77**), **5** (**SI = 3.33**), **15** (**SI = 1.96**), **23** (**SI = 7.77**), **27** (**SI = 6.07**), **34** (**SI = 3.56**), **41** (**SI = 2**), **53** (**SI = 2.77**), and **72** (**SI = 2.18**). Isoflavones are less active than flavones as inhibitors of ENT2 (compare compounds **78, 79, 80, 81, 82, 83, 97** and **99**). Compound **45** belonging to the chalcone class, is 6 times more selective towards ENT2 compared to ENT1. Coumarins are not good inhibitors of ENT2 (see compounds **91** and **93**). Compound **111** (IC_{50} of 1.90 μ M) is the most active ENT2 inhibitor in the series **101** to **115**. The results from this analysis, suggest that 2-amino-3-cyano- substitution is a fairly good structural feature for ENT2 inhibition compared to ENT1, and may be exploited to obtain selective ENT2 inhibitors, which are currently lacking.

Comparing the biological activity data of equilibrative nucleoside transporters vs concentrative nucleoside transporter inhibition, it appears that the active site of ENTs is more hydrophobic relative to CNTs. The most sensitive nucleoside transporter among the five is CNT3. Compound **49**, which is the most active against both CNT1 and CNT2, is inactive against the ENTs. Also, compounds **39** (IC_{50} of 0.57 μ M) and **50** (IC_{50} of 0.68 μ M), which show very potent inhibition against CNT3, are not significantly active against ENTs.

QSAR studies have been successfully applied for modeling biological activities of the flavones tested. In this work, we carried out 3D-QSAR studies for establishing correlations between structural properties of 95 flavones and analogous compounds such as coumarins and a quinoxaline and their inhibitory activities against ENT1 and ENT2. 3-D QSAR analysis was performed using CoMFA and CoMSIA methods.

The models generated show correlation coefficients (r^2) of 0.937 and 0.928 (ENT1), and 0.870 and 0.957 (ENT2) with cross-validated r^2 (q^2) of 0.585 and 0.523 (ENT1), and 0.510 and 0.565 (ENT2), respectively for CoMFA and CoMSIA. Taking into consideration the contributions made by different descriptors, electrostatic descriptors contributed the most, followed by the hydrogen bond donor descriptor. These two main descriptors were followed by H-bond acceptor and hydrophobic properties in ENT1 and ENT2 models, respectively.

The standard deviation (s), Fischer ratio (F) and the statistical results for the validation exercises performed to prove the robustness of these models demonstrated a

high degree of reliability of the models. The q^2 and r^2 values obtained from group cross-validation and bootstrapping respectively, are not significantly different from the original values. The negative q^2 values obtained for all models using randomized activity data indicate that correlations of the models were not due to chance. The predictive ability of the models was validated using an internal and external test set of compounds which had not been included in the training sets of compounds. The predictive r^2 values for these ligand-based CoMFA and CoMSIA models were significantly high in all the models in the case of the internal set, but in the case of the external test set, only the CoMFA model of ENT1 afforded good predictions (Table 4.8).

The models derived from 3D-QSAR were used to predict the activities of *in silico* designed molecules and some of the highly predicted molecules (**Pred 14**, **Pred 25**, **Pred 26**, **Pred 28**, **Pred 29**, **Pred 31**, **Pred 32**, **Pred 34**, **Pred 37**, **Pred 43**, **Pred 44** and **Pred 51** for ENT1, and **Pred 25**, **Pred 37** and **Pred 43** for ENT2) can be obtained and assayed to check the validity of the models in a practical sense and in an attempt to search for more potent compounds. From the results of the SAR and QSAR studies, a novel lead compound, **XI** was designed but the synthesis failed to yield the compound, but rather produced the mixture of compounds **XII** and **XIII**. A different synthetic route will have to be used to obtain compound, **XI**. The mixture of compounds **XII** and **XIII** will have to be separated to determine which one is more potent.

4.8 Conclusion

In the study, ninety five flavonoids and related compounds (Table 4.1) were studied by qualitative SAR and 3D-QSAR analyses. CoMFA and CoMSIA 3D-QSAR models provided insights regarding how different functional groups affect potency and transporter selectivity. The statistically validated models were used for *in silico* prediction of designed compounds which identified potential novel inhibitors, which are still to be obtained and biologically evaluated. Considering the combined activity of compounds **XII** and **XIII** for ENT1, some more analogs can be synthesized and their inhibitory activities can be examined. Thus, the work undertaken, including the biological evaluation, the analysis of 2-D and 3-D structure activity relationships and synthesis of compounds **XII** and **XIII** can help to better understand the structural determinants of equilibrative nucleoside transporter inhibition and rational design of new, specific and more effective inhibitors, but the obtained information may not be applied to structurally more diverse flavones. This work has also identified the first hENT2-selective inhibitors (compound **3**, **35** and **96**) relative to ENT1. In comparing the activity data of ENTs with CNTs (see Chapter 3), one distinct observation about the active sites is that the binding site for flavones at ENTs is more hydrophobic than that at CNTs.

4.9 Experimental Section: Chemistry

Thin-layer chromatography (TLC) was performed on silica gel plates (Analtech). Compounds were visualized by UV light (254 and 365 nm). 1D NMR spectra were

recorded on a Varian Inova 500 MHz NMR instrument using (CD₃)₂SO as solvent and tetramethylsilane (TMS) as an internal standard. Flash column chromatography was performed on Fischer silica gel (170-400 mesh). Mass spectra were obtained on Bruker HP ESQUIRE Ion Trap LC/MS (n) system. All solvents and reagents were purchased from Aldrich and used without further purification unless otherwise indicated.

4.9.1 Reaction Procedure

To a solution of potassium hydroxide, (100 mg, 1.6 mmol) in 12 mL water, 3, 4,5-trimethoxy benzyl chloride, **IX** (500 mg, 3.2 mmol), 2,3-dimethoxy phenol, **X** (690 mg, 3.2 mmol) and the ionic catalyst 1-ethyl-3-methylimidazolium tetrafluoroborate (0.4mL, 0.3 mmol) were added. The mixture was stirred at room temperature for 5 hours. The mixture of compounds **XII** and **XIII** (721 mg) was isolated from other impurities by extraction using ethyl acetate and purification by column chromatography with a solvent system containing n-hexane/ethyl acetate (8:2). The NMR and mass spectra of mixture of compounds XII and XII are reported in Figure A.1 and A.2 in the appendix section, respectively.

4.9.2 Mixture of Compounds XII and XIII

Yield 60 %; light yellow semisolid; (ESI, Pos) m/z 357.2 [(M + 23)]⁺; ¹H NMR (500 MHz, DMSO) 6.707 (H, dd, J = 8.5 Hz, ArH), 6.539 (2H, d, J = 9.5 Hz, ArH), 6.479 (H, s, ArH), 6.429 (1H, d, J = 8.5 Hz, ArH), 3.743 (6H, s, 2 OCH₃), 3.718 (9H, s, 3 OCH₃), 3.679 (2H, s, methylene H).

Chapter 5: Pharmacophore Mapping of Flavone Derivatives for hCNT3 Inhibition

5.1 Introduction

Human concentrative nucleoside transporters are being studied extensively by researchers to find out the exact features of the active sites of these 13 transmembrane domain proteins.¹⁶⁻²⁰ In the meantime, to identify new potent inhibitors, most of the methods rely on ligand-based drug design and one of such approaches is ligand-based pharmacophore mapping. The pharmacophore concept is based on the kinds of interaction observed in molecular recognition, i.e., hydrogen bonding, charge, aromatic, and hydrophobic interactions and their arrangements in 3D space. Pharmacophores generated can be used as queries in 3D database searching to identify new structural classes of potential lead compounds, and can also serve as templates for generating alignments for 3D-QSAR studies. Two types of pharmacophore hypothesis are well established: receptor-based and receptor-independent pharmacophores. Receptor based pharmacophore mapping cannot be performed in this case since X-ray crystal structures are still not available for human concentrative nucleoside transporters. Hence, the most suitable choice is receptor-independent and ligand-dependent pharmacophore mapping.¹⁴⁹⁻¹⁵¹ Consequently, the present work was undertaken to study the flavone scaffold with a view to deduce the active pharmacophore based on a receptor-independent hypothesis, using the PHASE¹⁵² program (Schrodinger Inc.), that can eventually aid in comprehending the effects of different compounds containing this unit.

5.2 Materials and Methods

In the present study, 62 compounds of a series of flavone analogs were considered. The general structure and activity data of flavones used in the study are presented in chapter 3, Table 3.1. The steps involved in the pharmacophore mapping undertaken are: 1) preparation of ligands, 2) creation of the pharmacophoric sites, 3) finding common pharmacophores, 4) scoring hypotheses and 5) deriving 3D-QSAR models. The compounds used in the pharmacophore mapping have the following general structure (Figure 5.1), and are listed in Table 5.1 with the activity and number of conformations generated.

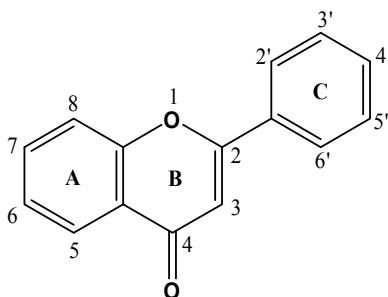


Figure 5.1: General structure of compounds used in the study

Table 5.1: Compounds used in pharmacophore mapping

Compound No.	Activity pKi	Pharm Set	No. of conformations^a
50	6.237	Active	7
84	6.056	Active	15
13	5.863	Active	4
83	5.591	Active	7
34	5.443	Active	20
12	5.395	Active	5
72	5.253	Active	11
49	5.216	Active	7
74	5.201	Active	3
51	5.145	Active	9
11	5.124	Active	5
57	5.093	Active	15
5	5.030	Active	4
3	5.019	Active	7
85	4.991	Active	9
62	4.942	Active	5
63	4.905	Active	4
52	4.874	Inactive	4
71	4.871	Inactive	2
33	4.863	Inactive	11
66	4.857	Inactive	3
67	4.842	Inactive	3
10	4.815	Inactive	9
23	4.815	Inactive	8
42	4.815	Inactive	7
70	4.766	Inactive	3
60	4.763	Inactive	2
8	4.724	Inactive	5
80	4.712	Inactive	4
27	4.711	Inactive	6
55	4.658	Inactive	3
75	4.656	Inactive	2
15	4.652	Inactive	4
81	4.652	Inactive	4
79	4.639	Inactive	7
17	4.637	Inactive	7
40	4.637	Inactive	3
31	4.622	Inactive	9
48	4.597	Inactive	5
64	4.588	Inactive	5
59	4.571	Inactive	3

Table 5.1: (continued)

Compound No.	Activity pKi	Pharm Set	No. of conformations
78	4.570	Inactive	7
32	4.565	Inactive	7
61	4.562	Inactive	2
54	4.560	Inactive	5
65	4.554	Inactive	5
16	4.536	Inactive	8
4	4.536	Inactive	4
77	4.531	Inactive	2
56	4.521	Inactive	3
68	4.475	Inactive	3
69	4.448	Inactive	2
58	4.432	Inactive	3
35	4.374	Inactive	9
2	4.326	Inactive	5
82	4.325	Inactive	4
30	4.321	Inactive	6
19	4.261	Inactive	3
9	4.216	Inactive	4
14	4.202	Inactive	4
6	4.055	Inactive	4
22	3.825	Inactive	2

^aThe more rotatable bonds in a molecule, the more the no. of conformations generated for it. This general concept is applicable to the molecules in the study.

5.2.1 Preparation of Ligands

The chalcones and glucoside (compound **43** – **47** and **73**) were not included in the data set due to differences in structure; and compound **39** was eliminated due to strong possibility of the existence of a different binding mode. The conformations of each molecule were generated using the OPLS_2005 force field¹⁵³ with a maximum relative energy difference of 10 kcal/mol, distance-dependent dielectric solvation treatment and minimum atom deviation of 2 Å. The activity cut off was set to pK_i equal to 4.9, above which compounds are defined as active and below which the compounds were considered as inactive. Hence, the entire data set was divided into 17 actives and 45 inactives.

5.2.2 Creation of Pharmacophoric Sites

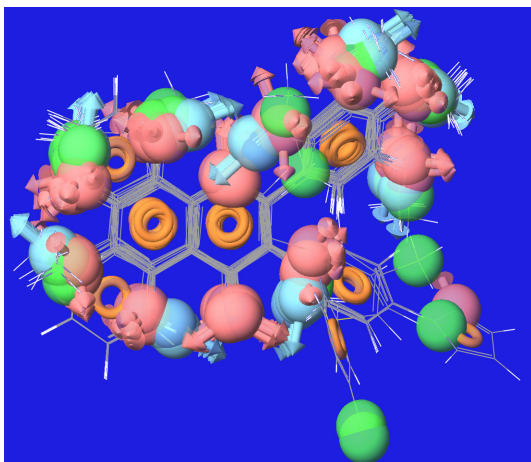
After generation of conformations for each ligand in the study, the different pharmacophoric sites were generated, using inbuilt parameters for H-bond acceptor (A), H-bond donor (D), hydrophobic (H), negative (N), positive (P) and aromatic (R) functional groups present in the molecules. The sites are represented as follow:
Acceptor= Red sphere with vectors pointing in the direction of possible interaction,
Donor= Blue sphere with vectors pointing in the direction of possible interaction,
Hydrophobic= Green sphere and Aromatic= Orange ring at the center of aromatic ring.
For the given set of molecules, no positive or negative features were generated due to their absence. There is an abundance of acceptor and donor sites in almost all molecules. Most distinguishing feature between active and inactive sets of molecules is presence of hydrophobic sites in inactive ligands with exceptions of two compounds in the active set (compounds **63** and **84**). Figure 5.2 shows all compounds with the pharmacophoric sites.

5.2.3 Finding a Common Pharmacophore

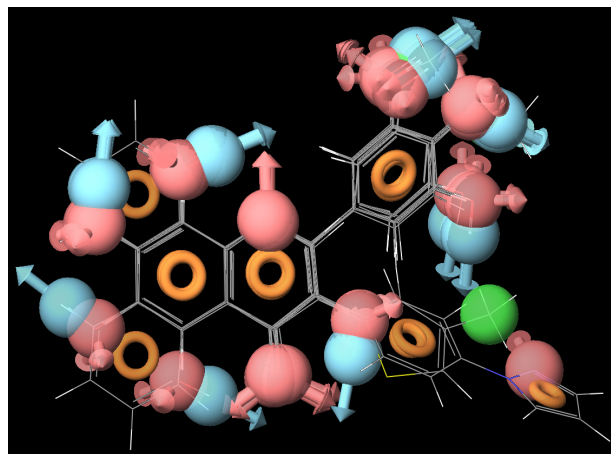
To find the common pharmacophore mapping all the active and inactive ligands, the number of pharmacophoric site features was varied from 5 through 7. The feature frequencies were adjusted to four for acceptor, two for donor, and three for aromatic ring. Also the minimum no. of actives to be matched to a common pharmacophore was set to at least 12 out of 17 active ligands. Attention was focused on the 7- site pharmacophore hypotheses, to derive more specific pharmacophore for CNT3. The two pharmacophores, **AAAADDR** and **AAADRRR** as marked in bold in Table 5.2 were finally selected for generating hypotheses and in all 20 hypotheses of these two combinations were derived which were common to most active ligands in the data set.

5.2.4 Scoring Hypotheses

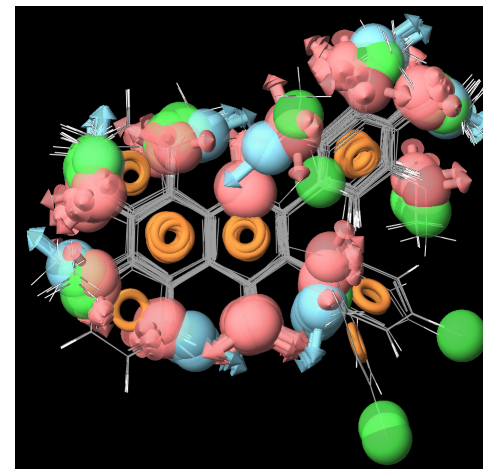
A scoring procedure is applied to identify the pharmacophore that yields the best alignment of the active ligands. The scoring procedure provides a ranking of the different hypotheses, allowing the making of rational choices about which hypotheses are most



(A)



(B)



(C)

Figure 5.2: (A) All ligands with pharmacophoric sites, (B) active ligand set and (C) inactive ligand set

Table 5.2: Pharmacophore generation

No. of sites	No. of variants	List of variants	No. of pharmacophores	No. of common pharmacophore
5	11	AAAAD, AAAAR, AAADD, AAADR, AAARR, AADDR, AADRR, AARRR, ADDRR, ADRRR, DRRR	1025	10
6	9	AAAADD, AAAADR, AAAARR, AAADDR, AAADRR, AAARRR, AADDRR, AADRDR, ADDRDR	247	7
7	6	AAAADDR , AAAADRR, AAAARRR, AAADDRR, AAADRRR , AADDRRR	35	2

appropriate for further investigation. In the scoring process, a survival box is built which contains a set of very similar pharmacophores culled from conformations of a minimum number of active ligands, and certain of these ligands may contribute more than one pharmacophore to a box. Each pharmacophore and its associated ligand are treated temporarily as a *reference* in order to assign a score. This means the other *non-reference* pharmacophores in the box are aligned, one-by-one, to the reference pharmacophore, using a standard least-squares procedure applied to the corresponding pairs of site points. At this stage, the quality of each alignment is measured using up to three terms: (1) the root-mean-squared deviation (RMSD) in the site point positions; (2) the average cosine of the angles formed by corresponding pairs of vector features (acceptors, donors and aromatic rings); and (3) a volume overlay term (Equation 5.1) based on van der Waals models of the non-hydrogen atoms in each pair of structures.

$$Svol_{(i)} = V_{common_{(i)}} / V_{total_{(i)}} \quad (\text{Eq. 5.1})$$

$V_{common_{(i)}}$ is the common or overlapping volume between ligand i and the reference ligand, while $V_{total_{(i)}}$ is the total volume occupied by both ligands. The volume term is computed only if the option to score by volume is selected. These two or three terms are combined with separate weights to yield a combined alignment score for each non-reference pharmacophore that has been aligned to the reference. If a non-reference ligand contributes more than one pharmacophore to the box, the pharmacophore yielding the best alignment to the reference is selected. The overall multi-ligand alignment score for a given reference pharmacophore is the average score from the best set of individual alignments.¹⁵²

For the current study, 20 hypotheses were selected, each of which contained 7 pharmacophoric sites. Hypothesis 1 and 11 scored the highest in AAADRRR and AAAADDR combinations. Table 5.3 lists the survival scores of each of those hypotheses with number of active ligands matched to it. The derived hypotheses are only used to obtain ligand alignments. It does not contribute in any way to the QSAR model itself. Instead, hypotheses have an association with the model, because they define how ligands should be pre-aligned before applying the model. Also, there is no necessary connection between the score and the quality of the QSAR models. Figure 5.3 and 5.4 show all of the hypotheses with compound 50 co-displayed with them. As seen in the Figure 5.3 (hypotheses 1 to 10), three acceptors, one donor and three aromatic features cover different parts of the molecule to give the common pharmacophore. Similarly, Figure 5.4 (hypotheses 11 to 20) shows four acceptors, two donors and an aromatic feature contributing to generation of the common hypothesis.

5.2.5 Building a QSAR Model

The building of most QSAR models requires alignment of ligands according to a “bioactive conformation”. Sixty two training and test set ligands cannot all be expected to match all seven sites in the hypotheses. Some weak inhibitors will be missing one or more features contained in the hypothesis. To deal with this possibility, PHASE uses

Table 5.3: Scoring results

No.	Hypotheses	Survival	No. of actives matched
1	AAADRRR	3.778	12
2	AAADRRR	3.756	12
3	AAADRRR	3.699	12
4	AAADRRR	3.656	11
5	AAADRRR	3.608	11
6	AAADRRR	3.600	11
7	AAADRRR	3.542	11
8	AAADRRR	3.297	11
9	AAADRRR	3.295	11
10	AAADRRR	2.809	12
11	AAAADDR	3.490	10
12	AAAADDR	3.490	10
13	AAAADDR	3.462	10
14	AAAADDR	3.366	10
15	AAAADDR	3.345	10
16	AAAADDR	3.345	10
17	AAAADDR	3.038	10
18	AAAADDR	2.936	10
19	AAAADDR	2.918	10
20	AAAADDR	2.918	10

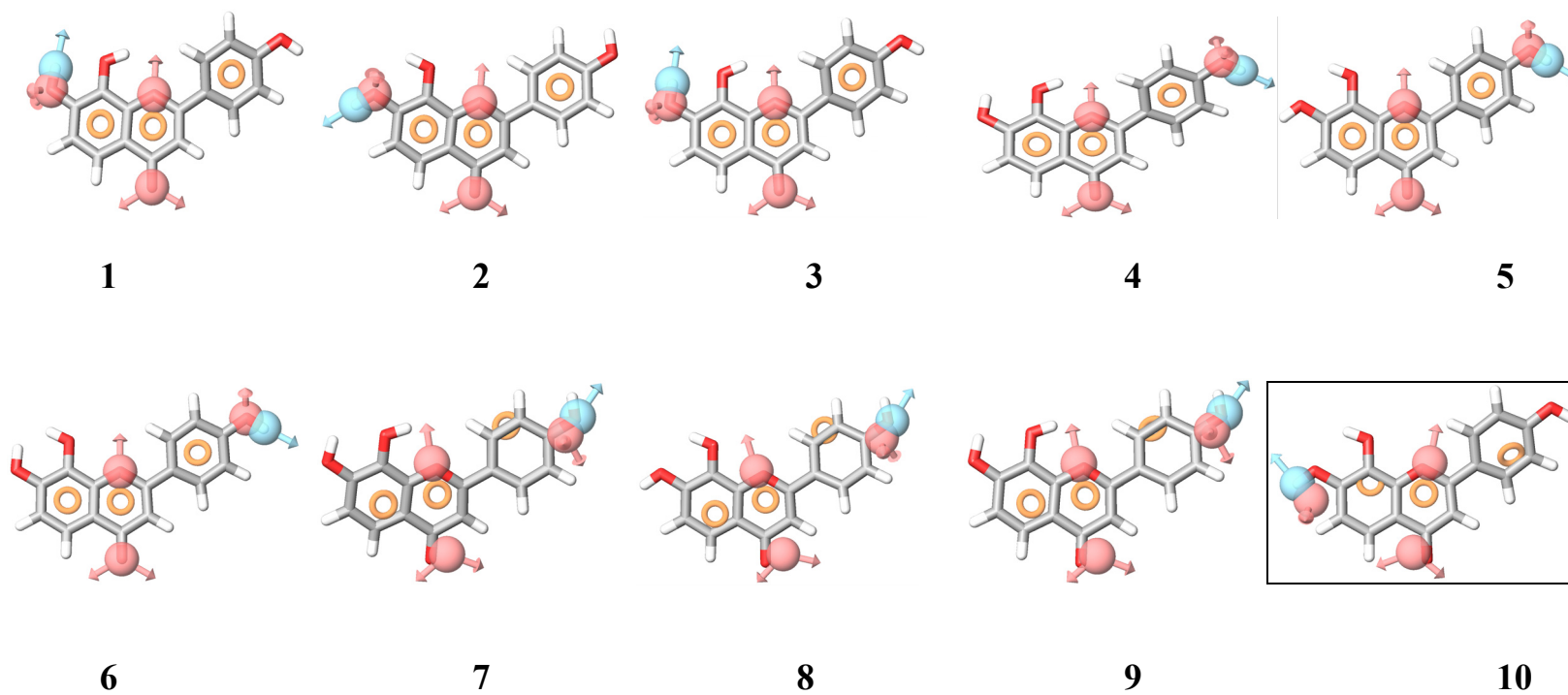


Figure 5.3: Hypotheses belonging to pharmacophore AAADRRR

represents selected pharmacophore for QSAR studies

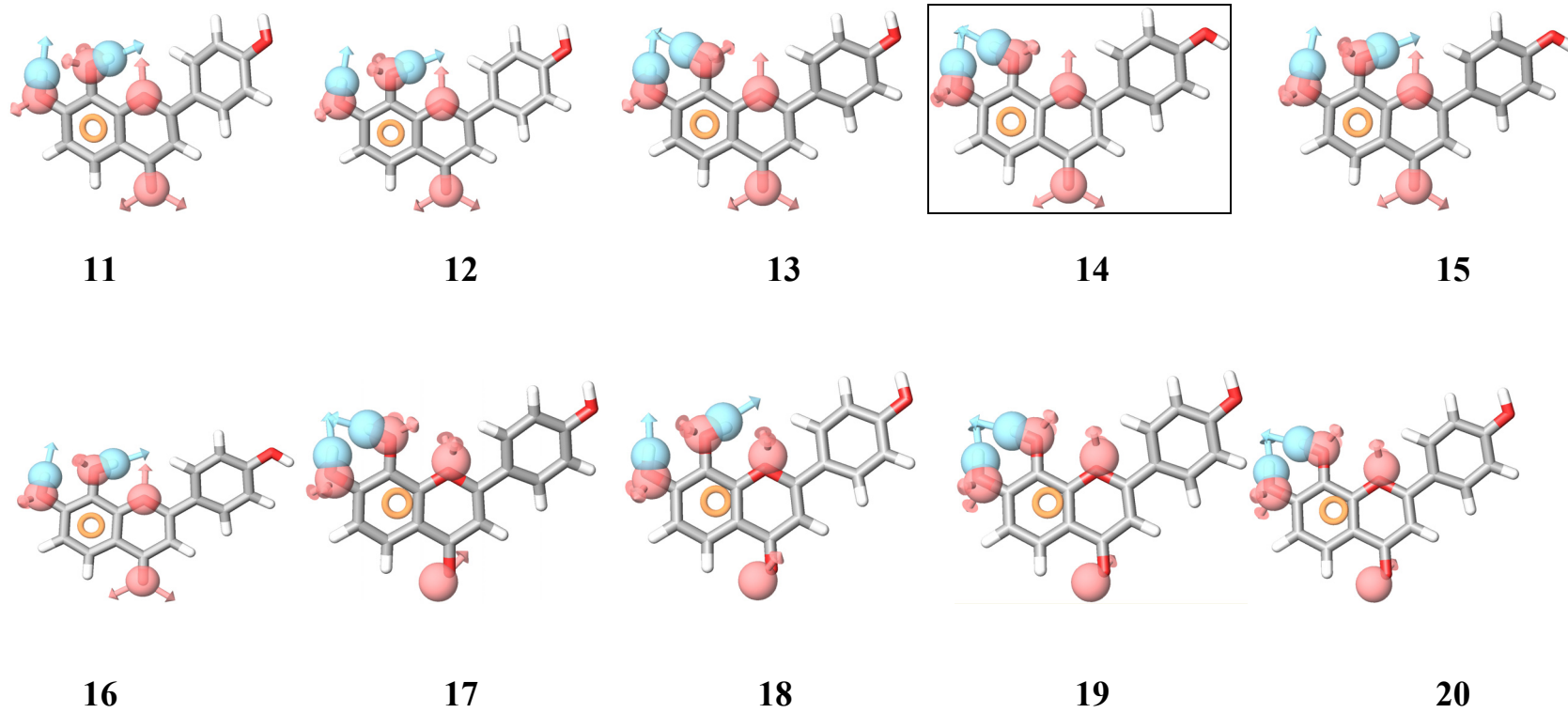


Figure 5.4: Hypotheses belonging to pharmacophore AAAADDR

represents selected pharmacophore for QSAR studies

partial matching to obtain alignment of inactive ligands in which, if at least three sites are matched, a proper alignment is obtained. For each ligand, outside the active set, then PHASE searches for matches involving the largest possible number of sites and identifies the match that yields the highest fitness score. These alignments can give information about which features are important and which are not, especially for actives that are not in the training set. PHASE QSAR models are based on partial least-squares (PLS) regression, applied to a large set of binary-valued variables that encode whether or not ligand atoms or features occupy various cube-shaped elements of space. PHASE can generate QSAR models that are atom-based or pharmacophore-based. The independent variables in the QSAR model are derived from a regular grid of cubic volume elements that span the space occupied by the training set ligands. For our study, after aligning the inactive set, all the listed hypotheses were subjected to pharmacophore based QSAR model development with a grid spacing of 1 Å and 5 PLS factors and by choosing the test set of 10 compounds randomly. Different combinations of compounds to comprise the test set were investigated. The results of the QSAR models have been listed in Table 5.4.

5.3 Results and Discussion

As mentioned in section 5.2.4, the high scoring hypothesis does not necessarily give a good model; the results reflected this fact. The hypotheses which scored highest in category AAADRRR, i.e., hypothesis 1, did not contribute to a better model. Instead, hypothesis 10, gave a good QSAR model. For the category AAAADDR, hypothesis 14 gave a reliable QSAR model.

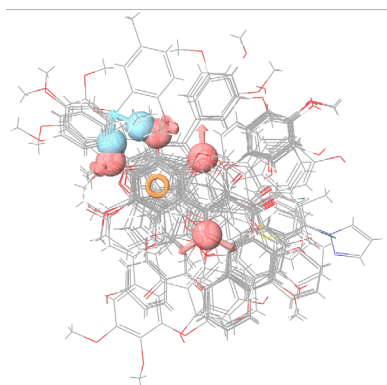
As seen in Table 5.4, the data set is divided into training and test set, and the compounds belonging to the test set were kept constant to compare the results obtained for both of the hypotheses. Hypothesis AAAADDR is better in terms of R^2 (equal to 0.6197) which means that the model accounts for 61.97 % of the variance in the observed activity data) and Q^2 (equal to 0.5196), compared to AAADRRR, but both of them have almost the same Pearson-R value which indicates the correlation between the predicted and observed activity for the test set. Figure 5.5 shows the alignment of training set and test set compounds for both high quality hypotheses AAADRRR and AAAADDR. The contributions of different pharmacophore features to the QSAR are shown in Figure 5.6 for both hypotheses.

All panels of Figure 5.6 contain compound **50** co-displayed with the hypothesis. For A, B, and C, the molecule has deflected from the hypothesis, due to a comparatively lower fitness ratio with the hypothesis AAADRRR. The red cube shows an unfavorable region and the blue one shows favorable regions of the ligand for a particular pharmacophoric feature. The QSAR results mapped to the cubes, for both hypotheses show that positions 1, 4, and 8 harbor strong concentrations of blue cubes, indicating their importance as major contributors to inhibitory activity. Position 7 of the flavone is favored for a H-bond donor as well as acceptor, but the donor feature predominates. The A and C rings of the flavone (shown in Figure 5.1) have to be aromatic in nature as shown by higher number of blue cubes accumulated in those parts of the flavone,

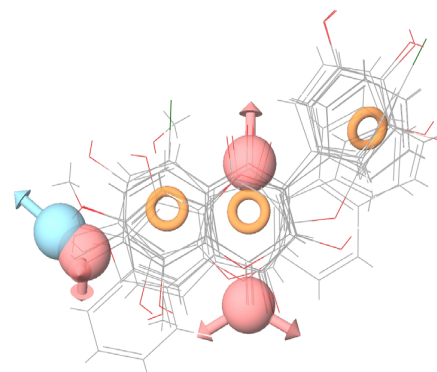
Table 5.4: QSAR results

Hypothesis	AAADRRR	AAAADDR
Survival rate	2.809	3.366
No. of compounds in training set	51	52
No. of compounds in test set	11	10
Test set compounds	11, 13, 34, 48, 55, 59, 65, 77, 78, 82, 85	11, 13, 34, 48, 55, 59, 65, 77, 82, 85
PLS factors	5	5
SD	0.3194	0.2817
R ²	0.5201	0.6197
F	9.8	15
P	2.314e - 06	9.998e-09
RMSE	0.3146	0.3187
Q ²	0.5005	0.5196
Pearson-R	0.7286	0.7281

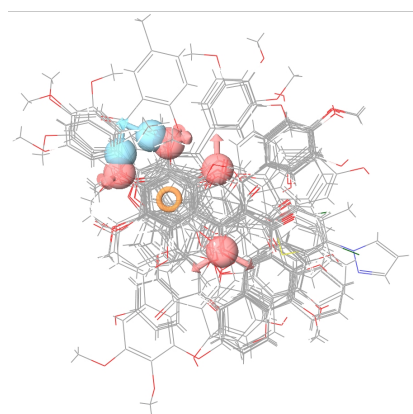
SD= Standard deviation of regression, R²= Coefficient of determination, F= Ratio of model variance to observed activity variance, P= Significance level of F, RMSE= RMS error in the test set prediction, Q²= Parameter directly proportional to R², Pearson-R= Correlation constant for predicted and observed activity for test set.



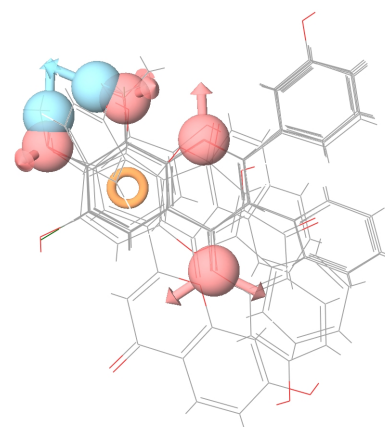
(A) AAADRRR Training Set



(B) AAADRRR Test Set

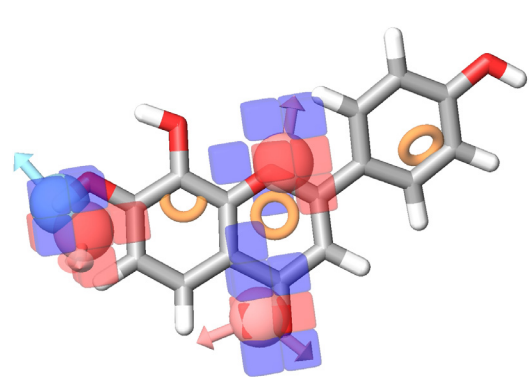


(C) AAAADDR Training Set

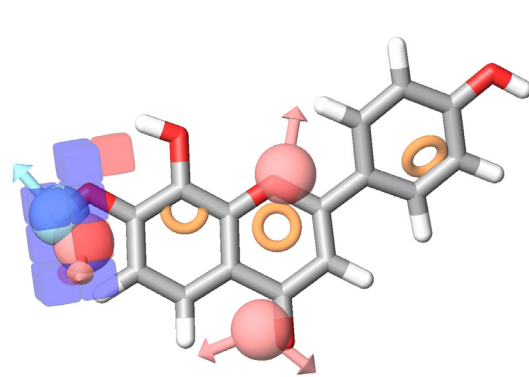


(D) AAAADDR Test Set

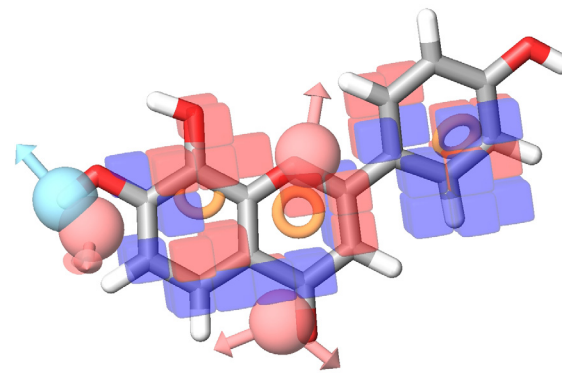
Figure 5.5: Training and test set used for building QSAR models for hypotheses AAADRRR (A, B) and AAAADDR (C, D)



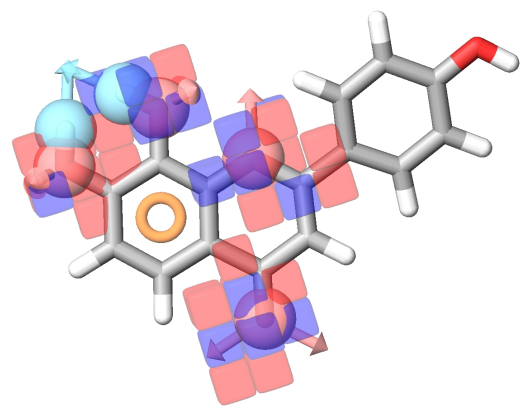
(A) Acceptor contribution



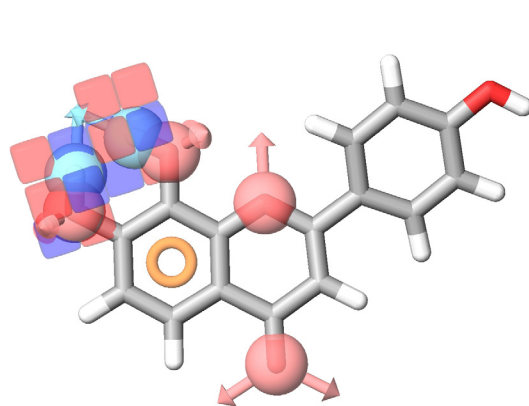
(B) Donor Contribution



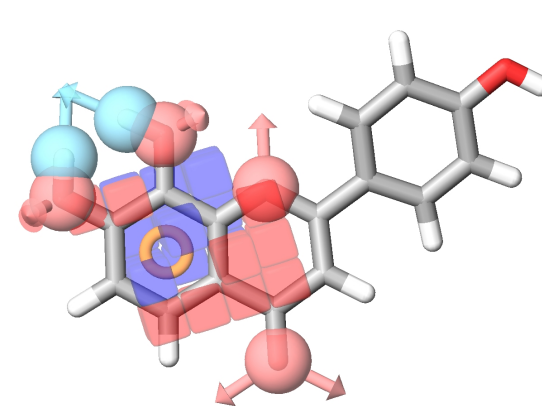
(C) Aromatic Ring Contribution



(D) Acceptor contribution



(E) Donor Contribution



(F) Aromatic Ring Contribution

Figure 5.6: Contribution of sites to pharmacophores AAADRRR (A, B, C) & AAAADDR (D, E, F)

whereas ring B does not display that much importance for an aromatic feature as do rings A and C.

5.4 Pharmacophore Based Database Searching

Although, docking and scoring have been the most widely employed techniques, ligand-based virtual screening has also gained momentum in recent years, and in the absence of a crystal structure, it is one of the most widely used computer-aided approaches for drug lead discovery.¹⁵⁴⁻¹⁵⁶ As mentioned at the beginning of the chapter, the main aim of this study was to derive a reliable pharmacophore model which can be applied for QSAR studies and pharmacophore-based database screening to identify hits with similar chemical features, which is the next step in the study. For this purpose, two methods were followed. One is the use of the PHASE derived pharmacophore models to find matches using different databases (Figures 5.7A and 5.7B). The other approach is to generate a 3D map of these pharmacophoric features by defining the distances and distance tolerance between them (Figures 5.7C and 5.7D) and then using this map as a query to perform UNITY database searching. Figures 5.7A and 5.7B contain the two pharmacophores that can be used as such for finding matches, and Figures 5.7C and 5.7D are the 3D maps of the pharmacophores built in the SYBYL UNITY module.

5.5 Summary

In view of these observations, the present study may have identified some important pharmacophores of flavone derivatives for concentrative nucleoside transporter type 3 inhibition. 3D-pharmacophore models were generated using a data set of 62 compounds which was split into training and test sets. The best models consisted of important chemical features, and mapped well to the ligands. The fairly good predictive abilities of these models are shown by Pearson-R values of 0.7286 and 0.7281 for hypothesis AAADRRR and AAAADDR, respectively. The study also supports the notion that the presence of three aromatic rings with 7- position donor and 8- position acceptor groups is the optimum for activity and can be used as a template pharmacophore for virtual screening using various available modeling programs and databases. Additionally, the presence of H-bond acceptors at position 1 and 4 contributes favorably to activity.

Thus, in conclusion, it can be stated that the pharmacophore models derived from this study may be used to retrieve inhibitors from databases and hence they could be used as a fast tool to assist the discovery of novel hCNT3 inhibitors either at the hit discovery (database screening) or lead optimization (activity prediction) stages.

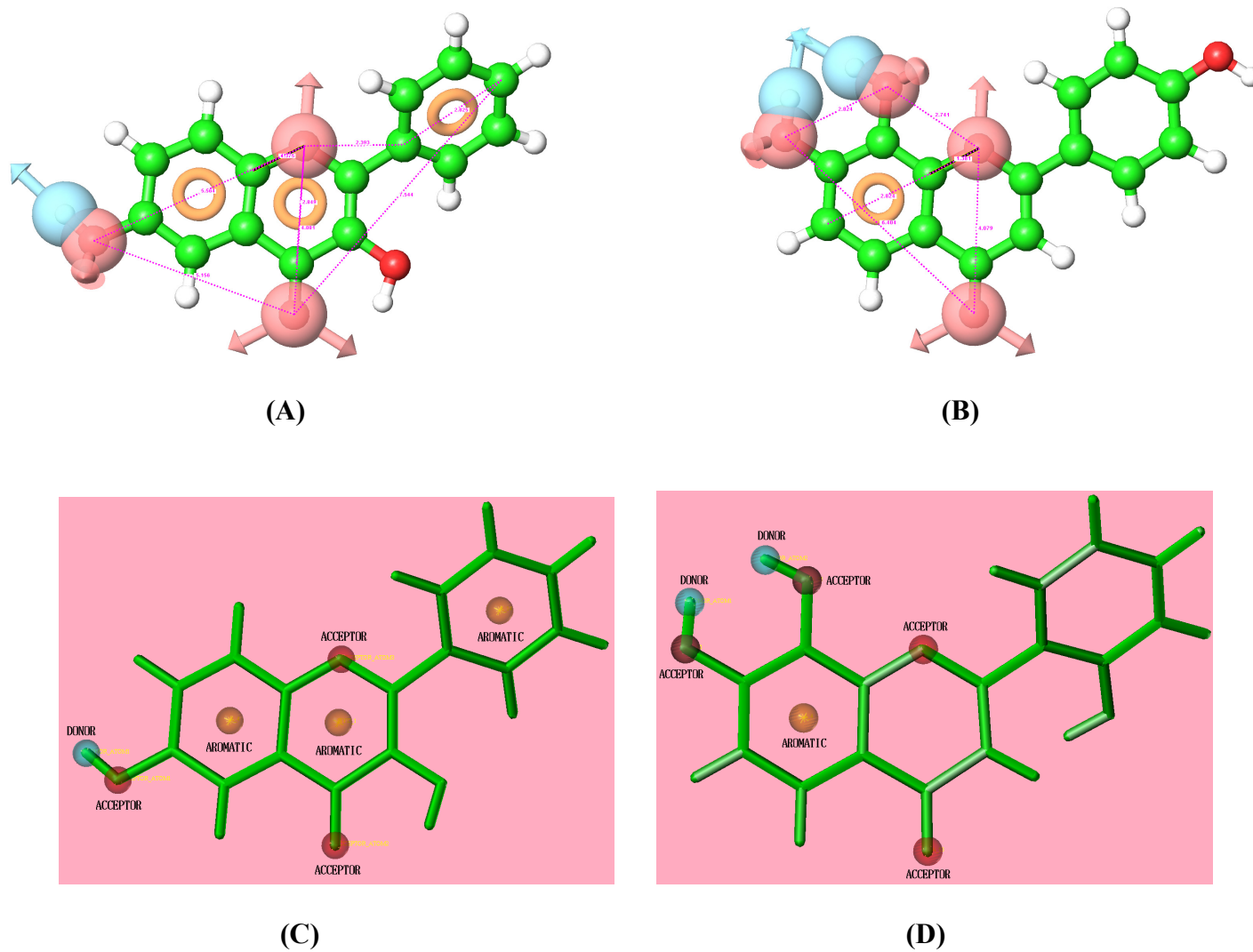


Figure 5.7: PHASE hypotheses (A and B) and UNITY query (C and D) to be used for database searching

List of References

1. Vranic, II; Matic, M.; Perunicic, J.; Simic, T.; Soskic, L.; Milic, N., Adenosine cardioprotection study in clinical setting of paroxysmal supraventricular tachycardia. *Prostaglandins Leukot Essent Fatty Acids* **2006**, 74, (6), 365-71.
2. Ciruela, F.; Casado, V.; Rodrigues, R. J.; Lujan, R.; Burgueno, J.; Canals, M.; Borycz, J.; Rebola, N.; Goldberg, S. R.; Mallol, J.; Cortes, A.; Canela, E. I.; Lopez-Gimenez, J. F.; Milligan, G.; Lluís, C.; Cunha, R. A.; Ferre, S.; Franco, R., Presynaptic control of striatal glutamatergic neurotransmission by adenosine A1-A2A receptor heteromers. *J Neurosci* **2006**, 26, (7), 2080-7.
3. O'Brien J, R., Platelet aggregation: Part I Some effects of the adenosine phosphates, thrombin, and cocaine upon platelet adhesiveness. *J Clin Pathol* **1962**, 15, (5), 446-52.
4. Moir, T. W.; Jones, P. K., Observations on the effect of changes in arterial oxygenation on adenosine induced coronary vasodilation. *Adv Exp Med Biol* **1973**, 39, 11-26.
5. Fain, J. N.; Pointer, R. H.; Ward, W. F., Effects of adenosine nucleosides on adenylate cyclase, phosphodiesterase, cyclic adenosine monophosphate accumulation, and lipolysis in fat cells. *J Biol Chem* **1972**, 247, (21), 6866-72.
6. Yamazaki, R. K., Glucagon stimulation of mitochondrial respiration. *J Biol Chem* **1975**, 250, (19), 7924-30.
7. Goldberg, A. L.; Singer, J. J., Evidence for a role of cyclic AMP in neuromuscular transmission. *Proc Natl Acad Sci U S A* **1969**, 64, (1), 134-41.
8. Matsushita, S.; Fanburg, B. L., Pyrimidine nucleotide synthesis in the normal and hypertrophying rat heart. Relative importance of the de novo and "salvage" pathways. *Circ Res* **1970**, 27, (3), 415-28.
9. Maguire, M. H.; Lukas, M. C.; Rettie, J. F., Adenine nucleotide salvage synthesis in the rat heart; pathways of adnosine salvage. *Biochim Biophys Acta* **1972**, 262, (2), 108-15.
10. Lech-Maranda, E.; Korycka, A.; Robak, T., Pharmacological and clinical studies on purine nucleoside analogs--new anticancer agents. *Mini Rev Med Chem* **2006**, 6, (5), 575-81.
11. Painter, G. R.; Almond, M. R.; Mao, S.; Liotta, D. C., Biochemical and mechanistic basis for the activity of nucleoside analogue inhibitors of HIV reverse transcriptase. *Curr Top Med Chem* **2004**, 4, (10), 1035-44.

12. Plagemann, P. G.; Wohlhueter, R. M.; Woffendin, C., Nucleoside and nucleobase transport in animal cells. *Biochim Biophys Acta* **1988**, 947, (3), 405-43.
13. Jacquez, J. A., Transport and enzymic splitting of pyrimidine nucleosides in Ehrlich cells. *Biochim Biophys Acta* **1962**, 61, 265-77.
14. Belt, J. A., Heterogeneity of nucleoside transport in mammalian cells. Two types of transport activity in L1210 and other cultured neoplastic cells. *Mol Pharmacol* **1983**, 24, (3), 479-84.
15. Plagemann, P. G.; Wohlhueter, R. M., Nucleoside transport in cultured mammalian cells. Multiple forms with different sensitivity to inhibition by nitrobenzylthioinosine or hypoxanthine. *Biochim Biophys Acta* **1984**, 773, (1), 39-52.
16. Gray, J. H.; Owen, R. P.; Giacomini, K. M., The concentrative nucleoside transporter family, SLC28. *Pflugers Arch* **2004**, 447, (5), 728-34.
17. Jakobs, E. S.; Paterson, A. R., Sodium-dependent, concentrative nucleoside transport in cultured intestinal epithelial cells. *Biochem Biophys Res Commun* **1986**, 140, (3), 1028-35.
18. Le Hir, M.; Dubach, U. C., Sodium gradient-energized concentrative transport of adenosine in renal brush border vesicles. *Pflugers Arch* **1984**, 401, (1), 58-63.
19. Le Hir, M.; Dubach, U. C., Uphill transport of pyrimidine nucleosides in renal brush border vesicles. *Pflugers Arch* **1985**, 404, (3), 238-43.
20. Huang, Q. Q.; Yao, S. Y.; Ritzel, M. W.; Paterson, A. R.; Cass, C. E.; Young, J. D., Cloning and functional expression of a complementary DNA encoding a mammalian nucleoside transport protein. *J Biol Chem* **1994**, 269, (27), 17757-60.
21. Che, M.; Ortiz, D. F.; Arias, I. M., Primary structure and functional expression of a cDNA encoding the bile canalicular, purine-specific Na(+)-nucleoside cotransporter. *J Biol Chem* **1995**, 270, (23), 13596-9.
22. Wang, J.; Su, S. F.; Dresser, M. J.; Schaner, M. E.; Washington, C. B.; Giacomini, K. M., Na(+)-dependent purine nucleoside transporter from human kidney: cloning and functional characterization. *Am J Physiol* **1997**, 273, (6 Pt 2), F1058-65.
23. Ritzel, M. W.; Ng, A. M.; Yao, S. Y.; Graham, K.; Loewen, S. K.; Smith, K. M.; Ritzel, R. G.; Mowles, D. A.; Carpenter, P.; Chen, X. Z.; Karpinski, E.; Hyde, R. J.; Baldwin, S. A.; Cass, C. E.; Young, J. D., Molecular identification and characterization of novel human and mouse concentrative Na⁺-nucleoside

- cotransporter proteins (hCNT3 and mCNT3) broadly selective for purine and pyrimidine nucleosides (system cib). *J Biol Chem* **2001**, 276, (4), 2914-27.
24. Huang, M.; Wang, Y.; Cogut, S. B.; Mitchell, B. S.; Graves, L. M., Inhibition of nucleoside transport by protein kinase inhibitors. *J Pharmacol Exp Ther* **2003**, 304, (2), 753-60.
 25. Loewen, S. K.; Ng, A. M.; Yao, S. Y.; Cass, C. E.; Baldwin, S. A.; Young, J. D., Identification of amino acid residues responsible for the pyrimidine and purine nucleoside specificities of human concentrative Na(+) nucleoside cotransporters hCNT1 and hCNT2. *J Biol Chem* **1999**, 274, (35), 24475-84.
 26. Ritzel, M. W.; Yao, S. Y.; Huang, M. Y.; Elliott, J. F.; Cass, C. E.; Young, J. D., Molecular cloning and functional expression of cDNAs encoding a human Na⁺-nucleoside cotransporter (hCNT1). *Am J Physiol* **1997**, 272, (2 Pt 1), C707-14.
 27. Mangravite, L. M.; Xiao, G.; Giacomini, K. M., Localization of human equilibrative nucleoside transporters, hENT1 and hENT2, in renal epithelial cells. *Am J Physiol Renal Physiol* **2003**, 284, (5), F902-10.
 28. Lai, Y.; Bakken, A. H.; Unadkat, J. D., Simultaneous expression of hCNT1-CFP and hENT1-YFP in Madin-Darby canine kidney cells. Localization and vectorial transport studies. *J Biol Chem* **2002**, 277, (40), 37711-7.
 29. Anderson, C. M.; Baldwin, S. A.; Young, J. D.; Cass, C. E.; Parkinson, F. E., Distribution of mRNA encoding a nitrobenzylthioinosine-insensitive nucleoside transporter (ENT2) in rat brain. *Brain Res Mol Brain Res* **1999**, 70, (2), 293-7.
 30. Dresser, M. J.; Gerstin, K. M.; Gray, A. T.; Loo, D. D.; Giacomini, K. M., Electrophysiological analysis of the substrate selectivity of a sodium-coupled nucleoside transporter (rCNT1) expressed in *Xenopus laevis* oocytes. *Drug Metab Dispos* **2000**, 28, (9), 1135-40.
 31. Crawford, C. R.; Cass, C. E.; Young, J. D.; Belt, J. A., Stable expression of a recombinant sodium-dependent, pyrimidine-selective nucleoside transporter (CNT1) in a transport-deficient mouse leukemia cell line. *Biochem Cell Biol* **1998**, 76, (5), 843-51.
 32. Yao, S. Y.; Ng, A. M.; Ritzel, M. W.; Gati, W. P.; Cass, C. E.; Young, J. D., Transport of adenosine by recombinant purine- and pyrimidine-selective sodium/nucleoside cotransporters from rat jejunum expressed in *Xenopus laevis* oocytes. *Mol Pharmacol* **1996**, 50, (6), 1529-35.
 33. Vickers, M. F.; Young, J. D.; Baldwin, S. A.; Ellison, M. J.; Cass, C. E., Functional production of mammalian concentrative nucleoside transporters in *Saccharomyces cerevisiae*. *Mol Membr Biol* **2001**, 18, (1), 73-9.

34. Mackey, J. R.; Mani, R. S.; Selner, M.; Mowles, D.; Young, J. D.; Belt, J. A.; Crawford, C. R.; Cass, C. E., Functional nucleoside transporters are required for gemcitabine influx and manifestation of toxicity in cancer cell lines. *Cancer Res* **1998**, *58*, (19), 4349-57.
35. Larrayoz, I. M.; Casado, F. J.; Pastor-Anglada, M.; Lostao, M. P., Electrophysiological characterization of the human Na⁽⁺⁾/nucleoside cotransporter 1 (hCNT1) and role of adenosine on hCNT1 function. *J Biol Chem* **2004**, *279*, (10), 8999-9007.
36. Mata, J. F.; Garcia-Manteiga, J. M.; Lostao, M. P.; Fernandez-Veledo, S.; Guillen-Gomez, E.; Larrayoz, I. M.; Lloberas, J.; Casado, F. J.; Pastor-Anglada, M., Role of the human concentrative nucleoside transporter (hCNT1) in the cytotoxic action of 5[Prime]-deoxy-5-fluorouridine, an active intermediate metabolite of capecitabine, a novel oral anticancer drug. *Mol Pharmacol* **2001**, *59*, (6), 1542-8.
37. Schaner, M. E.; Wang, J.; Zhang, L.; Su, S. F.; Gerstin, K. M.; Giacomini, K. M., Functional characterization of a human purine-selective, Na⁺-dependent nucleoside transporter (hSPNT1) in a mammalian expression system. *J Pharmacol Exp Ther* **1999**, *289*, (3), 1487-91.
38. Li, J. Y.; Boado, R. J.; Pardridge, W. M., Differential kinetics of transport of 2',3'-dideoxyinosine and adenosine via concentrative Na⁺ nucleoside transporter CNT2 cloned from rat blood-brain barrier. *J Pharmacol Exp Ther* **2001**, *299*, (2), 735-40.
39. Plagemann, P. G.; Aran, J. M., Characterization of Na⁽⁺⁾-dependent, active nucleoside transport in rat and mouse peritoneal macrophages, a mouse macrophage cell line and normal rat kidney cells. *Biochim Biophys Acta* **1990**, *1028*, (3), 289-98.
40. Ritzel, M. W.; Ng, A. M.; Yao, S. Y.; Graham, K.; Loewen, S. K.; Smith, K. M.; Hyde, R. J.; Karpinski, E.; Cass, C. E.; Baldwin, S. A.; Young, J. D., Recent molecular advances in studies of the concentrative Na⁺-dependent nucleoside transporter (CNT) family: identification and characterization of novel human and mouse proteins (hCNT3 and mCNT3) broadly selective for purine and pyrimidine nucleosides (system cib). *Mol Membr Biol* **2001**, *18*, (1), 65-72.
41. Osses, N.; Pearson, J. D.; Yudilevich, D. L.; Jarvis, S. M., Hypoxanthine enters human vascular endothelial cells (ECV 304) via the nitrobenzylthioinosine-insensitive equilibrative nucleoside transporter. *Biochem J* **1996**, *317* (Pt 3), 843-8.

42. Flanagan, S. A.; Meckling-Gill, K. A., Characterization of a novel Na⁺-dependent, guanosine-specific, nitrobenzylthioinosine-sensitive transporter in acute promyelocytic leukemia cells. *J Biol Chem* **1997**, 272, (29), 18026-32.
43. Vickers, M. F.; Mani, R. S.; Sundaram, M.; Hogue, D. L.; Young, J. D.; Baldwin, S. A.; Cass, C. E., Functional production and reconstitution of the human equilibrative nucleoside transporter (hENT1) in *Saccharomyces cerevisiae*. Interaction of inhibitors of nucleoside transport with recombinant hENT1 and a glycosylation-defective derivative (hENT1/N48Q). *Biochem J* **1999**, 339 (Pt 1), 21-32.
44. Cabrita, M. A.; Baldwin, S. A.; Young, J. D.; Cass, C. E., Molecular biology and regulation of nucleoside and nucleobase transporter proteins in eukaryotes and prokaryotes. *Biochem Cell Biol* **2002**, 80, (5), 623-38.
45. Zhang, J.; Visser, F.; Vickers, M. F.; Lang, T.; Robins, M. J.; Nielsen, L. P.; Nowak, I.; Baldwin, S. A.; Young, J. D.; Cass, C. E., Uridine binding motifs of human concentrative nucleoside transporters 1 and 3 produced in *Saccharomyces cerevisiae*. *Mol Pharmacol* **2003**, 64, (6), 1512-20.
46. Chang, C.; Swaan, P. W.; Ngo, L. Y.; Lum, P. Y.; Patil, S. D.; Unadkat, J. D., Molecular requirements of the human nucleoside transporters hCNT1, hCNT2, and hENT1. *Mol Pharmacol* **2004**, 65, (3), 558-70.
47. Zhang, J.; Smith, K. M.; Tackaberry, T.; Visser, F.; Robins, M. J.; Nielsen, L. P.; Nowak, I.; Karpinski, E.; Baldwin, S. A.; Young, J. D.; Cass, C. E., Uridine binding and transportability determinants of human concentrative nucleoside transporters. *Mol Pharmacol* **2005**, 68, (3), 830-9.
48. Toan, S. V.; To, K. K.; Leung, G. P.; de Souza, M. O.; Ward, J. L.; Tse, C. M., Genomic organization and functional characterization of the human concentrative nucleoside transporter-3 isoform (hCNT3) expressed in mammalian cells. *Pflugers Arch* **2003**, 447, (2), 195-204.
49. Nonaka, Y. T., K.; Hiratochi, M; Kuramochi, Y; Isaji, M Preparation of 5'-modified nucleoside derivatives as CNT-2 inhibitors. WO 2004101593, 2004.
50. Kikuchi, N. N., Y; Tatani, K; Hiratochi, M; Kuramohi, Y; Isaji, M; Shimizu, K; Miyagi, T Preparation of Ribofuranoside compounds having benzimidazole moiety as CNT2 inhibitors. WO 2005063788, 2005.
51. Tatani, K. N., Y; Kikuchi, N; Preparation of purine nucleoside derivatives modified in 8-position as inhibitors of concentrative nucleoside transporter 2. WO 2006030803, 2006.

52. Crespy, V.; Aprikian, O.; Morand, C.; Besson, C.; Manach, C.; Demigne, C.; Remesy, C., Bioavailability of phloretin and phloridzin in rats. *J Nutr* **2001**, 131, (12), 3227-30.
53. Baldwin, S. A.; Beal, P. R.; Yao, S. Y.; King, A. E.; Cass, C. E.; Young, J. D., The equilibrative nucleoside transporter family, SLC29. *Pflugers Arch* **2004**, 447, (5), 735-43.
54. Sundaram, M.; Yao, S. Y.; Ng, A. M.; Griffiths, M.; Cass, C. E.; Baldwin, S. A.; Young, J. D., Chimeric constructs between human and rat equilibrative nucleoside transporters (hENT1 and rENT1) reveal hENT1 structural domains interacting with coronary vasoactive drugs. *J Biol Chem* **1998**, 273, (34), 21519-25.
55. Vijayalakshmi, D.; Belt, J. A., Sodium-dependent nucleoside transport in mouse intestinal epithelial cells. Two transport systems with differing substrate specificities. *J Biol Chem* **1988**, 263, (36), 19419-23.
56. FitzGerald, G. A., Dipyridamole. *N Engl J Med* **1987**, 316, (20), 1247-57.
57. Griffiths, M.; Beaumont, N.; Yao, S. Y.; Sundaram, M.; Boumah, C. E.; Davies, A.; Kwong, F. Y.; Coe, I.; Cass, C. E.; Young, J. D.; Baldwin, S. A., Cloning of a human nucleoside transporter implicated in the cellular uptake of adenosine and chemotherapeutic drugs. *Nat Med* **1997**, 3, (1), 89-93.
58. Sundaram, M.; Yao, S. Y.; Ingram, J. C.; Berry, Z. A.; Abidi, F.; Cass, C. E.; Baldwin, S. A.; Young, J. D., Topology of a human equilibrative, nitrobenzylthioinosine (NBMPR)-sensitive nucleoside transporter (hENT1) implicated in the cellular uptake of adenosine and anti-cancer drugs. *J Biol Chem* **2001**, 276, (48), 45270-5.
59. Yao, S. Y.; Ng, A. M.; Muzyka, W. R.; Griffiths, M.; Cass, C. E.; Baldwin, S. A.; Young, J. D., Molecular cloning and functional characterization of nitrobenzylthioinosine (NBMPR)-sensitive (es) and NBMPR-insensitive (ei) equilibrative nucleoside transporter proteins (rENT1 and rENT2) from rat tissues. *J Biol Chem* **1997**, 272, (45), 28423-30.
60. Handa, M.; Choi, D. S.; Caldeiro, R. M.; Messing, R. O.; Gordon, A. S.; Diamond, I., Cloning of a novel isoform of the mouse NBMPR-sensitive equilibrative nucleoside transporter (ENT1) lacking a putative phosphorylation site. *Gene* **2001**, 262, (1-2), 301-7.
61. Kiss, A.; Farah, K.; Kim, J.; Garriock, R. J.; Drysdale, T. A.; Hammond, J. R., Molecular cloning and functional characterization of inhibitor-sensitive (mENT1) and inhibitor-resistant (mENT2) equilibrative nucleoside transporters from mouse brain. *Biochem J* **2000**, 352 Pt 2, 363-72.

62. Sundaram, M.; Yao, S. Y.; Ng, A. M.; Cass, C. E.; Baldwin, S. A.; Young, J. D., Equilibrative nucleoside transporters: mapping regions of interaction for the substrate analogue nitrobenzylthioinosine (NBMPR) using rat chimeric proteins. *Biochemistry* **2001**, 40, (27), 8146-51.
63. Crawford, C. R.; Patel, D. H.; Naeve, C.; Belt, J. A., Cloning of the human equilibrative, nitrobenzylmercaptapurine riboside (NBMPR)-insensitive nucleoside transporter ei by functional expression in a transport-deficient cell line. *J Biol Chem* **1998**, 273, (9), 5288-93.
64. Griffiths, M.; Yao, S. Y.; Abidi, F.; Phillips, S. E.; Cass, C. E.; Young, J. D.; Baldwin, S. A., Molecular cloning and characterization of a nitrobenzylthioinosine-insensitive (ei) equilibrative nucleoside transporter from human placenta. *Biochem J* **1997**, 328 (Pt 3), 739-43.
65. Griffith, D. A.; Jarvis, S. M., Nucleoside and nucleobase transport systems of mammalian cells. *Biochim Biophys Acta* **1996**, 1286, (3), 153-81.
66. Ward, J. L.; Leung, G. P.; Toan, S. V.; Tse, C. M., Functional analysis of site-directed glycosylation mutants of the human equilibrative nucleoside transporter-2. *Arch Biochem Biophys* **2003**, 411, (1), 19-26.
67. Pennycooke, M.; Chaudary, N.; Shuralyova, I.; Zhang, Y.; Coe, I. R., Differential expression of human nucleoside transporters in normal and tumor tissue. *Biochem Biophys Res Commun* **2001**, 280, (3), 951-9.
68. Musa, H.; Dobrzynski, H.; Berry, Z.; Abidi, F.; Cass, C. E.; Young, J. D.; Baldwin, S. A.; Boyett, M. R., Immunocytochemical demonstration of the equilibrative nucleoside transporter rENT1 in rat sinoatrial node. *J Histochem Cytochem* **2002**, 50, (3), 305-9.
69. Jennings, L. L.; Hao, C.; Cabrita, M. A.; Vickers, M. F.; Baldwin, S. A.; Young, J. D.; Cass, C. E., Distinct regional distribution of human equilibrative nucleoside transporter proteins 1 and 2 (hENT1 and hENT2) in the central nervous system. *Neuropharmacology* **2001**, 40, (5), 722-31.
70. Ward, J. L.; Sherali, A.; Mo, Z. P.; Tse, C. M., Kinetic and pharmacological properties of cloned human equilibrative nucleoside transporters, ENT1 and ENT2, stably expressed in nucleoside transporter-deficient PK15 cells. Ent2 exhibits a low affinity for guanosine and cytidine but a high affinity for inosine. *J Biol Chem* **2000**, 275, (12), 8375-81.
71. Yao, S. Y.; Ng, A. M.; Sundaram, M.; Cass, C. E.; Baldwin, S. A.; Young, J. D., Transport of antiviral 3'-deoxy-nucleoside drugs by recombinant human and rat equilibrative, nitrobenzylthioinosine (NBMPR)-insensitive (ENT2) nucleoside

- transporter proteins produced in *Xenopus* oocytes. *Mol Membr Biol* **2001**, 18, (2), 161-7.
72. Yao, S. Y.; Ng, A. M.; Vickers, M. F.; Sundaram, M.; Cass, C. E.; Baldwin, S. A.; Young, J. D., Functional and molecular characterization of nucleobase transport by recombinant human and rat equilibrative nucleoside transporters 1 and 2. Chimeric constructs reveal a role for the ENT2 helix 5-6 region in nucleobase translocation. *J Biol Chem* **2002**, 277, (28), 24938-48.
 73. Vickers, M. F.; Kumar, R.; Visser, F.; Zhang, J.; Charania, J.; Raborn, R. T.; Baldwin, S. A.; Young, J. D.; Cass, C. E., Comparison of the interaction of uridine, cytidine, and other pyrimidine nucleoside analogues with recombinant human equilibrative nucleoside transporter 2 (hENT2) produced in *Saccharomyces cerevisiae*. *Biochem Cell Biol* **2002**, 80, (5), 639-44.
 74. Appleford, P. J.; Griffiths, M.; Yao, S. Y.; Ng, A. M.; Chomey, E. G.; Isaac, R. E.; Coates, D.; Hope, I. A.; Cass, C. E.; Young, J. D.; Baldwin, S. A., Functional redundancy of two nucleoside transporters of the ENT family (CeENT1, CeENT2) required for development of *Caenorhabditis elegans*. *Mol Membr Biol* **2004**, 21, (4), 247-59.
 75. Governo, R. J.; Deuchars, J.; Baldwin, S. A.; King, A. E., Localization of the NBMPR-sensitive equilibrative nucleoside transporter, ENT1, in the rat dorsal root ganglion and lumbar spinal cord. *Brain Res* **2005**, 1059, (2), 129-38.
 76. Visser, F.; Zhang, J.; Raborn, R. T.; Baldwin, S. A.; Young, J. D.; Cass, C. E., Residue 33 of human equilibrative nucleoside transporter 2 is a functionally important component of both the dipyrindamole and nucleoside binding sites. *Mol Pharmacol* **2005**, 67, (4), 1291-8.
 77. Zhou, M.; Xia, L.; Engel, K.; Wang, J., Molecular determinants of substrate selectivity of a novel organic cation transporter (PMAT) in the SLC29 family. *J Biol Chem* **2007**, 282, (5), 3188-95.
 78. Barnes, K.; Dobrzynski, H.; Foppolo, S.; Beal, P. R.; Ismat, F.; Scullion, E. R.; Sun, L.; Tellez, J.; Ritzel, M. W.; Claycomb, W. C.; Cass, C. E.; Young, J. D.; Billeter-Clark, R.; Boyett, M. R.; Baldwin, S. A., Distribution and functional characterization of equilibrative nucleoside transporter-4, a novel cardiac adenosine transporter activated at acidic pH. *Circ Res* **2006**, 99, (5), 510-9.
 79. Paul, B.; Chen, M. F.; Paterson, A. R., Inhibitors of nucleoside transport. A structure-activity study using human erythrocytes. *J Med Chem* **1975**, 18, (10), 968-73.
 80. Lauzon, G. J.; Paterson, A. R., Binding of the nucleoside transport inhibitor nitrobenzylthioinosine to HeLa cells. *Mol Pharmacol* **1977**, 13, (5), 883-91.

81. Paterson, A. R.; Naik, S. R.; Cass, C. E., Inhibition of uridine uptake in HeLa cells by nitrobenzylthioinosine and related compounds. *Mol Pharmacol* **1977**, *13*, (6), 1014-23.
82. Stoeckler, J. D.; Rosenfield, C. G.; Chu, S. H.; Li, S. Y.; Acton, E. M.; Ryan, K. J.; Parks, R. E., Jr., Inhibition of nucleoside transport by nitrobenzylthioformycin analogs. *Biochem Pharmacol* **1990**, *40*, (3), 615-9.
83. Ziemnicka-Merchant, B.; Aran, J. M.; Plagemann, P. G.; Krafft, G. A., Effects of chemical modification of nitrobenzylthioinosine on its binding to high-affinity membrane binding sites and inhibition of nucleoside transport. *Biochem Pharmacol* **1992**, *44*, (8), 1577-83.
84. Zhu, Z.; Furr, J.; Buolamwini, J. K., Synthesis and flow cytometric evaluation of novel 1,2,3,4-tetrahydroisoquinoline conformationally constrained analogues of nitrobenzylmercaptapurine riboside (NBMPR) designed for probing its conformation when bound to the es nucleoside transporter. *J Med Chem* **2003**, *46*, (5), 831-7.
85. Tromp, R. A.; Spanjersberg, R. F.; von Frijtag Drabbe Kunzel, J. K.; AP, I. J., Inhibition of nucleoside transport proteins by C8-alkylamine-substituted purines. *J Med Chem* **2005**, *48*, (1), 321-9.
86. Kadatz, R., [Pharmacological properties of a new coronary dilator substance 2, 6-bis(diethanolamino)-4, 8-dipiperidino-pyrimido[5,4-d]pyrimidine.]. *Arzneimittelforschung* **1959**, *9*, (1), 39-45.
87. Nott, M. W., The possible role of adenosine in the coronary dilator action of some pyrimidopyrimidines and pteridines. *Br J Pharmacol* **1970**, *39*, (2), 287-95.
88. Ijzerman, A. P.; Thedinga, K. H.; Custers, A. F.; Hoos, B.; Van Belle, H., Inhibition of nucleoside transport by a new series of compounds related to lidoflazine and mioflazine. *Eur J Pharmacol* **1989**, *172*, (3), 273-81.
89. Pirovano, I. M.; Van Belle, H.; Ijzerman, A. P., Inhibition of nucleoside uptake in human erythrocytes by a new series of compounds related to lidoflazine and mioflazine. *Eur J Pharmacol* **1990**, *189*, (6), 419-22.
90. Huang, M.; Wang, Y.; Mitchell, B. S.; Graves, L. M., Regulation of equilibrative nucleoside uptake by protein kinase inhibitors. *Nucleosides Nucleotides Nucleic Acids* **2004**, *23*, (8-9), 1445-50.
91. Carrier, E. J.; Auchampach, J. A.; Hillard, C. J., Inhibition of an equilibrative nucleoside transporter by cannabidiol: a mechanism of cannabinoid immunosuppression. *Proc Natl Acad Sci U S A* **2006**, *103*, (20), 7895-900.

92. Balwierczak, J. L.; Krulan, C. M.; Wang, Z. C.; Chen, J.; Jeng, A. Y., Effects of adenosine A2 receptor agonists on nucleoside transport. *J Pharmacol Exp Ther* **1989**, 251, (1), 279-87.
93. Striessnig, J.; Zernig, G.; Glossmann, H., Human red-blood-cell Ca²⁺-antagonist binding sites. Evidence for an unusual receptor coupled to the nucleoside transporter. *Eur J Biochem* **1985**, 150, (1), 67-77.
94. Agrotis, A.; Little, P. J.; Saltis, J.; Bobik, A., Dihydropyridine Ca²⁺ channel antagonists inhibit the salvage pathway for DNA synthesis in human vascular smooth muscle cells. *Eur J Pharmacol* **1993**, 244, (3), 269-75.
95. Shank, R. P.; Baldy, W. J., Adenosine transport by rat and guinea pig synaptosomes: basis for differential sensitivity to transport inhibitors. *J Neurochem* **1990**, 55, (2), 541-50.
96. Hammond, J. R.; Clanachan, A. S., [3H]nitrobenzylthioinosine binding to the guinea pig CNS nucleoside transport system: a pharmacological characterization. *J Neurochem* **1984**, 43, (6), 1582-92.
97. Deckert, J.; Morgan, P. F.; Marangos, P. J., Adenosine uptake site heterogeneity in the mammalian CNS? Uptake inhibitors as probes and potential neuropharmaceuticals. *Life Sci* **1988**, 42, (14), 1331-45.
98. Loike, J. D.; Horwitz, S. B., Effect of VP-16-213 on the intracellular degradation of DNA in HeLa cells. *Biochemistry* **1976**, 15, (25), 5443-8.
99. Yalowich, J. C.; Goldman, I. D., Analysis of the inhibitory effects of VP-16-213 (etoposide) and podophyllotoxin on thymidine transport and metabolism in Ehrlich ascites tumor cells in vitro. *Cancer Res* **1984**, 44, (3), 984-9.
100. White, J. C.; Hines, L. H.; Rathmell, J. P., Inhibition of 1-beta-D-arabinofuranosylecytosine transport and net accumulation by teniposide and etoposide in Ehrlich ascites cells and human leukemic blasts. *Cancer Res* **1985**, 45, (7), 3070-5.
101. Leung, G. P.; Man, R. Y.; Tse, C. M., Effect of thiazolidinediones on equilibrative nucleoside transporter-1 in human aortic smooth muscle cells. *Biochem Pharmacol* **2005**, 70, (3), 355-62.
102. Osada, Y.; Tsuchimoto, M.; Fukushima, H.; Takahashi, K.; Kondo, S.; Hasegawa, M.; Komoriya, K., Hypouricemic effect of the novel xanthine oxidase inhibitor, TEI-6720, in rodents. *Eur J Pharmacol* **1993**, 241, (2-3), 183-8.

103. Plagemann, P. G.; Wohlhueter, R. M., Effect of sulfhydryl reagents on nucleoside transport in cultured mammalian cells. *Arch Biochem Biophys* **1984**, 233, (2), 489-500.
104. Jarvis, S. M.; Young, J. D., Nucleoside transport in rat erythrocytes: two components with differences in sensitivity to inhibition by nitrobenzylthioinosine and p-chloromercuriphenyl sulfonate. *J Membr Biol* **1986**, 93, (1), 1-10.
105. Weber, G., Biochemical strategy of cancer cells and the design of chemotherapy: G. H. A. Clowes Memorial Lecture. *Cancer Res* **1983**, 43, (8), 3466-92.
106. Weber, G.; Lui, M. S.; Natsumeda, Y.; Faderan, M. A., Salvage capacity of hepatoma 3924A and action of dipyridamole. *Adv Enzyme Regul* **1983**, 21, 53-69.
107. Weber, G.; Jayaram, H. N.; Pillwein, K.; Natsumeda, Y.; Reardon, M. A.; Zhen, Y. S., Salvage pathways as targets of chemotherapy. *Adv Enzyme Regul* **1987**, 26, 335-52.
108. Horber, D. H.; Schott, H.; Schwendener, R. A., Cellular pharmacology of N4-hexadecyl-1-beta-D-arabinofuranosylcytosine in the human leukemic cell lines K-562 and U-937. *Cancer Chemother Pharmacol* **1995**, 36, (6), 483-92.
109. Hendrix, C. W.; Flexner, C.; Szebeni, J.; Kuwahara, S.; Pennypacker, S.; Weinstein, J. N.; Lietman, P. S., Effect of dipyridamole on zidovudine pharmacokinetics and short-term tolerance in asymptomatic human immunodeficiency virus-infected subjects. *Antimicrob Agents Chemother* **1994**, 38, (5), 1036-40.
110. Van Belle, H., Nucleoside transport inhibition: a therapeutic approach to cardioprotection via adenosine? *Cardiovasc Res* **1993**, 27, (1), 68-76.
111. De Jonge, R.; Out, M.; Maas, W. J.; De Jong, J. W., Preconditioning of rat hearts by adenosine A1 or A3 receptor activation. *Eur J Pharmacol* **2002**, 441, (3), 165-72.
112. Miura, T.; Tsuchida, A., Adenosine and preconditioning revisited. *Clin Exp Pharmacol Physiol* **1999**, 26, (2), 92-9.
113. Delicado, E. G.; Rodrigues, A.; Sen, R. P.; Sebastiao, A. M.; Ribeiro, J. A.; Miras-Portugal, M. T., Effect of 5'-(N-ethylcarboxamido)adenosine on adenosine transport in cultured chromaffin cells. *J Neurochem* **1990**, 54, (6), 1941-6.
114. Mosca, S. M.; Gelpi, R. J.; Cingolani, H. E., Adenosine and dipyridamole mimic the effects of ischemic preconditioning. *J Mol Cell Cardiol* **1994**, 26, (10), 1403-9.

115. Abd-Elfattah, A. S.; Ding, M.; Wechsler, A. S., Intermittent aortic crossclamping prevents cumulative adenosine triphosphate depletion, ventricular fibrillation, and dysfunction (stunning): is it preconditioning? *J Thorac Cardiovasc Surg* **1995**, 110, (2), 328-39.
116. Masuda, M.; Chang-Chun, C.; Mollhoff, T.; Van Belle, H.; Flameng, W., Effects of nucleoside transport inhibition on long-term ex vivo preservation of canine hearts. *J Thorac Cardiovasc Surg* **1992**, 104, (6), 1610-7.
117. Flameng, W., New strategies for intraoperative myocardial protection. *Curr Opin Cardiol* **1995**, 10, (6), 577-83.
118. Parkinson, F. E.; Rudolphi, K. A.; Fredholm, B. B., Propentofylline: a nucleoside transport inhibitor with neuroprotective effects in cerebral ischemia. *Gen Pharmacol* **1994**, 25, (6), 1053-8.
119. Fredholm, B. B.; Lindstrom, K.; Wallman-Johansson, A., Propentofylline and other adenosine transport inhibitors increase the efflux of adenosine following electrical or metabolic stimulation of rat hippocampal slices. *J Neurochem* **1994**, 62, (2), 563-73.
120. Koroshetz, W. J.; Moskowitz, M. A., Emerging treatments for stroke in humans. *Trends Pharmacol Sci* **1996**, 17, (6), 227-33.
121. Cronstein, B. N., Adenosine, an endogenous anti-inflammatory agent. *J Appl Physiol* **1994**, 76, (1), 5-13.
122. Ohta, A.; Sitkovsky, M., Role of G-protein-coupled adenosine receptors in downregulation of inflammation and protection from tissue damage. *Nature* **2001**, 414, (6866), 916-20.
123. Revan, S.; Montesinos, M. C.; Naime, D.; Landau, S.; Cronstein, B. N., Adenosine A2 receptor occupancy regulates stimulated neutrophil function via activation of a serine/threonine protein phosphatase. *J Biol Chem* **1996**, 271, (29), 17114-8.
124. Parmely, M. J.; Zhou, W. W.; Edwards, C. K., 3rd; Borchering, D. R.; Silverstein, R.; Morrison, D. C., Adenosine and a related carbocyclic nucleoside analogue selectively inhibit tumor necrosis factor-alpha production and protect mice against endotoxin challenge. *J Immunol* **1993**, 151, (1), 389-96.
125. Bouma, M. G.; van den Wildenberg, F. A.; Buurman, W. A., Adenosine inhibits cytokine release and expression of adhesion molecules by activated human endothelial cells. *Am J Physiol* **1996**, 270, (2 Pt 1), C522-9.

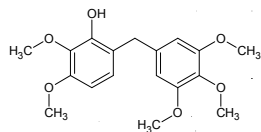
126. Le Vraux, V.; Chen, Y. L.; Masson, I.; De Sousa, M.; Giroud, J. P.; Florentin, I.; Chauvelot-Moachon, L., Inhibition of human monocyte TNF production by adenosine receptor agonists. *Life Sci* **1993**, 52, (24), 1917-24.
127. Izumino, K.; Iida, H.; Asaka, M.; Mizumura, Y.; Sasayama, S., Effect of the antiplatelet agents ticlopidine and dipyridamole on experimental immune complex glomerulonephritis in rats. *Nephron* **1986**, 43, (1), 56-61.
128. Lynch, T. P.; Paran, J. H.; Paterson, A. R., Therapy of mouse leukemia L1210 with combinations of nebularine and nitrobenzylthioinosine 5'-monophosphate. *Cancer Res* **1981**, 41, (2), 560-5.
129. Lynch, T. P.; Jakobs, E. S.; Paran, J. H.; Paterson, A. R., Treatment of mouse neoplasms with high doses of tubercidin. *Cancer Res* **1981**, 41, (8), 3200-4.
130. Kolassa, N.; Jakobs, E. S.; Buzzell, G. R.; Paterson, A. R., Manipulation of toxicity and tissue distribution of tubercidin in mice by nitrobenzylthioinosine 5'-monophosphate. *Biochem Pharmacol* **1982**, 31, (10), 1863-74.
131. el Kouni, M. H.; Diop, D.; Cha, S., Combination therapy of schistosomiasis by tubercidin and nitrobenzylthioinosine 5'-monophosphate. *Proc Natl Acad Sci U S A* **1983**, 80, (21), 6667-70.
132. el Kouni, M. H.; Messier, N. J.; Cha, S., Treatment of schistosomiasis by purine nucleoside analogues in combination with nucleoside transport inhibitors. *Biochem Pharmacol* **1987**, 36, (22), 3815-21.
133. el Kouni, M. H.; Knopf, P. M.; Cha, S. M., Combination therapy of *Schistosoma japonicum* by tubercidin and nitrobenzylthioinosine 5'-monophosphate. *Biochem Pharmacol* **1985**, 34, (21), 3921-3.
134. Ogbunude, P. O.; Ikediobi, C. O., Effect of nitrobenzylthioinosinate on the toxicity of tubercidin and ethidium against *Trypanosoma gambiense*. *Acta Trop* **1982**, 39, (3), 219-24.
135. Ogbunude, P. O.; al-Jaser, M. H., Experimental chemotherapy of leishmaniasis with adenosine analogue Formycin A, in combination with inhibitor of nucleoside transport, nitrobenzylthioinosinate. *Drugs Exp Clin Res* **1992**, 18, (10), 423-6.
136. Parker, M. D.; Hyde, R. J.; Yao, S. Y.; McRobert, L.; Cass, C. E.; Young, J. D.; McConkey, G. A.; Baldwin, S. A., Identification of a nucleoside/nucleobase transporter from *Plasmodium falciparum*, a novel target for anti-malarial chemotherapy. *Biochem J* **2000**, 349, (Pt 1), 67-75.

137. Gero, A. M.; Scott, H. V.; O'Sullivan, W. J.; Christopherson, R. I., Antimalarial action of nitrobenzylthioinosine in combination with purine nucleoside antimetabolites. *Mol Biochem Parasitol* **1989**, 34, (1), 87-97.
138. Schwartzman, J. D.; Pfefferkorn, E. R., Toxoplasma gondii: purine synthesis and salvage in mutant host cells and parasites. *Exp Parasitol* **1982**, 53, (1), 77-86.
139. Krug, E. C.; Marr, J. J.; Berens, R. L., Purine metabolism in Toxoplasma gondii. *J Biol Chem* **1989**, 264, (18), 10601-7.
140. Schwab, J. C.; Afifi Afifi, M.; Pizzorno, G.; Handschumacher, R. E.; Joiner, K. A., Toxoplasma gondii tachyzoites possess an unusual plasma membrane adenosine transporter. *Mol Biochem Parasitol* **1995**, 70, (1-2), 59-69.
141. Raghavan, K.; Kahn, S. D.; Buolamwini J. K., Building a hypothesis for nucleoside transport inhibitors, "Rational Drug Design- novel methodology and practical applications", ACS symposium series 719, **1999**, 153-164.
142. Cheng, Y.; Prusoff, W. H., Relationship between the inhibition constant (K₁) and the concentration of inhibitor which causes 50 per cent inhibition (I₅₀) of an enzymatic reaction. *Biochem Pharmacol* **1973**, 22, (23), 3099-108.
143. Cramer, I., R. D.; Patterson, D. E.; Bunce, J. D., Comparative Molecular Field Analysis. 1. Effect of Shape on Binding of Steroids to Carrier Proteins. *J. Am. chem. S.* **1988**, 110, 5959-5967.
144. Klebe, G.; Abraham, U.; Mietzner, T., Molecular similarity indices in a comparative analysis (CoMSIA) of drug molecules to correlate and predict their biological activity. *J. Med Chem* **1994**, 37, (24), 4130-46.
145. SYBYL, version 7.3; Tripos Inc.: 1699 South Hanley Road, St. Louis, MO 63144, USA.
146. Viswanadhan, V. N. G., A. K.; Revenkar, G. R.; Robins, R. J., *J. Chem. Info. and Comp. Sci.* **1989**, 29, 163.
147. Buolamwini, J. K. R., K.; Fesen, M. R.; Pommier, Y.; Kohn, K. W.; Weinstein, J. N., *Pharm. Research* **1996**, 13, 1891.
148. Xiao, Z.; Varma, S.; Xiao, Y.; Tropsha, A., Modeling of p38 mitogen-activated protein kinase inhibitors using the Catalyst™ HypoGen and *k*-nearest neighbor QSAR methods, *J. Mol. Grap. Mod.* , 23, **2004**, 129–138.
149. Mukherjee, S.; Nagar, S.; Mullick, S.; Mukherjee, A.; Saha, A., Pharmacophore mapping of arylbenzothiophene derivatives for MCF cell inhibition using classical and 3D space modeling approaches, *J. Mol. Grap. Mod.* 26, **2008**, 884–892.

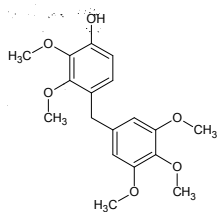
150. Lu, L.; Tsai, K.; Chiang, Y.; Jiaang, W.; Wu, S.; Mahindroo, N.; Chien, C.; Lee, S. J., A three-dimensional pharmacophore model for dipeptidyl peptidase IV inhibitors, *European J. Med. Chem.*, 20, **2007**, 1-9
151. Karki, R. G.; Kulkarni, V. M., A feature based pharmacophore for *Candida albicans* MyristoylCoA: protein *N*-myristoyltransferase inhibitors, *Eur. J. Med. Chem.*, 36, **2001**, 147–163.
152. MAESTRO, version 7.5; Schrodinger Inc.: 120 West 45th Street, New York, NY 0036, USA.
153. Kaminski, G. A.; Friesner, R. A.; Tirado-Rives, J.; Jorgensen, W. L., Evaluation and reparametrization of the OPLS-AA force field for proteins via comparison with accurate quantum chemical calculations on peptides, *J. Phys. Chem. B*, 105, **2001**, 6474-6487.
154. Gooda, A. C.; Cheney, D. L.; Sitkoff, D. F.; Tokarski, J. S., Analysis and optimization of structure-based virtual screening protocols 2. Examination of docked ligand orientation sampling methodology: mapping a pharmacophore for success, *J. Mol. Grap. Mod.*, 22, **2003**, 31–40.
155. Shaikh, M.S.; Mittal, A.; Bharatam, P.V., Design of fructose-2,6-bisphosphatase inhibitors: A novel virtual screening approach, *J. Mol. Grap. Mod.*, 26, **2008**, 900–906.
156. Axe, F. U.; Bembenek, S. D.; Szalma, S., Three-dimensional models of histamine H3 receptor antagonist complexes and their pharmacophore, *J. Mol. Grap. Mod.*, 24, **2006**, 456–464.

Appendix: Proton and Mass Spectrum of Compounds XII and XIII

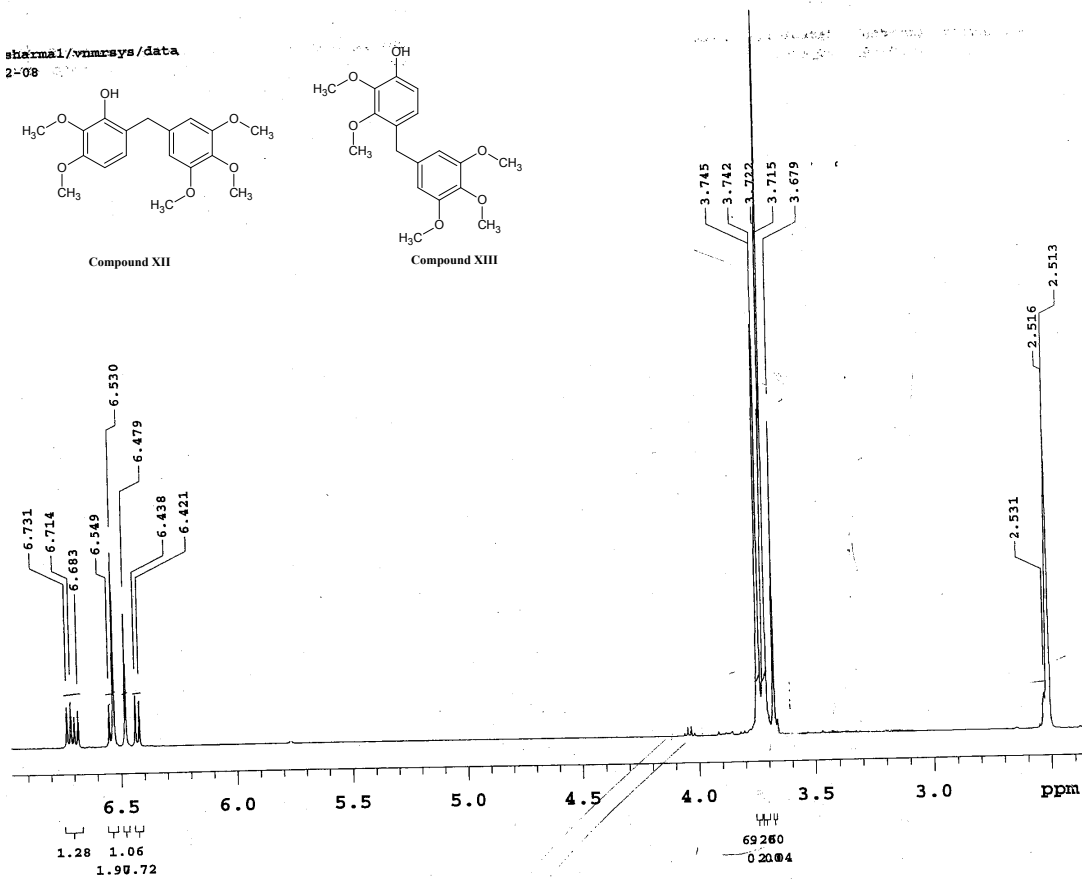
shamal/vnmrsva/data
2-08



Compound XII



Compound XIII



shamal/vnmrsva/data
2-08

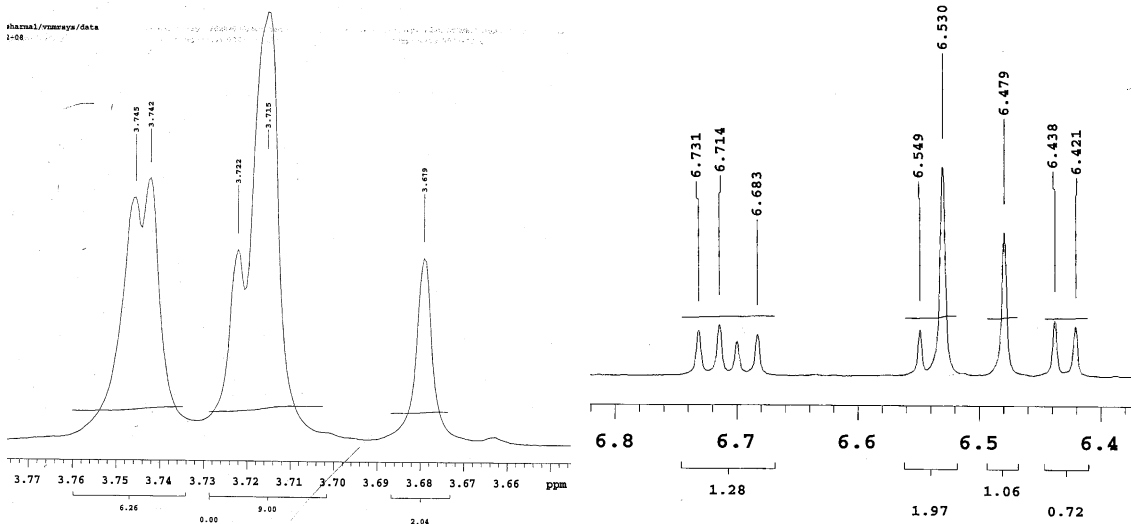


Figure A.1: Proton spectrum

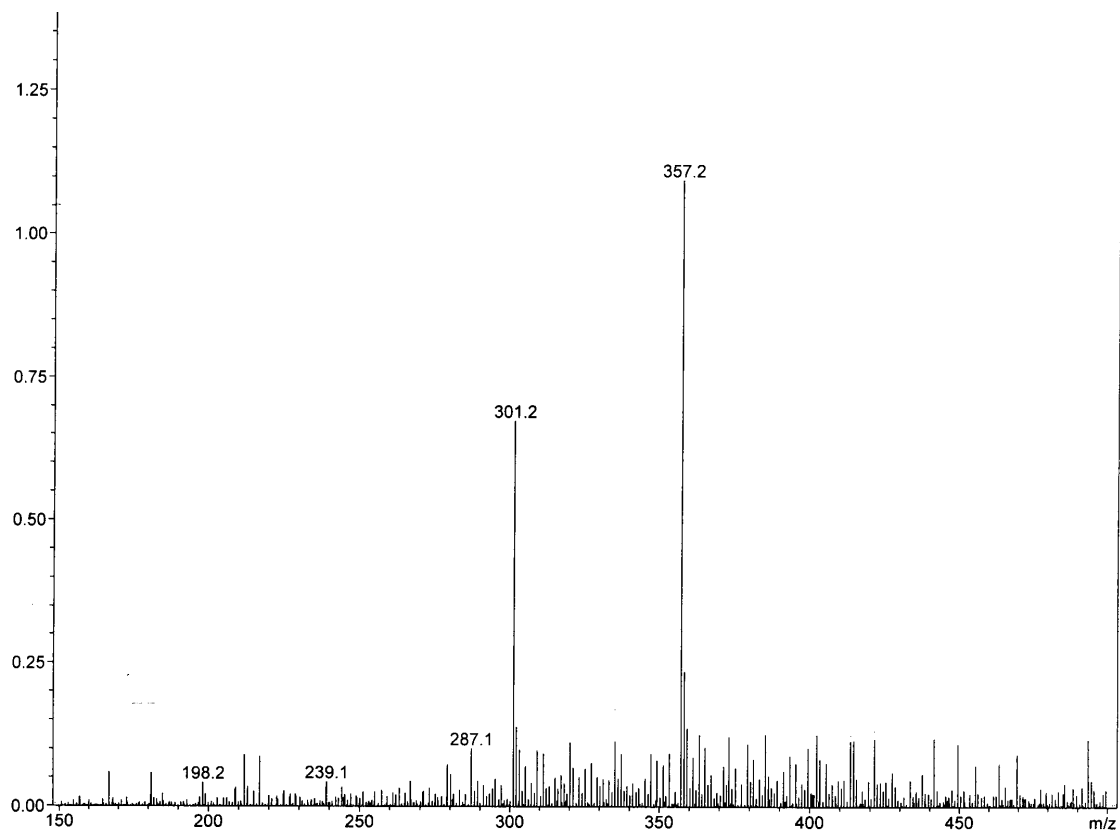


Figure A.2: ES mass spectrum

Vita

Surekha Ravaji Pimple was born in the city of Mumbai, India on August 20, 1979. She received the degree of Bachelor of Pharmacy in 2001 and the degree of Master of Pharmaceutical Sciences in 2004 from University of Mumbai, India. She joined the Department of Pharmaceutical Sciences at The University of Tennessee, Memphis, in August 2005 as a graduate student under the guidance of Dr. John K. Buolamwini.